# EXPERIMENTAL STUDY ON PLACEMENT OF TOE PROTECTION ELEMENTS OF RIVER BANK PROTECTION WORKS UNDER LIVE BED CONDITION

**Tanzim Ahmed**

**DEPARTMENT OF WATER RESOURCES ENGINEERING**

**BANGLADESH UNIVERSITY OF ENGINEERING AND TECHNOLOGY (BUET)**

**DHAKA-1000**

**May, 2014**

# EXPERIMENTAL STUDY ON PLACEMENT OF TOE PROTECTION ELEMENTS OF RIVER BANK PROTECTION WORKS UNDER LIVE BED CONDITION

A Thesis Submitted

by

Tanzim Ahmed

(0411162012 P)

In partial fulfillment of the requirements for the Degree of

**MASTER OF SCIENCE IN WATER RESOURCES ENGINEERING**

**DEPARTMENT OF WATER RESOURCES ENGINEERING**

**BANGLADESH UNIVERSITY OF ENGINEERING AND TECHNOLOGY (BUET)**

**DHAKA-1000**

**May, 2014**

## CERTIFICATION OF APPROVAL

The thesis titled **"Experimental Study on Placement of Toe Protection Elements of River Bank Protection Works Under Live Bed Condition"**, submitted by Tanzim Ahmed, Roll No. 0411162012P, Session: April 2011, to the Department of Water Resources Engineering, Bangladesh University of Engineering and Technology, has been accepted as satisfactory in partial fulfillment of the requirement for the degree of **Master of Science in Water Resources Engineering** on 26th May, 2014.

______________________________

**Dr. Md. Abdul Matin** — **Chairman (Supervisor)**
Professor,
Department of Water Resources Engineering
BUET, Dhaka-1000, Bangladesh

______________________________

**Dr. Md. Sabbir Mostafa Khan** — **Member (Ex-Officio)**
Professor and Head,
Department of Water Resources Engineering
BUET, Dhaka-1000, Bangladesh

______________________________

**Dr. Md. Mostafa Ali** — **Member**
Assistant Professor,
Department of Water Resources Engineering
BUET, Dhaka-1000, Bangladesh

______________________________

**Dr. M. R. Kabir** — **Member (External)**
Professor and Pro Vice-Chancellor
The University of Asia pacific,
Dhaka, Bangladesh

May, 2014

# DECLARATION

This is to certify that this thesis work has been done by me and neither this thesis nor any part thereof has been submitted elsewhere for the award of any degree or diploma.

| | |
|---|---|
| **Dr. Md. Abdul Matin** | **Tanzim Ahmed** |
| Countersigned by the Supervisor | Signature of the Candidate |

## TABLE OF CONTENTS

# LIST OF FIGURES

## LIST OF TABLES

## LIST OF NOTATIONS

| | |
|---|---|
| $D$ | Depth of scour |
| $D_n$ | Nominal thickness of protection unit |
| $d$ | Characteristics diameter |
| $d_n$ | nominal diameter |
| $dl$ | Length of a particle |
| $ds$ | Mean sieve size of a particle |
| $dt$ | Thickness of a particle |
| $dw$ | Width of a particle |
| $d_*$ | Dimensionless particle diameter |
| $d_{30}$ | Particle size for which 30% by weight is finer |
| $d_{50}$ | Median particle diameter for which 50% by weight is finer |
| $F$ | Freeboard |
| $F_D$ | Drag force |
| $g$ | Gravitational acceleration |
| $h$ | Depth of flow |
| $K_h$ | Depth Factor |
| $k_s$ | Effective bed roughness |
| $R$ | Lacey's regime scour depth |
| $R^2$ | Coefficient of determination |
| $R'$ | Rise of flood |
| $R_{e*}$ | Boundary Reynolds Number/ Particle Shear Reynolds Number |
| $S$ | Horizontal settling distance |
| $S_f$ | Safety factor |
| $T$ | Thickness of slope stone |
| $T_1$ | Thickness of stone on prospective slope below bottom of apron |
| $u$ | Depth averaged flow velocity |
| $u_*$ | Shear velocity/ Friction velocity |
| $u_{*c}$ | Critical friction velocity |
| $w$ | Fall velocity |
| $\rho$ | Mass density of water |

| | |
|---|---|
| $\rho_s$ | Mass density of particle |
| $\tau$ | Average shear stress |
| $\tau_c$ | Critical shear stress |
| $\tau_*$ | Shield's number/ Dimensionless shear stress/ Critical Shields stress |
| $\nu$ | Kinematic viscosity of water |
| $\mu$ | Dynamic viscosity of water |
| $\Delta$ | Relative density |
| $\theta$ | Angle of repose |
| u' | Turbulent fluctuations |
| $\mathcal{J}$ | Relative turbulence intensity |
| r.m.s u' | Turbulence intensity |
| $\sigma_u$ | Root-mean square of stream-wise velocity |

## LIST OF ABBREVIATIONS

| | |
|---|---|
| BWDB | Bangladesh Water Development Board |
| CC blocks | Concrete Cement blocks |
| FA | Falling Apron |
| FAP | Flood Action Plan |
| JMREMP | Jamuna-Meghna River Erosion Mitigation Project |
| PWD | Public Works Department (Datum level) |
| RRI | River Research Institute |

## ACKNOWLEDGEMENT

It is the greatest privilege of the author to acknowledge her supervisor Dr. Md. Abdul Matin, Professor, Department of Water Resources Engineering, BUET for providing an interesting idea of the work. His cordial and constant supervision, valuable suggestion, constructive comments, keen interest throughout the thesis work and enormous expertise helped the author for better understanding of the study.

The author is also highly grateful to Dr. Md. Sabbir Mostafa Khan, Professor and Head, Department of Water Resources Engineering, BUET and Dr. Md. Mostafa Ali, Assistant Professor, Department of Water Resources Engineering, BUET, for their valuable constructive comments on this thesis. The author is also grateful to Dr. M. R. Kabir, Professor and Pro-Vice-Chancellor, University of Asia Pacific, Dhaka, for his valuable and constructive suggestions.

The author acknowledges the staffs of the Hydraulics and River Engineering laboratory of DWRE, for their co-operation during the experimentation.

The author coveys her deepest and sincerest regards to her husband and family for their understanding and moral support. The author also wishes to give thanks to her colleagues and friends.

Above all, the author is grateful to almighty Allah, who has given her the opportunity to work hard.

**Tanzim Ahmed**

May, 2014

## ABSTRACT

Bank protection works are essentially important parts of river training works. In recent times, out of all types of river training structures, bank revetments works are common in Bangladesh. The purpose of bank revetments is to prevent bank erosion as a structural measure. They have to be designed to resist the current and wave and to protect the river bed and river bank against erosion. Toe scour is probably the most frequent cause of failure of riprap revetments. This is true not only for riprap, but also for a wide variety of protection techniques. A flexible toe protection in the form of a falling apron finds many applications in Bangladesh. For designing of bank protection works in perennial rivers, where low water level prevails, the construction works have always been a difficult task. Placing of underwater apron materials requires a considerably higher skill, equipment demand and standard and practical approaches. Such scenarios become more challenging as the channel bed composed of sand. In the sand bed channel flowing under equilibrium condition may be considered as live bed channel.

The present study has been undertaken to investigate experimentally two important aspect of underwater construction such as the placing behavior and incipient condition of toe protection elements under live bed condition. The experiments are conducted in the Hydraulics and River Engineering Laboratory of Water Resources Engineering Department, BUET. Three types of CC block and five types of geobag have been used to conduct fifteen experimental runs with two different hydraulic conditions to investigate placing behavior. For the incipient condition experimentation, four types of CC block and five types of geobag have been used to conduct nineteen experimental runs with various conditions. The measured data have been used to obtain various relationships at the incipient condition of the toe protection elements.

Experimental results are analyzed to develop relationships between shear velocities, depth averaged velocity, relative depth, turbulent intensity, depth factor, boundary Reynolds number and Shield’s number. Developed empirical relationships can be used to predict the shear velocity, depth averaged velocity, turbulent intensity and depth factor at incipient condition for selected types and sizes of toe protection elements. The proposed relationships are also compared with the equations available in previous studies. Comparisons show that the predictive capacity of the proposed

relationships is found to be satisfactory. Both CC block and geobag shows greater shear velocity and shear stress in case of live bed than that of fixed bed. Shear velocity on a live bed is about 2% greater than that of fixed bed for CC Block. For geobag shear velocity is about 8% greater on a live bed than that of fixed bed. The shear stress on live bed for CC block and geobag is about 4% and 16% greater than fixed bed respectively. However, a comparison has been made between underwater and dry bed toe protection to observe the incipient parameters.

It is suggested that the designer should consider the hydraulic parameters which should be commensurate with underwater constructional aspects. Therefore, this study will be helpful in designing of toe protection in case of underwater construction in real life practice.

# CHAPTER ONE

# INTRODUCTION

## 1.1 Background of the study

River training and bank protection works of alluvial rivers like Bangladesh is now a major challenge for engineers. However, still most of the relevant hydraulic and sedimentary processes arising from the coupling of flow and sediment are not fully understood. Artificial covering with erosion resistant material are being built to protect riverbank and bed from erosion. In recent time, concrete blocks and geobags are commonly used as toe protection elements of revetment works.

Toe scour is probably the most frequent cause of failure of riprap revetments. This is not only true for riprap, but also for a wide variety of protection techniques. A flexible toe protection in the form of a falling apron finds many applications in India and Bangladesh. The idea of dumping concrete cement blocks (CC blocks) or rock at the low waterline when a river endangers a village is copied for large structures. The first major application was at the Hardinge Bridge in India in 1912. Usually design rules formulated on the basis of experience, are made and applied in other river training works (Hoeven, 2002).

Number of study has been conducted for incipient motion of sediment particle. Dey and Raju (2002) conducted research on incipient motion of gravel and coal beds. Inglis (1949), Neill (1967), Maynord et al. (1989), USACE (1994), NHC (2006) proposed relationship regarding incipient motion. Limited study has been done on incipient behavior of toe protection elements. In Bangladesh, river bank and bed protection works are to be constructed in underwater condition. Therefore it is very important to understand the launching behavior of protection elements in real field condition. Hasan (2003) investigated local scour at the toe of protected embankment under clear water condition. Haque (2010) carried out an experimental investigation in a sand bed channel and observed the flow behavior around constructed apron for different flow condition. The apron materials were single sized geobag and concrete blocks of different sizes. Raju (2011) carried out an experimental study on settling behavior and incipient condition of toe protection elements in a fixed bed channel. It is anticipated that the behavior of protection elements will be different under such condition at which the channel bed is composed of sand, flowing under equilibrium condition which is considered as live bed channel. The precise discharge and time at which initial movement occurs is a subjective determination, therefore investigators have different point of views in this regard (Ashiq and Doering, 2006). Perng and Capart (2008) investigated underwater sand bed erosion and observed the bottom current acquires a higher density because of sediment suspension, allowing gravity to affect both the turbulence generation and the longitudinal balance of the flow. During construction and repair, geobags and concrete blocks are delivered directly from vessel with the intention to form a uniform coverage. This process is simple but their dumping behavior plays a significant role. RRI (2010) conducted physical model study to test the performance of geobags and concrete blocks as bank protection works. But they did not carry out detail tests for underwater condition. In underwater condition, identification of placement of protective elements in water flowing situation is found to be more difficult. This has been also reported by Stevens and Oberhagemann (2006). The river bed roughness, flow velocity and turbulent intensity affect the uniform coverage and launching behavior of protection elements. In designing toe protection elements, the depth factor (h/d) is one of the significant parameter (Pilarczyk, 2008). With the depth factor, the water depth is taken into account, which is necessary to convert depth- averaged flow velocity into the flow velocity just above the protection. The depth factor also depends on the development of the flow profile and the roughness of the protection. Review of literature shows that no mentionable studies have been conducted to investigate the underwater constructional aspects of toe protection under live bed condition. In this study, an attempt has been made to conduct experimental investigation on the placing and incipient behavior of toe protection elements under live bed condition.

## 1.2 Objectives of the study

The main objectives of the study are:

1) To observe the placement of different types of protection elements
2) To investigate the incipient condition of protection elements after placement
3) To develop depth factor correlation for the design of protection elements especially for the falling apron

## 1.3 Organization of the thesis

This thesis has been organized under six chapters. Chapter one describes the background and objectives of the study. In Chapter two the review of literature related to the study has been described. In Chapter three, theoretical basis of governing parameters of placing behavior and analysis technique for incipient condition is stated. Chapter four illustrates the experimentation set-up of the laboratory, size of protection elements used, test scenarios, test procedures followed during measurements and the observations noted at that time. In Chapter five, analyses and discussions of experimental results are presented. Finally, the main conclusions of this study and recommendations for further research are presented in Chapter six.

# CHAPTER TWO

# LITERATURE REVIEW

## 2.1 Introduction

In this chapter, some laboratory studies which are related to river bank protection works have been discussed. Furthermore, some modern and classical approaches which were practiced earlier for the development of different incipient condition formulas have been illustrated. Here, some formulas related to the shear stress at incipient condition of protection element have been studied. In addition to this, literatures dealing with shear velocity, depth averaged velocity, shear stress, turbulent intensity and design of protection elements have been reviewed.

## 2.2 Bank protection works

Bank protection works are essentially important parts of river training works. In recent times, out of all types of river training structures, bank revetments works are frequent in Bangladesh. The purpose of bank revetments is to prevent bank erosion that means they have to be designed to resist the current and wave and to protect the river bed and bank from erosion. Their principal function is to provide a stable river bank. To fulfill this role they must meet certain basic requirements out of which stability is of utmost importance. Construction methods, construction materials and dimensions of the selected structures depend mainly on the hydraulic loads acting on the structures. They must be capable of withstanding the imposed loads and must have the necessary strength characteristics to resist displacement.

## 2.3 Revetment structures

Revetment is artificial roughening of the bank slope with erosion-resistant materials. A revetment usually consists of three components: cover layer, filter layer and toe protection. The cover layer must be able to resist hydraulic impacts (current and wave). The intermediate layers between cover and core material are required for drainage and filtering to allow for a stable foundation of the overall system. The toe of a revetment structure requires special attention during design. Toe protection is provided as an integral part at the foot of the bank to prevent undercutting caused by scour. The protection can be divided as falling apron or launching apron, which can be constructed with different materials, e.g., CC blocks, rip-rap, and geobags. Figure 2.1 shows a typical revetment and its different components (BWDB, 2010).

Launching apron consists of interconnected elements that are placed horizontally on the floodplain and normally anchored at the toe of the embankment. The interconnected elements are not allowed to rearrange their positions freely during scouring but launch down the slope as a flexible unit. The falling apron, on the other hand, consists of loose elements (e.g., CC blocks, geobags, stones) placed at outer end of the structure. When scour hole approaches the apron, the elements can adjust their position freely and fall down the scouring slope to protect it.

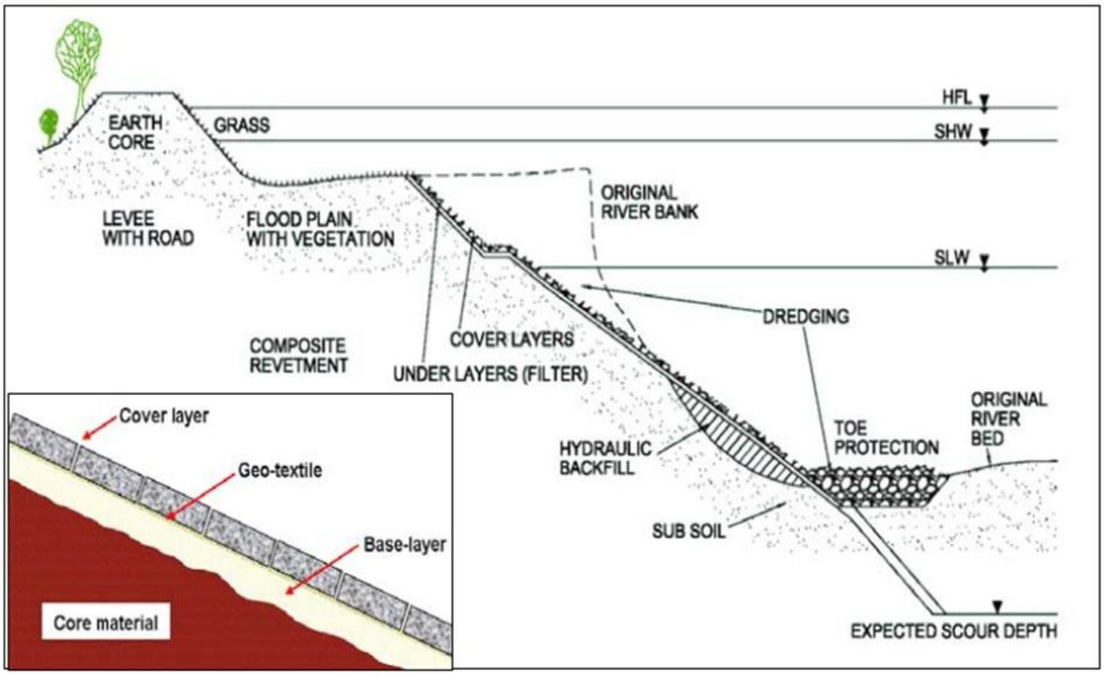


**Figure 2.1:** Components of a typical revetment on river bank (Source: BWDB, 2010)

Revetments built along the riverbank provide a number of advantages:

- the land used for construction is minimized, as it only requires to cut back a small strip along the bank line above low water level
- the protection under water follows the alignment of the existing river bank
- the toe protection or falling apron is placed at a deeper level, where more consolidated soils support a more even launching and more stable slopes after launching (Figure 2.2)

For revetments covering the underwater river bank, systematic dropping of material should start from the outer edge of the falling apron in the river and proceed towards the water edge near the bank. This type of dropping should be done in such a way that the underwater river bed and bank are covered with a specified uniform layer of protection material. The slope above low water may be covered by placing hard material over a filter layer. The filter should be extended to at least 1.0 m below the average low water level.

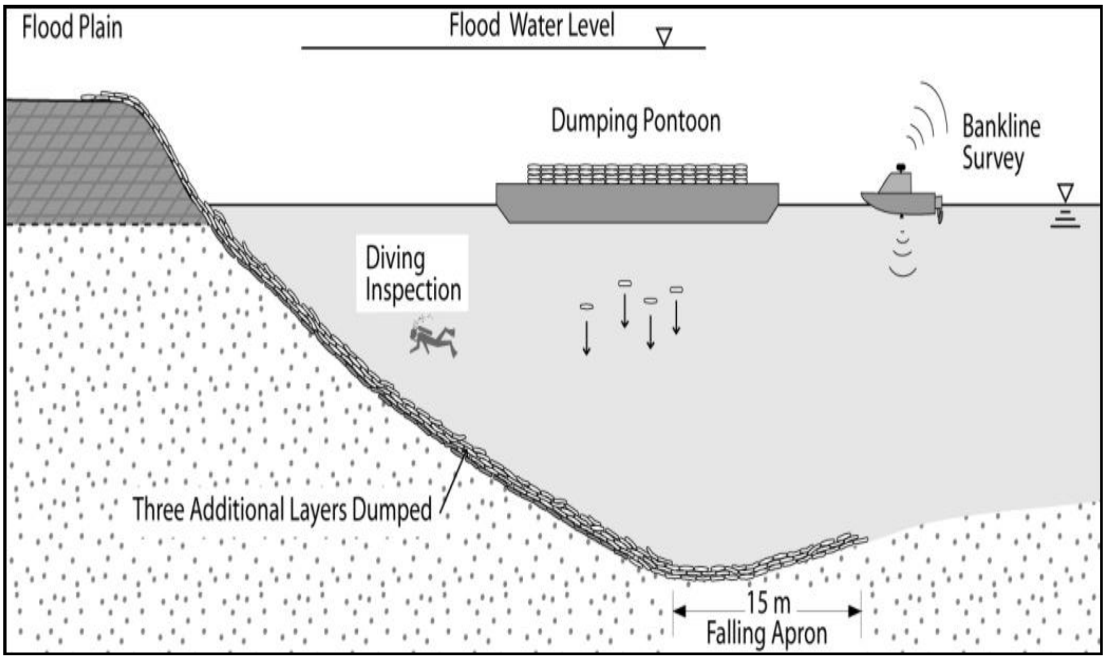


**Figure 2.2:** Protection of the underwater slope starting from the existing river bank

### 2.3.1 Toe protection

Toe scour is probably the most frequent cause of failure of riprap revetments. This is not only true for riprap, but also for a wide variety of protection techniques. Toe scour is the result of several factors, including these three (USACE, 1994): i) Change in cross section that occurs after a bank is protected in meandering channels: In meandering channels the thalweg often moves toward the outer bank after the bank is protected. The amount of change in cross section that occurs after protection is related to the erodibility of the natural channel bed and original bank material. Channels with highly erodible bed and banks can experience significant scour along the toe of the new revetment. ii) Scour at high flows in meandering channels*:* Bed profile measurements have shown that the bed observed at low flows is not the same bed that exists at high flows. At high flows the bed scours in channel bends and builds up in the crossings between bends. On the recession side of the flood, the process is reversed. Sediment is eroded from the crossings and deposited in the bends, thus obscuring the maximum scour that had occurred. iii) Braided channels: Scour in braided channels can reach a maximum at intermediate discharges where flow in the channel braids attacks banks at sharp angles.

### 2.3.2 Toe protection methods

Toe protection of revetments may be provided by two methods. Firstly, extensions to maximum scour depth: Lower extremity of revetment placed below expected scour depth or founded on non-erodible bed materials. These are preferred method, but can be difficult and expensive when underwater excavation is required. Secondly, placing of launchable stones: Launchable stones are defined as stones that are placed along expected erosion areas at an elevation above the zone of attack. As the attack and the resulting erosion occur below the stone, the stone is undermined and rolls/slides down the slopes, forming a surface cover layer reducing the erosion. In general, the design implies that, the scouring and undermining process of the developing scour hole in front of the structure initiates the deformation process of the toe protection. At the estimated maximum scour depth, the launching apron is assumed to cover and stabilize the bank-sided river profile, reducing further erosion of the bank.

A flexible toe protection in the form of a falling apron finds many applications in Bangladesh. The idea of dumping concrete cement blocks (CC blocks) or rock at the low waterline when a river endangers a village is copied for large structures. The first major application was at the Hardinge Bridge in India in1912. Usually design rules formulated on the basis of experience, are made and applied in other river training works (Hoeven, 2002).

### 2.3.3 Falling apron

Falling apron is a multi layer system of protection element placed on a sloping or horizontal surface as protection against scour. The individual units are rearranged freely with the morphodynamic forces of the river and stabilize the eroding bank. The single weight of each unit and the volume of protective material within a defined area are the decisive factors for designing an efficient falling apron. Apron is intended to launch when the underlying sand/sandy soil is scoured by the river current so as to form a continuous protection below the water level. Placing of underwater apron materials require a considerably higher skill, equipment demand and standard of control.

### 2.3.4 Dimension of falling apron

Among the various methods, launching apron or falling apron has been considered to be most economic and common method of toe protection of revetment. Falling aprons are generally laid horizontally on river bed at the foot of the revetment, so that when scour occurs, the material will launch and will cover the surface of the scour hole in a natural slope. Historically, starting from the limited understanding of Spring (1903) and Gales (1938) the launched quantity was computed assuming a launched apron thickness similar to the thickness of pitching work above water. The quantities were calculated as geometrical area depending on launched thickness, depth of scour, and slope of the launching apron. This approach has proven substantiated by the result of the systematic model tests published by Ingles in 1949 and follow on model tests conducted in Bangladesh during the Flood Action Plan in the early 1990s.

Spring (1903) recommended a minimum thickness of apron equal to 1.25 times the thickness of stone riprap of the slope revetment. He recommended further that the thickness of apron at the junction of apron and slope should be same as that lay on the slope but should be increased in the shape of a wedge towards the river bed, where intensity of current attack is severe and hence probability of loss of stone is greater.

Since apron stone shall have to be laid mostly under water and cannot be hand placed, thickness of apron at junction of toe and apron according to Rao (1946, after Varma, Saxena and Rao, 1989) should be 1.5 times the thickness of riprap in slope. Thickness at river end of apron in such case shall be 2.25 times the thickness of riprap in slope.

The slope of the launched apron was suggested by Spring and Gales as 1:2 and according to Joglekar (1971) it should not be steeper, but also not flatter than 1:3. Different shapes and dimensions were suggested by the above mentioned authors for the apron to be placed in the river bed expecting/estimating a thickness of the launched apron as about 1.25 times the thickness of the slope cover layer. The face slope of the launching apron may be taken as 2:1 for loose stone as suggested by Spring (1903) and Gales (1938). A schematic diagram of an apron is shown in Figure 2.3. Table 2.1 presents a summary of these dimensions.

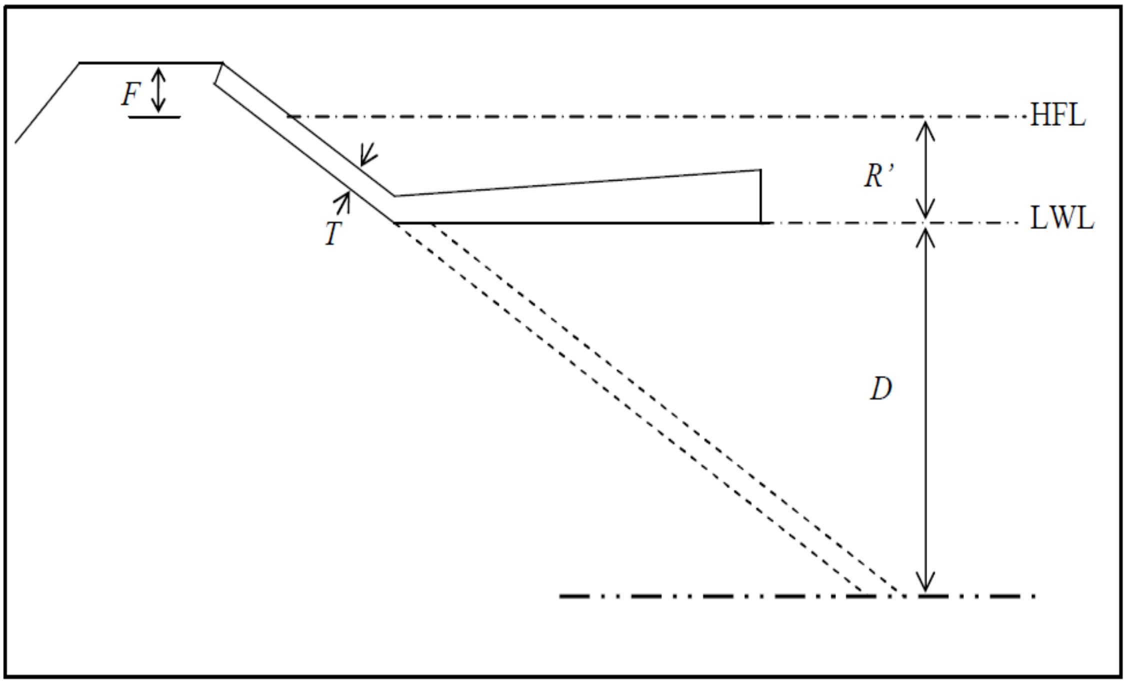


**Figure 2.3**: Schematic diagram of an Apron

**Table 2.1**: Dimension of Apron

| Parameter | Spring (1903) | Gales (1938) | Rao (1946) |
|---|---|---|---|
| Area of slope stone | 2.25 T(R'+F) | 2.24 T(R'+F) | 2.25 T(R'+F) |
| Area of apron stone | 2.82 DT | 2.24 $DT_1$ | 2.82 DT |
| Width of apron | 1.50 D | 1.50 D | 1.50 D |
| Mean thickness of apron | 1.88 T | 1.5 $T_1$ | 1.88 T |
| Inside thickness of apron | T | 1.5 $T_1$ | 1.5 T |
| Outside thickness of apron | 2.76 T | 1.5 $T_1$ | 2.25 T |
| Inclination of slope stone | 1V:2H | 1V:2H | 1V:2H |
| Desired inclination of apron stone | 1V:2H | 1V:2H | 1V:2H |

Where F = freeboard, R′ = rise of flood, D = deepest known scour, T = thickness of slope stone, $T_1$ = thickness of stone on prospective slope below bottom of apron. Table 2.1 shows minor difference among these approaches. Gales (1938) shape of apron includes a berm and provides allowance for scour. Therefore, any approach can be followed for construction of an apron.

### 2.3.5 Underwater falling apron construction

During construction of falling apron, geobags and CC blocks are delivered directly from vessel for placement of protective elements at designated position in the settling fashion. This process is simple but their dumping behavior plays a significant role. However, in such a condition, identification of placement of protective elements in underwater flowing situation is found to be more difficult (Raju, 2011). During the field visits at Sirajgonj Hard Point, the present practice of dumping geobags was observed and is shown in Figure 2.4

**Figure 2.4:** Geobags dumping at Sirajgonj Hard Point (Field visit on 15.08.2013)

Stability of underwater elements is computed as per Pilarczyk (1990) Formula for rock and rock related unit. Pilarczyk's publications provide different approaches for determining depth factor ($K_h$). In Pilarczyk (2000) publication, he mentioned that the value of 0.035 is chosen as a reference value for a critical shear stress parameter.

In JMREMP the average flow velocity of 3 m/s was selected as design velocity for revetments. In case of spurs or groynes, protruding into the flow, much higher flow velocities were observed resulting in much heavier protective elements, greater thickness of the protective layer, and higher cost per unit area of protection.

The depth factor $K_h = 2 \log [1+12h/k_s]^{-2}$ converts the local mean bottom velocity to the mean velocity. In this form, it applies to a fully developed logarithmic velocity profile. However, in rivers like Jamuna and Padma, this often does not apply. Pilharczyk gives the alternative formula for non-fully developed velocity profiles $K_h = (h/D_n+1)^{-0.2}$. This factor plays a major role for the purpose of calculation of stable protection element size, $D_n$ as stated in Zaman, M. U., and Oberhagemann, K. (2006).

## 2.4 Live bed condition

In live bed condition, the bed shear stress is larger than the critical shear stress of the bed. When the average shear stress on the bed of alluvial channel exceeds the critical shear stress of the bed material, the particle on the bed begin to move and live bed condition prevails. The rate of sediment transport is dependent on the shape, size and density of the bed particles and their placement among the surrounding particles.

According to Bridge Scour Manual (2013), if mostly suspended bed material transport is found, it is clear-water scour. On the other hand, some suspended bed material transport creates live bed condition. As for an example, pier scour at live bed condition is shown in Figure 2.5.

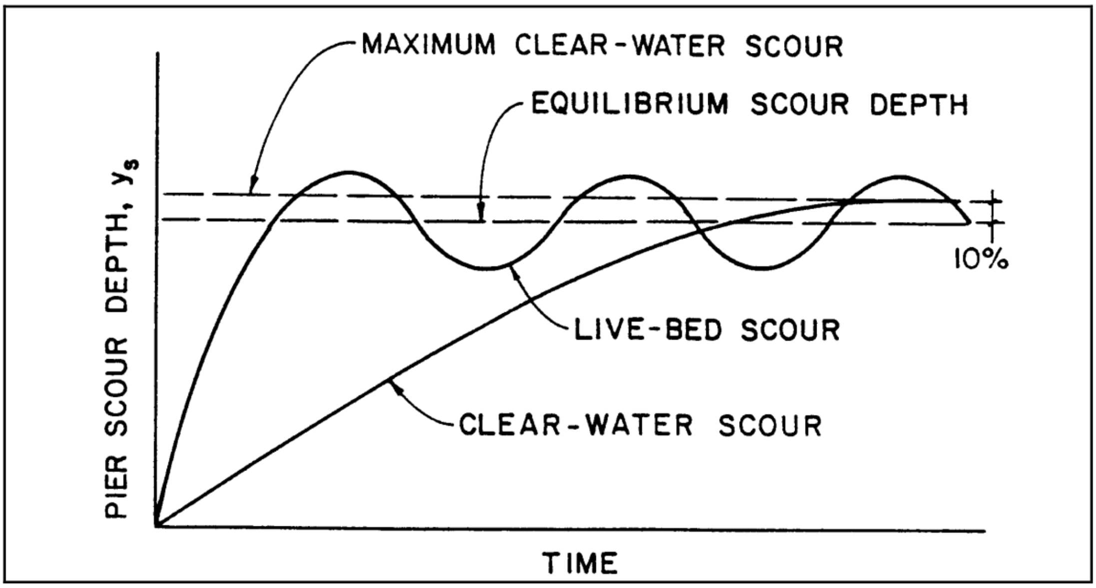


**Figure 2.5:** Pier scour at live bed condition

### 2.4.1 Bed form

Turbulent open-channel flows with mobile, flat (without distinct bed forms) granular beds have complex boundary conditions due to effects of bed mobility and permeability. They have attracted much less attention than their fixed-bed counterparts, and in many studies researchers implicitly have assumed that mobile-bed flows have the same structure and follow the same scaling laws as those over fixed beds. However, different boundary conditions may cause the structure of mobile-bed flows to differ from that of fixed-bed flows (Nikora and Goring, 2000). Bed forms are flow induced and directly affect the roughness or flow resistance. Forms of bed roughness observed in the flumes and in alluvial stream are illustrated by Simons and Richardson (1961), as shown in the Figure 2.6 (Source: Hasan, 2003).

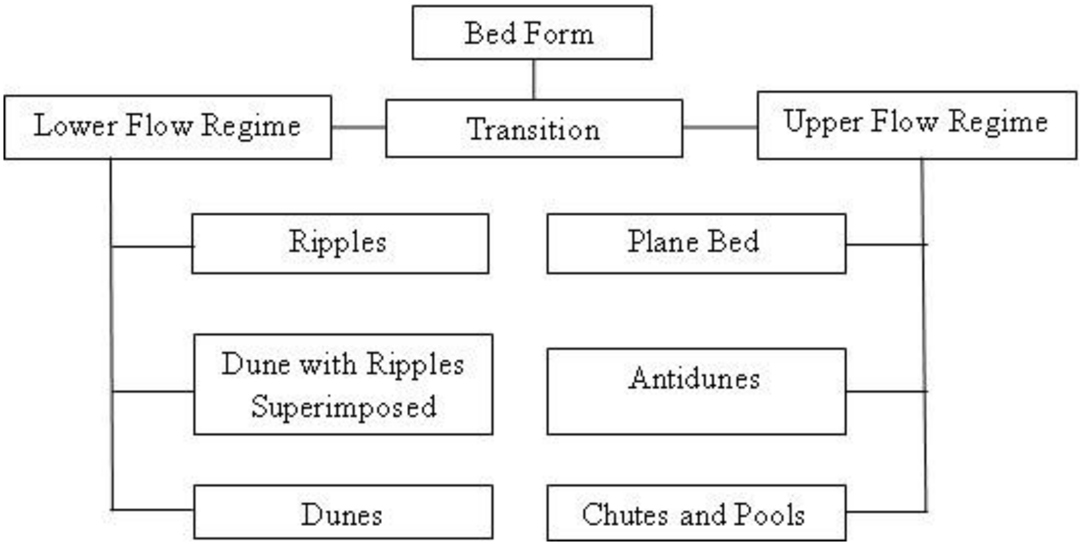


**Figure 2.6**: Types of bed form

Therefore, computation of the river stage and flow velocity relies on the determination of bed form roughness. Sediments move with the flow in such a way that bed forms are established. Bed particle configuration is particularly important in the presence of a sediment bed that is hydrodynamically rough (Cheng, 2006).

### 2.4.2 Classification of bed forms

Based on similarities in form, resistance to flow and sediment transport these bed forms are divided into categories of lower flow regime, transition zone, and upper flow regime in the order of increasing flow velocity. The characteristics associated with these flow regimes, in terms of bed-material concentration, mode of sediment transport, type of roughness and phase relation between bed and water surface are compared and summarized in Table 2.2.

Other characteristics features of different bed forms can be recognized on the basis of bed material size and the relative velocity of stream or Froude Number. Ripples are only observed with the fine material (generally with d< 0.5-0.7 mm) and do not form with coarse material (when d> 0.9-1.0 mm). Ripples are independent of depth of flow, but dunes are strongly dependent of flow depth.

**Table 2.2:** Classification of bed forms and their characteristics (After Simons et al., 1995); (Source: Chang, 1988)

| **Flow Regime** | **Bed Form** | **Bed-material concentration (ppm)** | **Mode of sediment Transport** | **Type of Roughness** | **Phase Relation Between Bed and Water Surface** |
|---|---|---|---|---|---|
| Lower regime | Ripples | 10-200 | Discrete steps | Form roughness predominates | Out of phase |
| | Ripples on dunes | 100-1200 | | | |
| | Dunes | 200-2000 | | | |
| Transition zone | Washedout dunes | 1000-3000 | | Variable | |
| Upper Regime | Plane beds | 2000-6000 | Continuous | Grain roughness predominates | In phase |
| | Antidunes | Above 2000 | | | |
| | Chute and Pools | Above 2000 | | | |

Simons and Richardson (1961) developed a bed-form predictor as shown in Figure 2.7. Bed forms are given in terms of the median fall diameter of the bed material in the sand-sized range and the stream power.

Athaullah(1968), working with Simons, studied many groups of dimensionless parameters. He presented a graphical relationship, shown in Figure 2.8 delineating different flow regimes based on the Froude number and the relative roughness R/d, where R is the hydraulic radius and d is the median bed-material size.

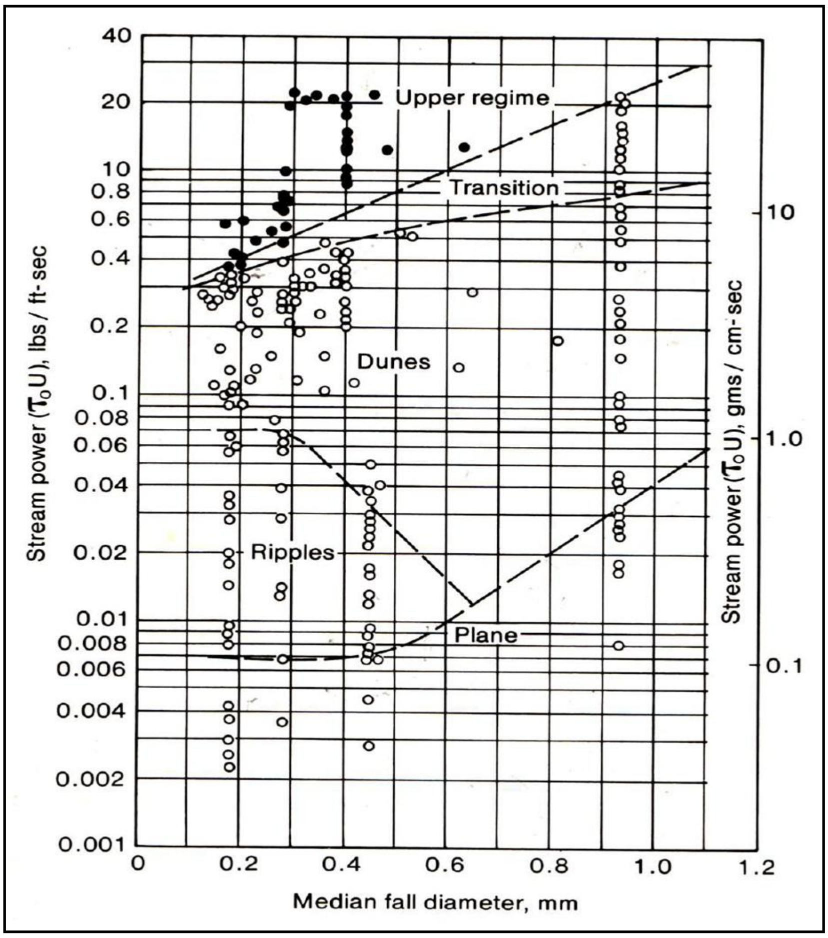


**Flgure 2.7:** Relationships among bed form, stream power per unit area, and median fall diameter (Simons and Richardson, 1961) (Source: Chang, 1988)

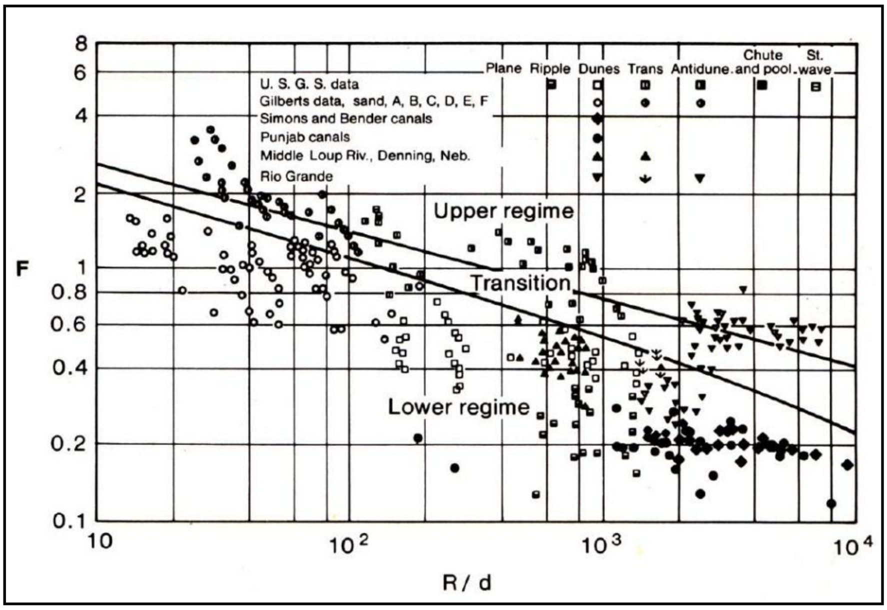


**Flgure 2.8:** Bed form prediction as function of Froud number and R/d (Athaullah 1968); (Source: Chang, 1988)

In Van Rijn's (1984) approach, the classification of bed form is assumed to be controlled mainly by bed-load transport, which is described by a dimensionless particle parameter, $d_*$ and a transport- stage parameter, T. The T parameter expresses the grain shear stress in relation to the critical or Shields stress (Chang, 1988).

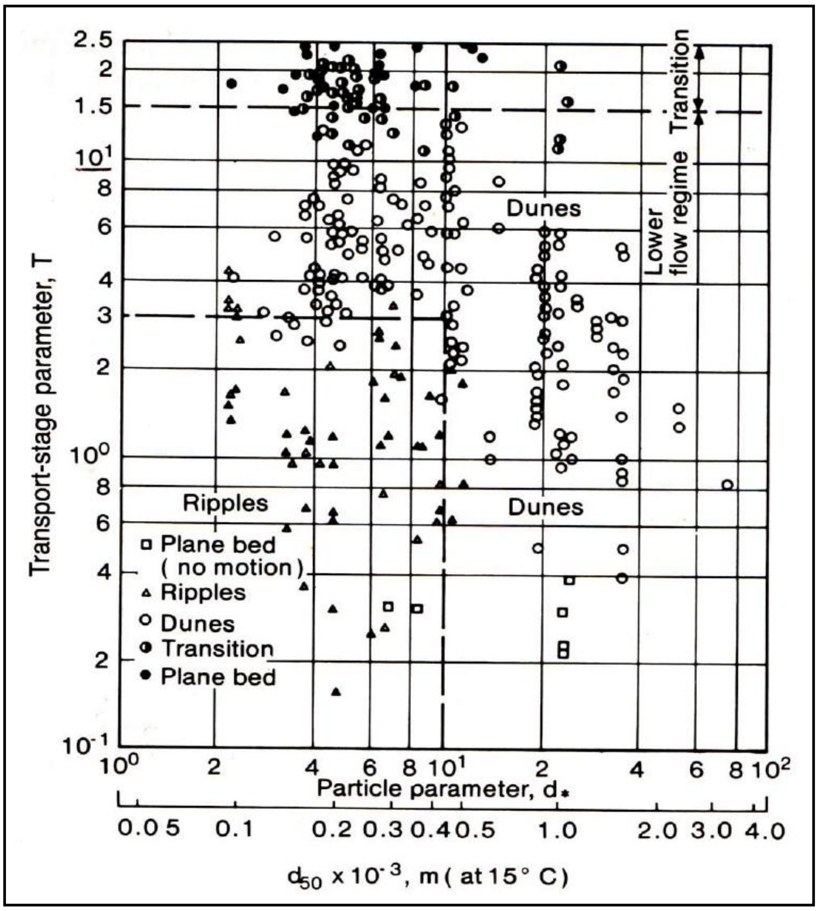


**Flgure2.9:** Diagram for bed-form classification in lower and transitional flow regimes (Van Rijn, 1984) (Source: Chang, 1988)

### 2.5 Reviews on previous studies

Maynord et al. (1989) developed the riprap design procedure based on local average velocity and local depth. This procedure addresses the influence of riprap gradation, blanket thickness, side slope angle, and channel bends. Many engineers prefer design procedures based on velocity. This is particularly true in riprap design because shear stress relations have not gained wide acceptance. Some of the existing riprap design procedures (OCE 1970; Liu et al. 1976) use the logarithmic velocity laws to convert shear stress into velocity for use in sizing riprap. However, significant problems arise in applying the logarithmic velocity relations to rough surfaces like riprap where relative roughness is high. The appropriate velocity for use in the riprap design procedure must be determined. The velocity used must be representative of flow conditions at the riprap and must be able to be determined by the designer by relatively simple methods.

Sediment movement under unidirectional flows was investigated by Paphitis (2001). A selection of threshold data sets from previous investigations were used to re-examine, selectively, some of the empirical curves that are most commonly used for the prediction of sediment threshold. Simple analytical formulae were derived describing single line curves for mean threshold values and envelopes for the initial movement of discrete particles and the commencement of mass sediment transport phases of the critical condition. The complexity of factors governing the prevailing conditions at threshold, together with the randomness of events, limits deterministic solutions; however, the curves provide an approach that can be used readily in practical applications. In contrast, the envelope presentation was more of a stochastic approach to the definition of threshold. It recognizes that there is no definitive threshold condition under which a particular particle size can be displaced, but rather that a range of threshold values exist. The empirical threshold relationships were derived on the basis of a relatively large amount of data. However, the sources utilized have interpreted the ‘critical condition’ in various ways, implying that the formulae must be treated with caution in applications.

Theoretical and experimental investigations on the threshold of noncohesive sediment motion under a steady-uniform stream flow on a combined transverse (across the flow direction) and longitudinal (streamwise direction) sloping bed was presented by Dey (2003). Theoretical analysis of the equilibrium of a sediment particle lying on a combined transverse and longitudinal sloping bed showed that the critical shear stress ratio (ratio of critical shear stress for a sloping bed to that for a horizontal bed) was a function of the transverse bed slope, longitudinal bed slope, angle-of-repose of sediment particles and lift-drag ratio. As in laboratory flume study, the uniform flow is difficult to establish in a steeply sloping channel and is impossible to obtain in an adversely sloping channel, experiments were conducted in two inverted semicircular ducts (closed-conduit flow) for three sizes of uniform sediments. The critical shear stresses for experimental runs were determined considering side-wall correction. The model can be applicable to both the channel beds and banks.

Marsh et al. (2004) conducted important study for comparing methods for predicting the incipient motion conditions of a uniform sand bed. The four methods are: (1) the Shields diagram, (2) an empirical approach, (3) a method derived from resolution of rotational forces, and (4) a simplified resolution of rotational forces with a variable lift force coefficient. The four methods were used to predict the incipient motion conditions for 97 experimental runs taken from seven independent experimental flume studies. The effectiveness of predicting depth averaged incipient motion velocity for each of the four methods was compared. The simplified resolution of rotational forces model (4) and Shields method (1) were most successful in predicting the incipient motion velocity. The empirical method was the least successful at predicting the measured incipient motion conditions.

Smith (2004) examined the initiation of motion of four natural and five sieved calcareous sand samples in unidirectional flow. Flume experiments yielded the sediment transport rate as a function of bed shear stress up to bed-form development. Reference-based criteria were supplemented by visual observations to determine the critical shear stress. The results were compared with published data for rounded and irregular particles in terms of the median sieve size and the corresponding nominal and equivalent diameters as functions of particle Reynolds number. The comparison showed that the critical shear stresses of the irregular particles were higher than the Shields curve in the hydraulically smooth flow regime and lower in the rough turbulent flow regime.

Two hydrodynamic parameters that are essential for the construction of submerged dikes in rivers with sand-filled geosynthetic bags were studied by Zhu et al. (2004). First, laboratory study and field observation were conducted to investigate the horizontal settling distance of sandbags in open channel flows. Sandbag models used for laboratory tests were prepared according to similarity requirements. An analytical formula for evaluating the settling distance was then derived based on the experimental data. The predictions were then compared to the field measurements. The observed settling distance varied significantly and its probability density distribution was positively skewed. This study also presented a formula for computing the critical flow velocity at incipient sandbag motion for two extreme conditions.

Göğüş, and Defne (2005) investigated the effect of shape and size of solid particles on their initiation of motion in open channel flows. Initial motions of 22 solitary particles having different shapes and sizes were observed in a tilting flume of rectangular cross section. A smooth fixed bed and an obstructing element of smaller height with respect to the particle size was used throughout the experiments. The ratio of the height of the obstructing element to the height of the particle was kept constant at 1/5. By either changing the slope of the tilting flume or the discharge, or both, a range of shear stress values was obtained. Various equations and graphical representations in terms of dimensionless bed shear stress, grain Reynolds number, and the ratio of flow depth to grain diameter were presented to determine the flow conditions corresponding to the initiation of motion of solitary particles of given shapes. The experiments revealed that critical flow conditions are dependent not only on the particle size and shape but also on the ratio of flow depth to grain diameter. Some authors suggested that, for the same bed shear stress, an increase in relative roughness causes a decrease in flow velocity around bed particles [e.g., Ashida and Bayazit, 1973; Bayazit, 1978; Graf, 1991; Shvidchenko and Pender, 2000; Vollmer and Kleinhans, 2007]. This hypothesis is partially supported by the experiments of Chiew and Parker (1994). They measured the conditions of incipient motion on variable slopes in a sealed duct and were thus able to vary slope while holding the relative roughness constant. Contrary to the open-channel experiments Chiew and Parker (1994) showed that $\tau_{*c}$ decreased with increasing channel slope due to the increased gravitational component in the downstream direction. These experiments, therefore, indicated that the observed increase in critical shear stress with increasing slope in open-channel flow is fundamentally due to the coincident increase in relative roughness (for the same boundary shear stress and particle size), although lack of aeration also might have been a factor (Lamb et al., 2008).

Scour of non cohesive sediment beds (uniform and non uniform sediments) downstream of an apron due to a submerged horizontal jet issuing from a sluice opening was investigated by Dey and Sarkar (2006). Using experimental scour depth at different times, the time variation of scour depth was scaled by an exponential law.

The variation of equilibrium scour depth with tail water depth indicates a critical tail water depth corresponding to a minimum equilibrium scour depth. The effect of sediment gradation on scour depth was pronounced for non uniform sediments, which reduced scour depth significantly due to formation of an armor layer, and therefore prompted study of the reduction of scour depth, by a launching apron placed downstream of the rigid apron. The maximum equilibrium depth of scour reduced significantly when a launching apron was placed downstream of a rigid apron, as the upstream slope of the scour hole was covered by the launching apron and the submerged jet was unable to erode the bed sediments after the initial period of scour. It was observed that the maximum scour depth occurred just at the edge of the launching apron. In some runs, a few stones detached from the launching apron were scattered at the zone of maximum scour; extra scour took place around the stones in addition to the scour by the flow, as was also observed by Hoeven (2002).

Comparisons of existing empirical threshold curves proposed for Shields diagram, a method based on the concept of probability of sediment movement, and an empirical method based on movability number was exercised by Beheshti, A. A. and Ataie-Ashtiani, B. (2007). These methods are used to predict the incipient motion conditions for experimental runs taken from various studies. Most of the experimental data, used in this work, was not used before in derivation of alternative formulations for Shields diagram and other methods. The empirical threshold curves based on the Shields entrainment function was the least successful at predicting the measured incipient motion conditions, while the use of the movability number gave good predictions of critical shear velocity compared with experimental data. Armitage and Rooseboom (2010) investigated the link between movability number and incipient motion in river sediments. They established a new look at the use of the movability number for the prediction of incipient motion – which is defined in terms of a defined intensity of motion. Using data from other researchers for particle Reynolds numbers up to nearly 12000, a relationship between movability number and intensity of motion was developed for flow with turbulent boundaries. This allowed for a firmer definition of incipient motion as well as a new bedload transportation equation.

Peirson et al. (2008) investigated two layers of armor overlying a filter, consistent with conventional rock protection designs in a large-scale flume for different slopes.

Two sizes of sandstone and basalt were tested. He found that, the additional resistance to erosion due to flows down steep slopes can be achieved by placing rock instead of dumping randomly.

Investigation in a sand bed channel and observation of the flow behavior around constructed apron for different flow condition was carried out by Haque (2010). The presence of apron at the toe of revetment caused a change in the velocity distribution near bed. Analysis of velocity contour revealed the trend of shifting maximum velocity away from the revetment. This study found that, when apron material was laid around a structure, the apron behaved like a submerged extension of the revetment. It was found that placing of apron in different arrangement not only reduced the maximum scour depth but also had changed the deposition pattern around revetment.

Oberhagemann and Hossain (2011) conducted a study on geotextile bag revetments for large rivers in Bangladesh. This study reported the outcome of the last eight years of development work under the ADB-supported Jamuna-Meghna River Erosion Mitigation Project (ADB, 2002), implemented by the Bangladesh Water Development Board. Besides substituting geotextile bags for concrete blocks as protective elements, the project involved in development of a comprehensive planning system to improve the overall reliability and sustainability of riverbank protection works. Geotextile bags also provide the potential for substantial cost reduction, due to the use of locally available resources. The use of the abundant local sand reduces transport distance and cost, while local labor is used for filling, transporting, and dumping of the 75 to 250 kg bags. In addition, there were strong indications that geotextile bags perform better than concrete blocks as underwater protection, largely due to their inherent filter properties and better launching behavior when the toe of the protected underwater slope was under-scoured.

The mechanism responsible for initiation of sediment motion under turbulent flow conditions was investigated by Celik, A.O. (2011). The impulse concept was investigated by utilizing appropriate measurement methods in the laboratory for determining the condition of incipient motion. The experimental program included measurements of particle entrainment rates of a mobile grain and turbulence induced forces acting upon a fixed grain for a range of flow conditions. In addition, near bed flow velocities were measured synchronously with both the entrainment and pressure measurements at turbulent resolving frequencies. Results of this work covered the limitations and uncertainties associated with the experimental methods employed, and the description of the inadequacies of existing incipient motion models via the impulse framework.

An experimental study in a fixed bed channel on settling behavior of toe protection elements of river bank protection was done by Raju (2011). The experiments were conducted to determine the fall velocity in a square shaped settling column of 30 cm X 30 cm X 130 cm and in the large tilting flume of the Hydraulics and River Engineering Laboratory of Water Resources Engineering Department, BUET. Sixteen different sizes of elements ranging from 1.6 cm X 1.6 cm X1.3 cm to 4.1 cm X 4.1 cm X 2.7 cm were used to conduct sixty four experimental runs with the discharges range from $0.033m^3/s$ to $0.203m^3/s$. During experimentation various observations were made and the measured data were used to obtain various relationships for the settling behavior of the toe protection elements in fixed bed condition.

Elkholy and Chaudhry (2012) carried out investigation to understand the mechanics of motion of large sandbags and to compute their trajectories. An equation was developed for the normalized maximum horizontal settling distance from the experimental data. It was found that the particle velocity normal to the flow depends mainly on the characteristic diameter of the particle and the Froude number of the flow while the particle velocity in the stream wise direction showed lower dependency on the Froude number. A model for the particle motion was developed by solving the Lagrangian equation numerically. Two approaches for computing the trajectory of the sandbags were investigated. The results showed that the approach in which the drag coefficient was varied based on the orientation of the particle gave better results than if the drag coefficient was kept constant and was based on the broadside orientation of the particle.

The turbulent characteristics in an open channel using the PIV method were measured by Pechlivanidis et al. (2012). This method assumed that the particles of a fluid faithfully follow the flow dynamics, hence the motion of these seeding particles were used to calculate velocity information of the flow. The experiments were conducted for both impermeable and permeable beds in a channel of 6.5m length, 7.5 cm width and 25 cm height. Two grass-like vegetation types of different height (2 and 6 cm) were used to represent permeable beds. Hydraulic characteristics such as distributions of velocities, turbulent intensities and Reynolds stress were investigated at a fine resolution using the PIV. Velocity was measured above the vegetation at different heights. Results showed that, velocity over the vegetation region was a function of the vegetation height and the total flow depth; velocity decreases as the vegetation height increases. In addition, velocities above the vegetation region were much lower than velocities above an impermeable bed. This was due to the turbulent shear stresses and the existence of turbulence in the vegetation region, which reduced the mean velocity above the vegetation region.

In order to derive guidelines to account for bed degradation in the design of rock protection at circular piers under currents a laboratory experiments was conducted by Desonneville, B. et al (2012). The analysis focused on the successive failure stages, the redistribution of stones over the slope and the evolution in time. The results showed that, as the undermining progressed, the stones at the edges of the protection were redistributed through a combination of rolling, sliding and sinking. Finally, a protective mound was formed, with stones covering the slopes on all sides. The observed stone layer thickness on the slopes gradually reduced towards the outside. A design rule was derived to account for bed degradation by quantifying the stone volume required for a falling apron.

Recking and Pitlick (2013) compared two equations (Shields and the Isbash equations) for predicting the stability of rocks exposed to a turbulent flow were both proposed in 1936, and since then, both equations have been used widely in the analysis of transport thresholds for coarse sediment. These two equations were obtained using two very different approaches, but as demonstrated in this paper, the equation developed by Isbash was consistent with the relation formulated by Shields for predicting the motion of sediments either in the flume or in the field. Comparison of the two equations suggests that standard approaches tend to oversize riprap in mountain streams.

### 2.6 Settling distance relationship

Most of the river bank toe protection structures are usually constructed in underwater condition. In such condition, the placement of toe protection elements at designated location is a difficult task. Placement of protection elements is mainly governed by its settling behavior and incipient condition under various hydraulic conditions. Hydrodynamic characteristics, especially the settling behavior of geobags and blocks, are of practical significance particularly for the construction of toe of a revetment. Study related to these hydrodynamic characteristics is very scarce in literature. Raju (2011) carried out an experimental study on settling behavior and suggested the following relationship for the prediction of settling distance of toe protection elements.

$$\frac{S}{h} = 1.49\left(\frac{u}{w}\right)^{1.06} \tag{2.1}$$

Where, S = Horizontal settling distance, h =flow depth, u= depth-averaged velocity, w =fall velocity of the protection element.

In this equation, fall velocity (w) can be substituted using equation (2.2) for CC block and equation (2.3) for geobags as presented in Raju and Matin (2013).

$$w = 3.965\,\frac{\nu}{d}\,d_*^{1.33} \tag{2.2}$$

$$w = 6.124\,\frac{\nu}{d}\,d_*^{1.21} \tag{2.3}$$

In which, $\nu$ = kinematic viscosity of the water; d= protection element (CC block and geobag) diameter and $d_*$ = dimensionless particle (protection element) diameter.

### 2.7 Incipient condition of protection element

Incipient motion of particles on a river bed can, in principle, be understood and predicted from a balance of the forces acting on the particles. Prediction of the forces acting on streambed particles is important for investigating the morphological evolution of river beds and constructing adequate bed and bank protection near weirs, spillways or other structures (Vollmer and Kleinhans, 2007). Incipient motion has been studied extensively over the past 60 years following the work by Shields (1936) who presented a semi empirical approach to incipient motion. Much of the subsequent research into incipient motion builds on the original work of Shields. Reviews and extensions of the Shields diagram have been undertaken by several authors e.g., White 1970; Mantz 1977; Miller et al. 1977, while only limited comparisons of Shields method against alternative methods for predicting incipient motion have been presented previously Marsh et al (2004).

The Shields (1936) method does not explicitly predict incipient motion of protection elements, but was presented as a non dimensional framework for comparing experimental results of protection elements with bed material. The well-known Shields curve is essentially an empirical result where a line of best fit has been applied to the scattered experimental data. Some of the same variables are present on both the x and y axes of the Shields curve (Equation 2.4 and 2.5) hence an iterative approach is needed for predicting incipient motion values. Here the particle shear Reynolds number ($R_{e*}$) values calculated from experimental data to predict a dimensionless shear stress ($\tau_*$) value from the Shields diagram (Figure 2.10)

$$R_{e*} = \frac{u_* d}{\nu} \tag{2.4}$$

$$\tau_* = \frac{\tau}{\Delta\rho\, gd} \tag{2.5}$$

Where $u_*$ = shear velocity (m/s) ($u_* = \sqrt{\tau/\rho}$, or $\sqrt{gRS}$); d = particle diameter (m); $\nu$ = kinematic viscosity of the water ($m^2/s$); $\Delta$ = relative density =( $\rho_s - \rho$)/ $\rho$ ; $\rho$ = density of fluid (1000 $kg/m^3$) ; $\rho_s$ = density of particle ($kg/m^3$); g=acceleration due to gravity ($m/s^2$); $\tau$ = average shear stress at the point of sediment motion (Pa), where the average shear stress $\tau$ is a function of the hydraulic radius (*R*) and water surface slope (*S*) ($\tau = \rho g R S$).

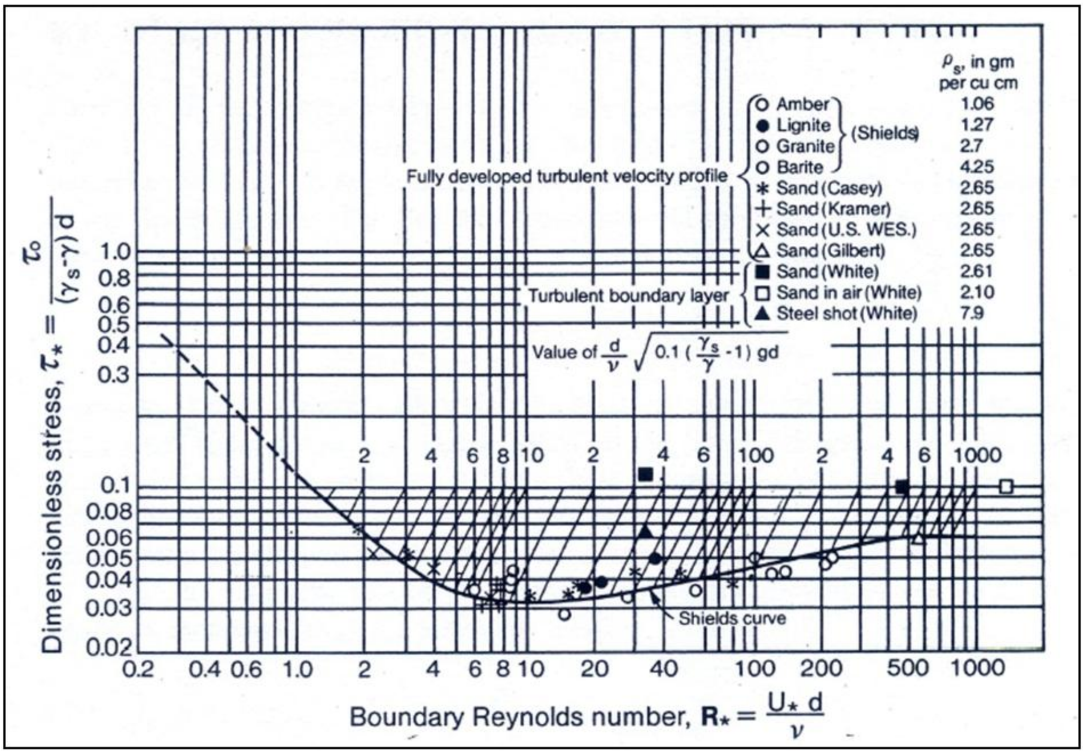


**Figure 2.10**: Shield's diagram for incipient motion (Source: Chang, 1988)

Incipient Motion, in the context of sediment transport in rivers, is that critical point at which sediment particles on the solid boundaries of the river flow (e.g. the bed or banks of a river) begin to move. From a theoretical point of view, if the fluid forces are below that required for the motion of a particle, there will not be any movement. If they are greater than that required for motion, there will be movement. The boundary between the two may be described as 'incipient' motion i.e. the particle is about to move (Armitage and Rooseboom, 2010).

### 2.7.1 Shear velocity equations

The theoretical investigations of Prandtl and Karman, and the experimental work of Nikuradse, have led to rational formulas for velocity distribution and hydraulic resistance for turbulent flow in circular pipes. With certain assumptions regarding the effects of secondary currents and of the free surface, and with the adoption of the hydraulic radius as the characteristic length, similar rational formulas were deduced by Keulegan (1938) for open channels. The hydraulic effect of roughness elements of arbitrary shape and of arbitrary distribution can be described very conveniently by comparing it with the effect of a rough surface consisting of closely packed sand grains of the type used by Nikuradse in his studies of rough pipes. Such a comparison leads to the concept of equivalent sand roughness. The size of sand grains as a measure of roughness was first suggested and used by von Karman as cited in Keulegan (1938). The basis of the comparison is the similarity of velocity distribution near a rough surface. In general according to Keulegan (1938),

$$\frac{u}{u_*} = a_{r0} + 5.75 \log\left(\frac{h}{k}\right) \quad (2.6)$$

where k is a roughness height. In Nikuradse's results $a_{r0}$ was found to have the value 8.5, so that

$$\frac{u}{u_*} = 8.5 + 5.75 \log\left(\frac{h}{k_s}\right) \quad (2.7)$$

where $k_s$ is the size of the closely packed sand grains. Eliminating $u/u_*$ between these two equations,

$$5.75 \log k_s = 8.5 - a_{r0} + 5.75 \log k \quad (2.8)$$

This is the expression which gives the equivalent sand roughness $k_s$ for the particular roughness k. Physically, if a velocity, u is observed at a point distant, h from a wall of an arbitrary roughness, k under a known shear, the same velocity will be obtained at the same point and for the same shear if the particular roughness is replaced by sand grains of size $d_{50}$ as given by equation 2.6.

An advantage of this procedure is that it is not necessary to make a geometrical specification of roughness in any given case for the purpose of description. With $d_{50}$ known, the expression for the mean flow in rough channels by Keulegan (1938) obtained as

$$\frac{u}{u_*} = 6.25 + 5.75 \log\left(\frac{R}{d_{50}}\right) \quad (2.9)$$

If Manning’s equation is used instead of Keulegan’s equation with Manning’s n in terms of a Strickler-type expression, then the critical velocity for a wide channel can be expressed as cited by Helbar and Farhoudi (2008) is

$$\frac{u}{u_*} = 7.66 \left(\frac{h}{d_{50}}\right)^{1/6} \quad (2.10)$$

Melville (1988) presented a design method for the estimation of equilibrium depths of local scour at bridge piers. Scour at clear-water condition becomes a special case, as does scour of uniform material, a rare event in practice.

At live-bed condition, scour introduces two further processes. Threshold or critical flow conditions became significance and were described by the mean flow velocity, u appropriate for the stated sediment and channel slope. Of equal importance were the flow conditions beyond which armoring of the channel bed was impossible. They were also characterized by the mean flow velocity, which again depends on the sediment characteristics and channel slope. Threshold and limiting armor conditions were discussed first. The general framework for scour estimation was then presented, and the effect of the significant parameters was described.

The Shields diagram remains the most effective way of determining threshold conditions for uniform sediments. For given fluid density and viscosity and sediment density, the Shields diagram can be used to obtain a plot of shear velocity against grain size. In Melville (1988) a useful relation for the coarser grain sizes $d_{50} > 6$ mm is found as

$$u_{*_c} = 0.03\, d_{50}^{\frac{1}{2}} \tag{2.11}$$

where $u_{*_c}$ is in m/s, and $d_{50}$ in mm. Threshold shear velocity was converted to threshold mean flow velocity, u using, as an approximation, the logarithmic form of the velocity profile by Melville (1988),

$$\frac{u}{u_*} = 5.75 \log\left(\frac{5.53\, h}{d_{50}}\right) \tag{2.12}$$

Where, h = flow depth. For uniform sediments, u marks the transition from clear-water to live-bed conditions scour.

### 2.7.2 Depth averaged velocity equations

During the decades of research in this area, numerous investigators have defined incipient motion in different ways. The present study focuses on the incipient motion of toe protection elements. Incipient motion commences when the attacking forces exceed the resisting forces (Vollmer and Kleinhans, 2007).

The earliest studies were related to critical velocities of stones (Brahms, 1753 and Sternberg, 1875). They studied the critical near bed velocity and found that it was related to the particle diameter, as follows:

$$u_{oc}^2 \sim d_s \tag{2.13}$$

in which $u_{oc}$ is the fluid velocity near the bed under critical conditions. Rubey (1948) found that the near bed velocity is, however, not very well defined and it is preferable to use the critical depth averaged velocity, u as the characteristic parameter.

Neill (1967), on the basis of experiments with natural gravels, glass spheres and low-density spheres, proposed a relationship of incipient depth averaged velocity designed to just maintain stability of stones on a flat bed, cited by Parola (1993),

$$\frac{\rho u^2}{(\gamma_s-\gamma)d_{50}} = 2.5\left(\frac{d_{50}}{h}\right)^{-0.2} \tag{2.14}$$

Where $d_{50}$ = median size of stone; u = depth averaged flow velocity; g = gravitational acceleration; and h = depth of flow.

The use of stones for scour protection has a long tradition in both river and coastal engineering. Breusers et al. (1977) recommended using boulders with a critical entrainment velocity, u, of twice the extreme flood velocity around the pier. This was because scouring at bridge piers starts at approximately half of velocity, u in normal flow conditions. In other words, when the approach velocity is less than 0.5u of the bed sediment, scouring will not occur. Based on this understanding, the Isbash (1935) formula can be used to estimate the incipient velocity of the protection (Chiew, 1992).

$$u = 0.85(2g\Delta d)^{\frac{1}{2}} \tag{2.15}$$

Inglis (1921) proposed a relationship for incipient motion of a single layer of stones on a flat bed on the basis of small scale experiments as:

$$\frac{\rho u^2}{(\gamma_s-\gamma)d_{50}} = 2.29\left(\frac{d_{50}}{h}\right)^{-0.23} \tag{2.16}$$

Maynord (1989), on the basis of more extensive experiments at larger scales, presented a relationship for incipient movement of riprap on a flat bed or on side slopes of 1V:2H or flatter that can be arranged as follows:

$$\frac{\rho u^2}{(\gamma_s - \gamma) d_{30}} = 2.62 \left(\frac{d_{30}}{h}\right)^{-0.2} \tag{2.17}$$

Where $d_{30}$ = riprap size for which 30% is finer by weight.

### 2.7.3 Turbulent fluctuations

According to Lamb et al. (2008), many studies have shown that the local average velocity, u is not the only relevant velocity scale in determining sediment mobility and, in addition, the fluctuations due to turbulence should be considered (e.g., Grass,1970; Wu and Yang, 2004; Hofland et al., 2005; Cheng, 2006; Vollmer and Kleinhans, 2007). The critical condition for initial sediment motion could be overestimated if the Shields diagram was applied for the condition of flows with high turbulence intensities (Cheng, 2006).

The intensity of turbulent fluctuations (i.e., $\sigma_u / u_*$, where $\sigma_u$ is the root-mean square of stream-wise velocity varies with height above the bed and has a peak value near the bed in hydraulically smooth flow, or near the top of the roughness elements in hydraulically rough flow ( Nikora and Goring, 2000).

Figure 2.11 shows a compilation of $\sigma_{u,max}/u_*$ for a wide range of relative roughness (Lamb et al., 2008). The resultant data clearly shows that the peak value in the turbulence intensity increases with decreasing relative roughness $k_s/h$.

The trend of increasing $\sigma_u$,max/$u_*$ with decreasing $k_s/h$ in this figure is significant despite the fact that the data cover a wide range of roughness types including boulders and gravel in natural streams (Nikora and Goring, 2000).

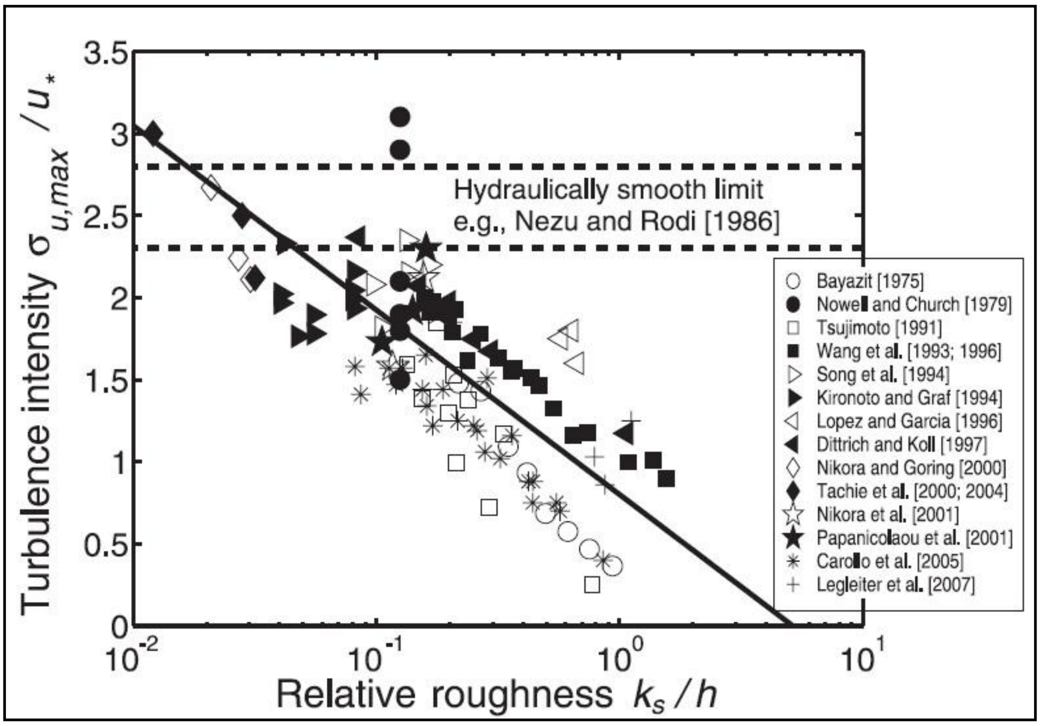


**Figure 2.11:** Near-bed peak turbulence intensity versus relative roughness (Source: Lamb et al. (2008)

On the basis of the evidence for scaling of turbulent sweeps to the outer-flow variables, Lamb et al. (2008) considered that turbulence intensity also should scale with the depth averaged flow velocity, u which in turn is a function of relative roughness. They therefore proposed that

$$\frac{\sigma_{u,max}}{u_*} = \alpha_2 \frac{u}{u_*} \qquad (2.18)$$

where $\alpha_2$ is a constant of proportionality between the depth averaged velocity and the peak near-bed turbulence intensity.

Many formulas have been proposed for the depth averaged flow velocity of rivers and streams. One of the most widely used is that of Bathurst (1985),

$$\frac{u}{u_*} = 5.62 \log\left(\frac{h}{k_s}\right) + 4 \qquad (2.19)$$

Combining equations (2.18) and (2.19) results in a semi empirical model for the peak turbulence intensity

$$\frac{\sigma_{u,max}}{u_*} = \alpha_2 \left[5.62 \log\left(\frac{h}{k_s}\right) + 4\right] \qquad (2.20)$$

Where, based on a best fit with data in Figure 2.11, $\alpha_2 = 0.2$. Thus the peak turbulent fluctuations are typically 20% of the depth-averaged velocity, and decrease with increasing relative roughness.

The model indicated that turbulent fluctuations affect incipient motion significantly. Fluctuations increase the drag and lift forces on the particle, so that mobility is increased.

# CHAPTER THREE

# THEORETICAL CONSIDERATIONS AND METHODOLOGY

## 3.1 Introduction

Inception of motion is a critical condition that involves many measurable and non-measurable factors. Dimensional analysis is a useful method to obtain a functional relationship between these variables. The variables defining the flow characteristics are include the depth-averaged velocity of the flow, u; shear velocity, $u_*$; the depth of flow section, h; the channel width, B; the slope of the channel, S and the gravitational acceleration, g. The properties of the fluid are its density, ρ and the kinematic viscosity, ν. The variables related to the properties of the protection elements are their shape, size and their density, $\rho_s$. The theoretical knowledge gained from the analysis of various parameters will be investigated in laboratory experiment.

## 3.2 Analysis of incipient condition based on shear velocity

Under critical conditions, also, the particle is about to move by rolling about its point of support. The gravitational force or submerged weight force is given by

$$F_g = c_1 g \left(\rho_s - \rho\right) d_n^3 \tag{3.1}$$

In which $\rho =$ density of fluid, $\rho_s$ = density of particle, g = acceleration due to gravity and $c_1 d_n^3$ = the volume of the particle where $c_1$ is a constant; $d_n$ = nominal diameter of the particle defined as the diameter of a sphere having the same volume and mass as the measured particle. It can be calculated as:

$$d_n = \left(\frac{6V}{\pi}\right)^{1/3} = \left(d_l\, d_w\, d_t\right)^{1/3} \tag{3.2}$$

where, V = original volume of the particle; dl, dw, and dt are the respective length, width and thickness of the particle.

The critical drag force is

$$F_D = c_2 \tau_c\, d_n^2 \tag{3.3}$$

here $c_2$ is a constant; $c_2 d_n^2$ = the effective surface area of the particle exposed to the critical shear stress, $\tau_c$.

Equating moments of the gravitational force and drag force about the support yields:

$$F_g\, a_1 \sin(\theta - \phi) = F_D\, a_2 \cos\theta$$

$$\text{Or, } c_1 g\left(\rho_s - \rho\right) d_n^3\, a_1 \sin(\theta - \phi) = c_2 \tau_c d_n^2\, a_2 \cos\theta$$

$$\text{or, } \tau_c = \frac{c_1 a_1}{c_2 a_2} g\left(\rho_s - \rho\right) d_n \cos\phi\ (\tan\theta - \tan\phi) \tag{3.4}$$

For a horizontal bed, $\phi = 0$, and Equation (3.4) becomes:

$$\tau_c = \frac{c_1 a_1}{c_2 a_2} g\left(\rho_s - \rho\right) d_n \tan\theta \tag{3.5}$$

When $a_1$ and $a_2$ are equal the forces on the particle act through its center of gravity and the fluid forces are caused predominantly by pressure. Also, when $a_1$ and $a_2$ are equal it will be seen that the ratio of the forces on the particle parallel to the bed i.e. hydrodynamic force, to those acting normal to the bed i.e. immersed weight, is equal to tan $\theta$, resulting Equation (3.5) as:

$$\frac{\tau_c}{g\,(\rho_s - \rho) d_n} = c \tan\theta \tag{3.6}$$

The left-hand side of equation (3.6) represents the ratio of two opposing forces: hydrodynamic force and immersed weight, which governs the initiation of motion.

Major variables that affect the incipient motion of a particle through a fluid include $\tau_c$, $d_n$ , $\rho_s$, $\rho$ and $\nu$.

From dimensional analysis they may be grouped into the following dimensionless parameters

$$f\left(\frac{\sqrt{(\tau_c/\rho)}}{\nu}, \frac{\rho W'}{\mu^2}\right) = 0 \tag{3.7}$$

in which $u_{*c} = \sqrt{(\tau_c/\rho)}$ is the critical friction velocity or the critical shear velocity, $W' = g\,(\rho_s - \rho) d_n{}^3$ is the submerged weight.

again, $u_*$ = shear velocity = $\sqrt{(\tau/\rho)}$ ; $\tau_c$ = average shear stress at the point of particle motion, where $\tau$ is the average shear stress is a function of the hydraulic radius (R) and slope of the energy line (S) ($\tau = \rho gRS$).

Thus (3.7) becomes

$$f\left(\frac{u_* d_n}{\nu}, d_n\left(\frac{\Delta g}{\nu^2}\right)^{1/3}\right) = 0 \quad (3.8)$$

Using particle shear Reynolds number or boundary Reynolds number, $R_{e*}$ as

$$R_{e*} = \left(\frac{u_* d_n}{\nu}\right) \quad (3.9)$$

and the dimensionless particle diameter, $d_*$ defined as

$$d_* = d_n\left(\frac{\Delta g}{\nu^2}\right)^{1/3} \quad (3.10)$$

The first and second non-dimensional term of equation (3.8) can be replaced by boundary Reynolds number ($R_{e*}$) defined in equation (3.9) and dimensionless particle diameter ($d_*$) defined in equation (3.10).

Inserting $d_*$ and $R_{e*}$ into equation (3.8) results in:

$$R_{e*} = f(d_*) \quad (3.11)$$

### 3.3 Analysis of incipient condition based on depth-averaged velocity

At incipient condition of toe protection elements i.e. when a protection element is about to move, the following dynamic similarity law must be true,

$$\frac{\tau_c}{g\,(\rho_s - \rho) d_n} = \frac{u_{*c} d_n}{\nu} \quad (3.12)$$

in which $u_{*c} = \sqrt{(\tau_c/\rho)}$. Shields determined equation (3.12) experimentally. A drawback of the Shields diagram is that the shear velocity appears on both axes. It has been argued by some investigators (Yalin, 1972; Yang, 1973) that the use of critical shear velocity, $u_{*c}$ and bottom shear stress, $\tau_c$ on both the abscissa and ordinate of the Shields curve (as dependent and independent variables, respectively) can present difficulties in interpretation, since they are interchangeable (Source: Beheshti, and Ashtiani, 2008).

In order to avoid trial and error solutions, alternative parameters are proposed in equation (3.10) allowing direct computation of the critical shear velocity by equation (3.11).

Neill and Hey (1982) have noted that many engineers prefer design procedures based on velocity. The appropriate velocity for use in the toe protection design procedure must be determined. The velocity used must be representative of flow conditions at the riprap and must be able to be determined by the designer by relatively simple methods. Average channel velocity can usually be determined but is not representative of conditions at the rock surface because of the wide diversity of channel shapes. Some form of local velocity must be used to account for the differences in channel shape. Local bottom velocity is the most representative velocity but is difficult for the designer to predict. Local average velocity, also called depth-averaged velocity, is representative of flow conditions at the point of interest and can be estimated by the designer.

In this study an attempt has been made to predict critical shear velocity through a simple relationship as in (3.11). To determine the incipient velocity of protection elements, first the critical shear velocity along with flow depth (h) at different incipient condition were observed. Having the values of shear velocity, $u_*$ and depth of flow, h the values of depth averaged velocity, u can be determined by using following dimensionless relationship:

$$\frac{u}{u_*} = f\left(\frac{h}{d}\right) \qquad (3.13)$$

Where $d = d_n$ = nominal diameter of the particle.

### 3.4 Analysis of depth factor for the design of protection elements

The design of the recommended falling apron is motivated by construction constraints. Different methods regarding calculations of unit dimensions of revetment cover layers and toe protections (e.g. PIANC, 1987; Pilarczyk, 1990; FAP 21, 1993) show only marginal deviations within the range of application for the rivers of Bangladesh. Hence, the widely used Pilarczyk method includes the turbulence intensity, velocity, shear stress and depth factor to determine the nominal thickness of a protection unit. With the flow velocity well known, or can be calculated reasonably accurately, Pilarczyk's relation (1990) is applicable. The general formula for the design against current loads is:

$$D_n \geq \frac{0.035\, u^2}{2g\Delta} \frac{\phi_{sc}\; K_\tau\; K_h}{K_s\; \Psi_{cr}} \tag{3.14}$$

Here, Dn = nominal thickness of protection unit, m; u = depth averaged flow velocity, m/s; $\phi_{sc}$ =stability factor (0.8 for CC blocks, cubical shape, randomly placed in multi layer; 0.5 for geobags); $K_\tau$ = turbulence factor (2 for CC blocks, 1 for geobags as high turbulence, local disturbances); $\Delta$ = relative density =( $\rho_s - \rho$ )/ $\rho$ ; $K_s$ = slope reduction factor = $\sqrt{(1-\sin^2 \alpha / \sin^2 \theta)}$ = 0.72, $\alpha$ = slope angle = $26.57^0$ (for 1V:2H), $\theta$ = angle of repose ( $40^0$ for blocks, $30^0$ for geobags); $\Psi_{cr}$ = critical value of dimensionless shear stress (0.035 for CC blocks, 0.05 for geobags); $K_h$ = depth factor.

With the depth factor, $K_{h,}$ the water depth, h is taken into account, which is necessary to convert the depth averaged flow velocity into the flow velocity just above the protection. The depth parameter also depends on the measure of development of the flow profile and the roughness of the protection. In a river, the turbulent boundary layer may never be fully developed because the depth of flow simply is not great enough (Hickin, 2004). Logarithmic velocity profiles exist for long stretches with constant bed roughness. For most engineering works as bottom protection or slope protection, the non developed velocity profile is usually present.

The following formulas for depth factor, $K_h$ are recommended by Pilarczyk, 2008:

For fully developed velocity profile:

$$K_h = 2.\, [\log (1+\frac{12h}{k_s})]^{-2}$$

Non-developed velocity profile:

$$K_h = (1+\frac{h}{k_s})]^{-0.2}$$

Where $k_s$ = size of block mats and thickness of bags.

Thus depth factor ($K_h$) becomes:

$$K_h = f\left(\frac{h}{d}\right) \quad (3.15)$$

### 3.5 Analysis of turbulent intensity

Turbulence intensity is an important physical quantity for turbulent flow. Turbulence intensity, u′, is defined by the corresponding fluctuating velocity as

$$\text{r.m.s } u' = \sqrt{\overline{u'^2}} \quad (3.16)$$

Otherwise, in analyzing turbulence intensity, many scholars prefer the relative turbulence intensity,

$$\mathcal{I} = \left(\sqrt{\overline{u'^2}}\right)/u \quad (3.17)$$

Many studies have shown that the local average velocity, u is not the only relevant velocity scale in determining sediment mobility and, in addition, the fluctuations due to turbulence should be considered (e.g., Grass, 1970; Wu and Yang, 2004; Hofland et al., 2005; Cheng, 2006; Vollmer and Kleinhans, 2007).

The intensity of turbulent fluctuations varies with height above the bed and has a peak value near the bed in hydraulically smooth flow, or near the top of the roughness elements in hydraulically rough flow (Nikora and Goring, 2000). The turbulence intensity is a function of relative roughness (d/h). The turbulent fluctuations affect incipient motion significantly. Fluctuations increase the drag and lift forces on the particle, so that mobility is increased (Lamb et al. 2008).

Incipient condition of the toe protection element is observed when turbulent fluctuations act to increase the local velocity around the elements above the average velocity. These downstream directed turbulent fluctuations, therefore, are included in this study.

Having the values of $u_*$ and h the values of turbulence intensity can be determined by using following dimensionless relationship:

$$\frac{\text{r.m.s } u'}{u_*} = f\left(\frac{h}{d}\right) \quad (3.18)$$

### 3.6 Methodology

The study has been carried out according to following steps of activities:

(i) Theoretical analysis of governing parameters

(ii) Design of experiments

(iii) Test scenarios and experimental run

(iv) Measurements and observations

(v) Analysis of data and development of equations

(vi) Predictive performance of proposed equation and comparison with others

The stepwise methodology can be better explained in a flow diagram as shown in Figure 3.1.

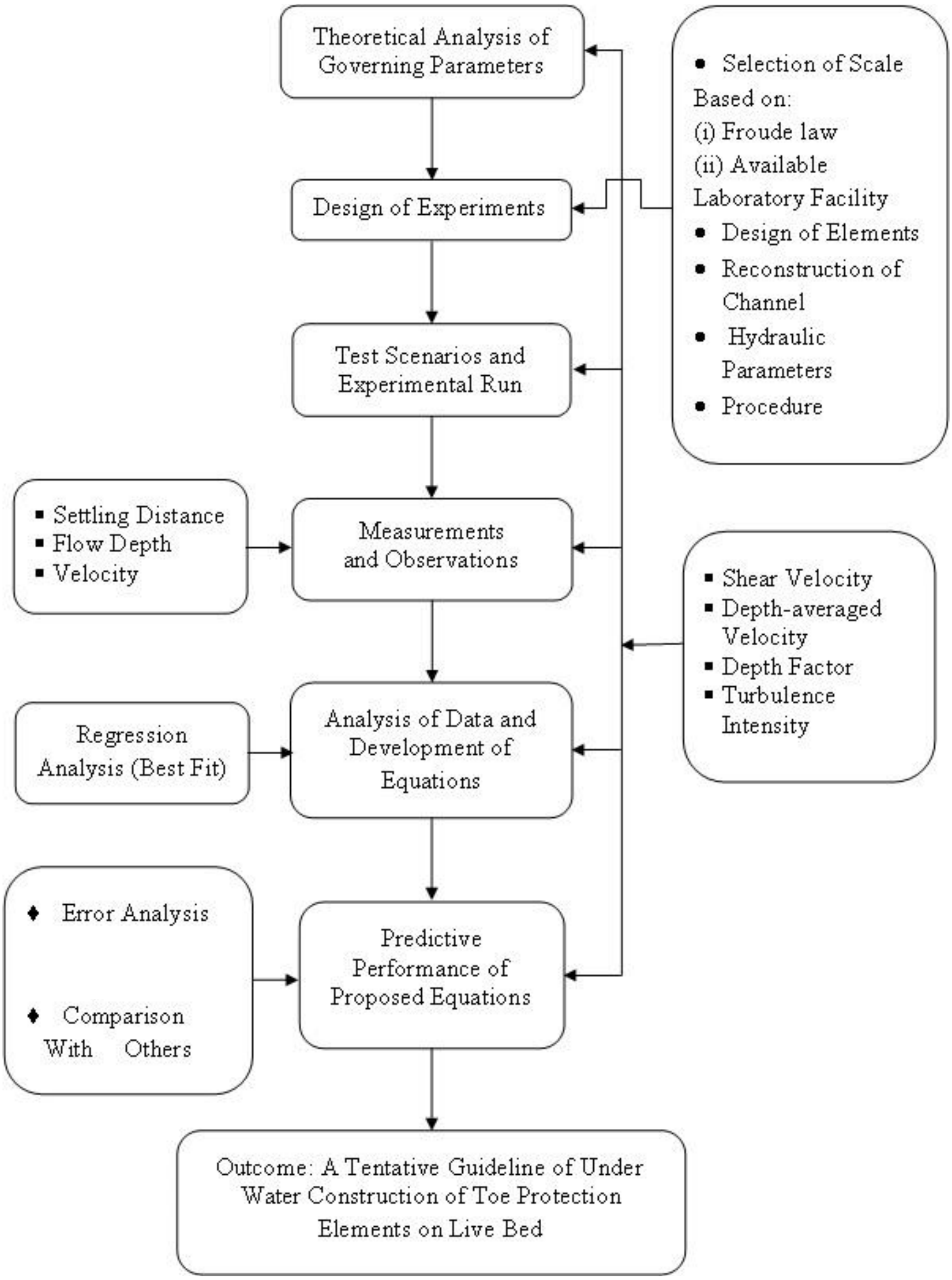


**Figure 3.1:** Flow diagram of methodology of the study

# CHAPTER FOUR

# EXPERIMENTAL SETUP AND OBSERVATION

## 4.1 Introduction

This chapter describes the detailed experimental setup, experimental procedure and data collection techniques. A brief description of the observations during experimentation is also presented here.

## 4.2 Reconstruction of laboratory channel

To carry out the experimental study of falling apron, the existing rigid bed channel made of concrete situated in the Hydraulics and River Engineering Laboratory of the Water Resources Engineering Department (DWRE) of the Bangladesh University of Engineering and Technology (BUET), Dhaka was utilized. However to fulfill the requirements as set in the objectives, a number of modifications in the test facility was required.

### Sand bed preparation

A 20-cm thick layer of sand was distributed evenly on the channel bottom. Figure 4.1 shows the prepared sand bed channel.

**Figure 4.1:** Sand bed channel at Hydraulics and River Engineering Laboratory, DWRE, BUET

The bed material used was fine sand. The grain size distribution is shown in Figure 4.2.


**Figure 4.2:** Grain size distribution of bed material

### 4.3 Experimental setup

The experimental setup consists of two separate parts; the experimental reach and experimental facilities. The experimental facilities are necessary for the storage and regulation of the water, circulating through the model and act as guiding part. The experimental reach contains the actual experimental model of a river. Schematic diagram of flow circulation system in the experimental setup is shown in Figure 4.3.

#### 4.3.1 Experimental reach

The test section is selected in the experimental reach of the setup. The experimental reach is a sand bed trapezoidal channel of length about 12.75 meters, bottom width 0.60 m, top width 1m and height 0.4m. The right bank of the channel is vertical and left bank is sloping with 1:1 slope. Figure 4.4 is showing the dimensions of experimental reach.

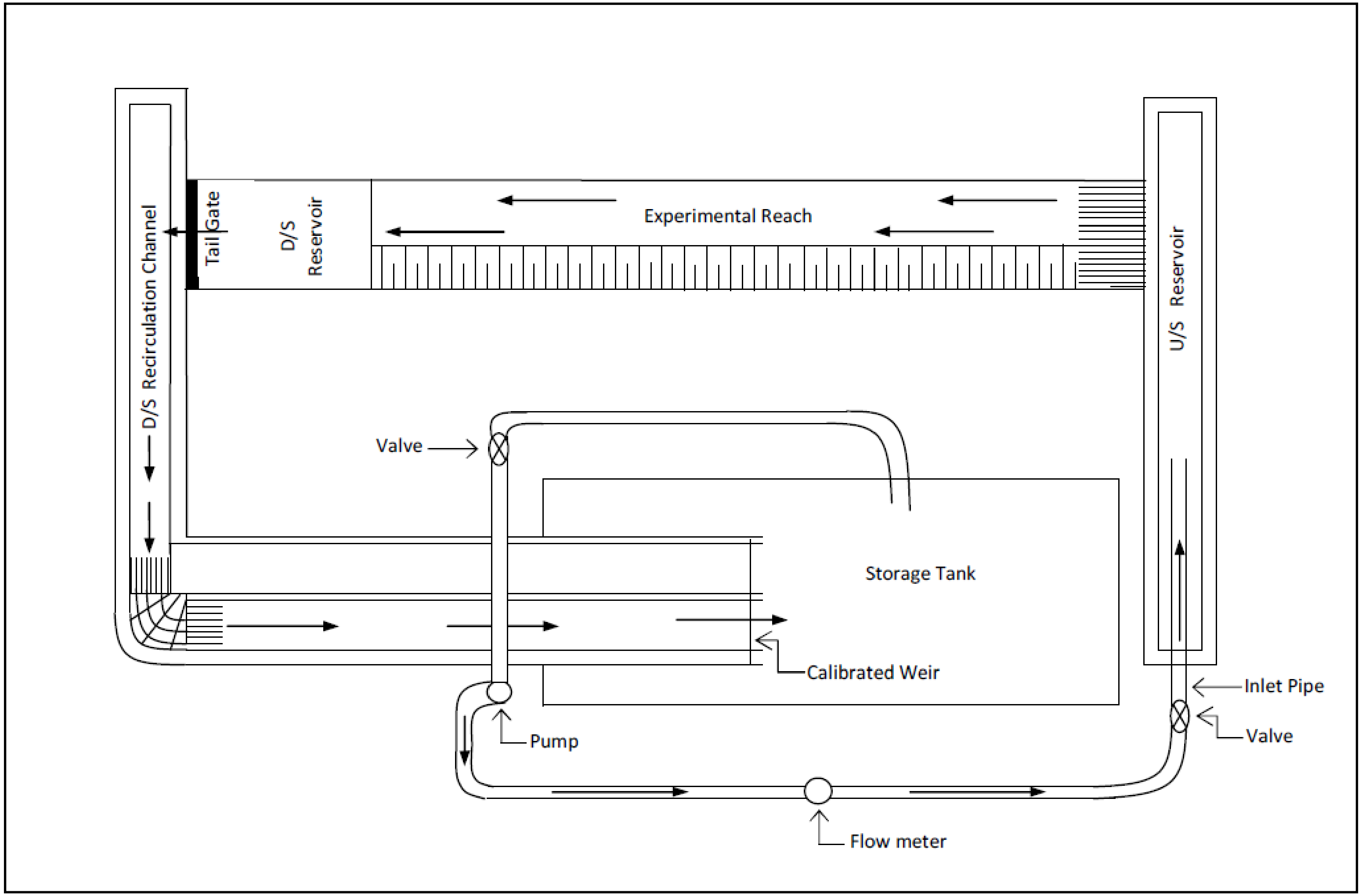


**Figure 4.3:** Schematic diagram of flow circulation system in experimental setup

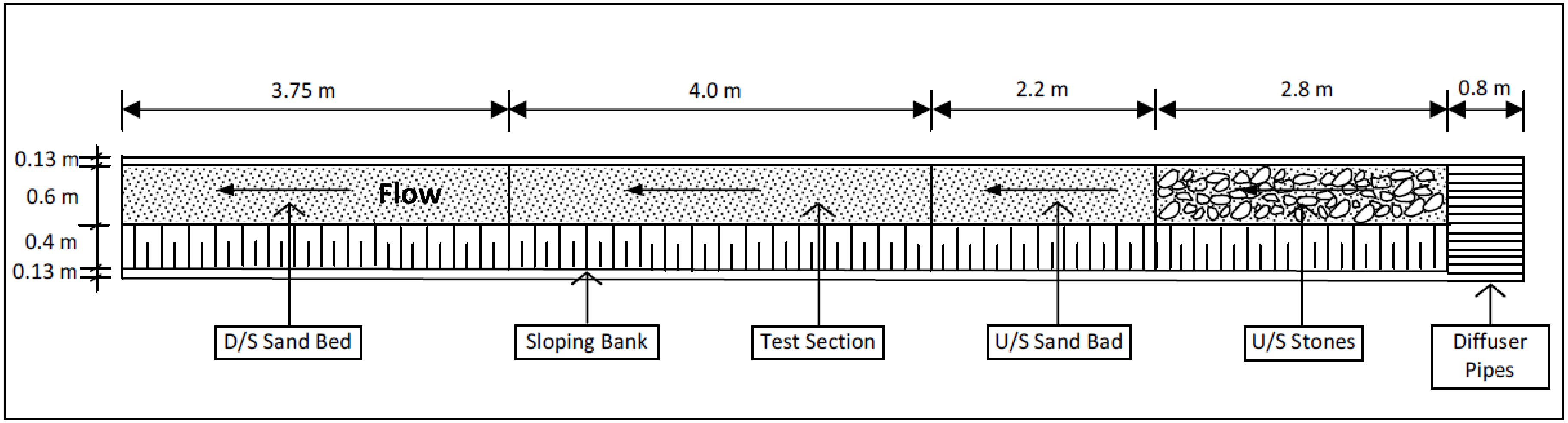


**Figure 4.4**: Dimensions of experimental reach

**Inflow zone**

An inflow section and an inflow branch of considerable length are needed to ensure stable flow conditions before the water reaches the test section. Water flows from the upstream reservoir to main channel via the inflow section. PVC tubes (D=2.7cm; L= 40 cm) are placed over the width of the entrance to get rid of the larger eddies present in the water coming from the upstream reservoir and thus the flow is stabilized. Just after the PVC tubes, about 2.8 m of the sand bed is filled with stone to ensure uniform flow in the test section (Figure 4.5).

**Figure 4.5**： Diffuser pipes and upstream stone bed

**Test Section**

The test section in the experimental reach of the setup is selected based on two considerations. Firstly, water approaching towards the channel from upstream reservoir, becomes stabilized within inflow zone. Thus, before reaching the test section the flow becomes uniform. Secondly, within the test section there should be no backwater effect from downstream of the test section. The test section has been selected based on numbers of trial run when the uniform flow achieved and no backwater effect in the reach was found.

**Outflow section**

At the downstream end of the model, the water in the channel flows over a tail gate into the experimental facilities of the model.

### 4.3.2 Experimental facilities

The experimental facilities are usually the permanent part of the setup. It acts as a facility to conduct all types of experiment in the channel reach. The components of the experimental facilities are briefly described below.

#### Downstream reservoir

The downstream reservoir (Figure 4.6) serves as storage reservoir with a volume of $1.5m^3$. The maximum water level can be at 0.77m elevation with respect to reservoir bottom. The tank had to be cleaned and emptied every week.

**Figure 4.6**: Downstream reservoir

The fine particles of the sediment deposited at the bottom have been removed through a valve placed at the lowest level of overflowing portion.

#### Pump

The circulating pump near the measuring flume draws water from the downstream reservoir (Figure 4.7). The pump has a maximum delivery of up to 90 cusec and head of 7m.

## Pipe line

The rate of water flow was controlled by the pipe line system (Figure 4.7). The pump sucks the water from the downstream reservoir into the pipe line. The T-joint on top of the pump divide the water over the excess pipe and the delivery or supply pipes, depending on the regulation of the valves in the respective pipes. As the pump delivers a constant discharge, the required discharge through the model must be regulated by these valves.

**Figure 4.7:** Pump and pipe line

## Upstream reservoir

The pump draws water from the downstream reservoir and discharges into the upstream reservoir through the pipe line system. The volume of the upstream reservoir is 4.8 $m^3$. The maximum water depth in the upstream reservoir can be 1.25 m. It has two chambers; one big and other is small. Water is dropped into the small chamber of the reservoir from the delivery pipe line. The main purpose of making the small chamber is to dampen the turbulence in the water. This small chamber is separated by a wall (with a number of openings in it) from the large chamber of the upstream reservoir. This is done to create a smooth inflow into the main channel. In this way, the disturbance was removed. For maintenance purpose, the upstream reservoir can be emptied through a small regulated opening placed at the lower level of the reservoir wall. This also acts as a storage reservoir.

### Regulating and measuring system

The regulating and measuring system of the model consists of the following:

### Tail gate

The downstream end of the channels the tail gate is placed (Figure 4.8). The tail gate is made of cast iron and surrounded by rubber flaps, so that water flows only over the gates. A wheel attached to the gate helps to rotate it up and down and thereby performs the downstream regulation. For a particular discharge, if the tailgate is raised it increases the water level and vice versa.

**Figure 4.8**: Tail gate

### Stilling basin and transition flumes

Behind the tail gate, water falls into a stilling basin. The width of the transition flume is equal to the width of the approach channel which is 0.50 m. Besides, transporting water to the measuring part of the permanent facility, the stilling basin as well as the transition flumes helps destroy turbulence.

**Figure 4.9:** Stilling basin and transition flumes

**Guiding vanes and tubes**

To ensure a more smooth flow towards the approach channels, guiding vanes are placed between the transition flumes and the approach channels which are at right angle to each other. These vanes guide the water around the corner. In order to prevent creation of extra unwanted turbulence in the approach channels, PVC tubes (diffuser pipes) are used on both the upstream and downstream side of the guiding vanes (Figure 4.10).

**Figure 4.10**: Guiding vanes and tubes

### Approach channels

The water flows over the tail gate into the stilling basin before entering the approach channel. The approach channel is 5.27 m long and 0.50 m wide. The approach channel is designed according to ISO standards, thus avoiding an extra cumbersome calibration. These standards can be found in the ISO standard Handbook 16, ISO 1438-1975 (E). The approach channel should have a minimum length of ten times the width of the channel and must be straight and must have smooth walls, all these conditions are fulfilled here.

**Figure 4.11:** Approach channels

### Electromagnetic flow meter

Discharge measurements are taken from the electromagnetic flow meter in the unit of $m^3/h$. The flow meter is 200 mm diameter. The flow through the pipe is controlled by the valve. Figure 4.12 shows an electromagnetic flow meter.

**Figure 4.12:** Flow meter

**Valves**

The flow in the channel is controlled with the help of two valves, one in the delivery pipe and another in the excess discharge pipe. When more discharge is required in the channel, the valve in the delivery pipe line had to be opened and the other valve had to be closed accordingly. In this way, flow of water is controlled in the channel. Figure 4.13 shows the valve.

**Figure 4.13:** Valve

**Point gage**

The point gage is used to measure water level in the channel. This point gage was installed on top of wooden bar in a measuring bridge in different locations of channel.

**Figure 4.14:** Point gage and measuring bridge

**Acoustic Doppler Velocimeter (ADV)**

The SonTek 10-MHz ADV (Acoustic Doppler Velocimeter) from the original SonTek is used to measure 3-axis (3D) velocity measurements in a wide variety of settings from the laboratory to the ocean. An acoustic Doppler velocimeter measures three-dimensional flow velocities using the Doppler shift principle, and the instrument consists of a sound emitter, three sound receivers, and a signal conditioning electronic module. The sound emitter generates an acoustic signal that is reflected back by sound-scattering particles present in the water, which are assumed to move at the water's velocity. The scattered sound signal is detected by the receivers and used to compute the Doppler phase shift, from which the flow velocity in the radial or beam directions is calculated (Garcia et al., 2005). In the present study, ADV was placed on a measuring bridge with the help of a steel clamp to collect velocity measurements at different locations of test section as shown in Figure 4.15 (a). the ADV accurately measures the three components of water velocity in both high and extremely low flow conditions. The sampling volume is about 5 cm below the tip of the probe. The maximum sampling rate is 25 Hz and sampling volume 0.25 $cm^3$. This 10-MHz ADV can measure velocity within the range is 1 mm/s to 250 cm/s. Figure 4.15 (b) is showing the beam design of the ADV.


**Figure 4.15 (a):** Acoustic Doppler Velocimeter (ADV)

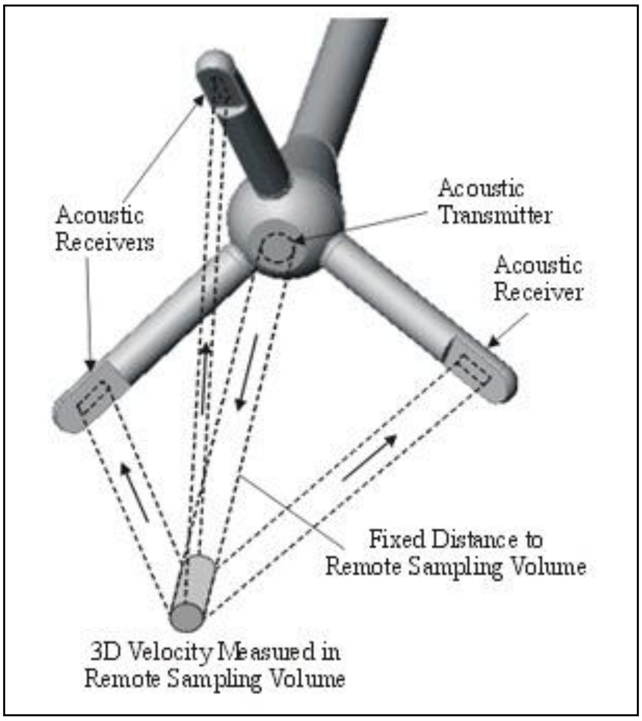


**Figure 4.15 (b):** ADV beam

After setup of the ADV with the software package it is used for taking high-quality three dimensional Velocity data at different points of the flow area are received to the ADV-processor. Computer shows the raw data after compiling the software package of the processor. At every point the instrument is recording a number of velocity data for a minute. With the statistical analysis using the installed software, the point velocities (three dimensional) were recorded for each flow depths.

### 4.4 Experimental size of protection elements

Following sections describe the process to determine the dimension of blocks and geobags.

#### 4.4.1 Selection of scale for experimentation

A geometrically similar undistorted scale factor 20 was selected to conduct the experiment. This selection of scale was based on (i) the available laboratory flume facilities and (ii) the Froude law criteria.

#### 4.4.2 Design of various model parameters

From the above considerations, various scale ratios of model parameters were designed as shown in Table 4.1.

**Table 4.1:** Scale ratios of model parameters

| Quantity | Dimension | Scale ratio |
|---|---|---|
| Length | $L$ | 1:20 |
| Volume or weight | $L^3$ | 1:8000 |
| Velocity | $L^{1/2}$ | 1:4.47 |
| Discharge | $L^{5/2}$ | 1:1789 |

It was assumed that the material and porosity remained unchanged for the experiment and prototype. Therefore, protection elements used for the laboratory experiment should be the same as those designed for field construction except for the reduced dimension.

#### 4.4.3 Design of CC block

CC blocks of different sizes were prepared using iron mold. The cement-sand ratio was 1:4. After one day of preparation, curing of blocks was done for 48 hours. As the protection elements were used in underwater condition, more curing time was considered so that better representation of relative density could be obtained. The blocks were cubical shaped prism. The cube shaped blocks are commonly used in Bangladesh context. The dimensions of blocks are listed in Table 4.2.

**Table 4.2**: Dimension of CC blocks used in the experiment

| Type of block | Length (mm) | Width (mm) | Thickness (mm) |
|---|---|---|---|
| Concrete block (C1) | 22.90 | 23.16 | 24.10 |
| Concrete block (C2) | 20.98 | 20.72 | 20.48 |
| Concrete block (C3) | 15.96 | 15.98 | 16.02 |
| Concrete block (C4) | 10 | 9.3 | 9.6 |

Different methods regarding calculations of unit dimensions of revetment cover layers and toe protections (e.g. PIANC, 1987; Pilarczyk, 1989; FAP 21/22, 1993) show only marginal deviations within the range of application for the rivers of Bangladesh. Since the widely used Pilarczyk formula (Pilarczyk, 1989; Przedwojski et al., 1995) includes the turbulence intensity, velocity and shear stress, it was followed to determine the nominal thickness of a protection unit. Design of the protection element size was considered as in Raju (2011).

### 4.4.4 Design of size of Geobag

Geobags of five different sizes were prepared by expert technician. For a bag, the exact amount of sand was weighted first. Then it was put in the one side open bag made of cloth. After that it was sewed to get a complete one. The shape was rectangular and square. The length to width ratio ranges from 1.73 to 1.09. The dimensions of the bags are listed in Table 4.3.

**Table 4.3**： Dimension of geobags used in the experiment

| Type of geobag | Length (mm) | Width (mm) | Thickness (mm) |
|---|---|---|---|
| Geobag (G1) | 71.20 | 40.90 | 10.9 |
| Geobag (G2) | 51.60 | 29.80 | 8.60 |
| Geobag (G3) | 42.90 | 38.00 | 9.04 |
| Geobag (G4) | 60.24 | 38.60 | 7.02 |
| Geobag (G5) | 51.94 | 47.70 | 7.02 |

For some typical block sizes, the equivalent sizes of geobags are provided in FAP 21 (2001). The design of geobag was done as in FAP 21 (2001) and NHC, (2006). Consequently block type C1 and C2 is equivalent to geobag type G4, G5 and G2, G3, respectively. Different protection elements used for the present study are shown in Figure 4.16.

**Figure 4.16:** CC blocks and geobags used in the experiment

### 4.4.5 Design of Apron

Design scour depth was estimated by Lacey's regime formula as it is widely used in this subcontinent in alluvial rivers. This empirical regime formula is:

$$R = 0.47\left({}^{Q}/_{f}\right)^{\frac{1}{3}} \tag{4.1}$$

With $D_s = XR\text{-}h$ (4.2)

Where $D_s$ = Scour depth at design discharge (m) Q = Design discharge ($m^3/s$), h = Depth of flow (m), may be calculated as (HWL-LWL), f = Lacey's silt factor = 1.76 $(d_{50})^{1/2}$; $d_{50}$ = Median diameter of sediment particle (mm), X = Multiplying factor for design scour depth.

Considering a typical field condition as presented in Table 4.4 and from equation 4.1 and 4.2, $D_s$ =7.23 m Therefore,

Width of apron, $W_{apron} = 1.5\ D_s = 11$ m.

Width of apron in the flume, $W_{apron} = 11/20 = 55$ cm.

Thickness of protection over scoured slope, $T = 1.25\ D_n$.

Shape of the apron for blocks was followed according to Rao, 1946, discussed previously and shown in Figure 4.17.

**Table 4.4**: Hydraulic parameters of typical field condition

| | |
|---|---|
| High Water Level, HWL | 8.0 m PWD |
| Low Water Level, LWL | 2.0 m PWD |
| Design discharge, Q | 15,000 $m^3/s$ |
| Median diameter of sediment particle, $d_{50}$ | 0.23 mm |
| Multiplying factor for design scour depth, X | 1.25 for straight reach of channel |

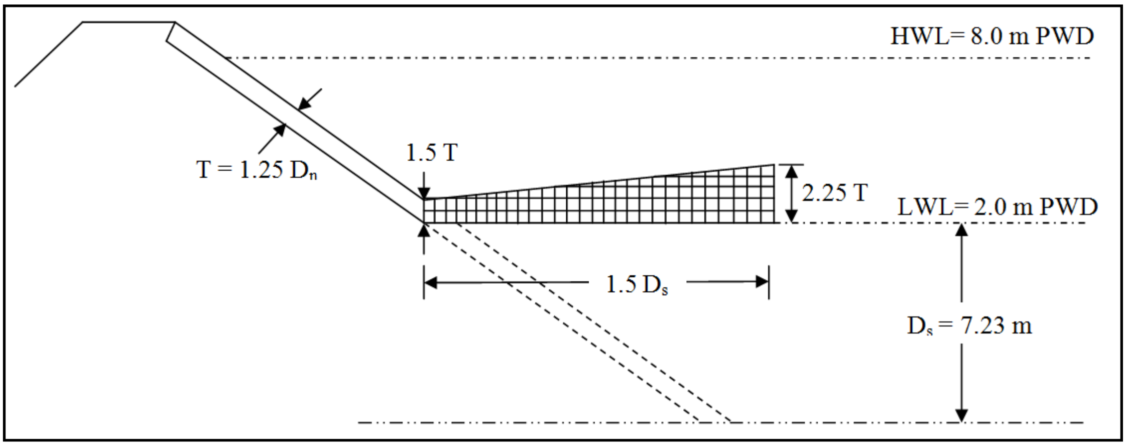


**Figure 4.17**: Schematic diagram for shape of Apron for a typical field condition

**Quantity of block:**

Inside thickness of apron = 1.5 T

Outside thickness of apron = 2.25 T

Quantity of block, $V_{block} = L\ (1.5T + 2.25T)/2\ m^3/m$

Number of block per unit length = $V_{block}/D_n^3$

This amount of block is dumped so as to achieve the shape according to Figure 4.17, over the width of apron per unit length to investigate its incipient condition.

**Quantity of geobag:**

In mass dumping concept, a falling apron is developed from the water line by dumping a calculated quantity of geobags as a heap below LWL along the river section. The geobags were assumed to launch in a slope of 1V:2H, to cover the slope and future scour holes. According to Halcrow and Associates (2002), a protection thickness of 0.61 m on the scour surface for a scour depth up to 17 m is required. For a typical condition as mentioned above, the calculated scour depth was 7.23 m.

Therefore,
Volume of geobag, $V_{geobag} = (10^2+20^2)^{0.5}$ x 0.61 $m^3/m$
Number of geobag per unit length = $V_{geobag}/D_n^3$
This amount of geobag was dumped from the water surface over the width of apron per unit length in the channel to investigate its incipient condition.

### 4.4.6 Hydraulic parameters

Utility of an experimental investigation infield practice lies in the simulation of the field situations in the experimental setup. In order to simulate field conditions observed in different bank protection works already undertaken in Bangladesh, it was necessary to keep the velocity, water depth within a range. The flow depth was selected considering the High Water Level (HWL) and Low Water Level (LWL) in a typical field condition. This will facilitate the tasks of engineers and researchers to compare the test results with the field circumstances and to search for the option best suited for a given site condition for sustainable bank protection works. The hydraulic parameters are presented in Table 4.5.

**Table 4.5**: Initial hydraulic parameters regarding experimental study

| Type of element | Discharge, Q ($m^3/h$) | Experimental value | | Corresponding field value | |
|---|---|---|---|---|---|
| | | Depth of flow, h (m) | Velocity, V (m/s) | Depth of flow, h (m) | Velocity, V (m/s) |
| CC Block | 195 | 0.175 | 0.30 | 3.5 | 1.34 |
| CC Block | 150 | 0.15 | 0.30 | 3 | 1.34 |
| Geobag | 165 | 0.175 | 0.25 | 3.5 | 1.12 |
| Geobag | 130 | 0.15 | 0.25 | 3 | 1.12 |

### 4.4.7 Test duration

After dumping the elements from water surface, they were allowed to be stable on the bed and then the measurements were made. For incipient motion tests, the duration of a run was about 60 minutes to 90 minutes for CC blocks and geobags, depending on their sizes.

## 4.5 Test scenarios

Experiments were conducted with four types of CC block and five types of geobag with two different hydraulic conditions to investigate placing behavior and incipient condition as presented in Table 4.6(a) and Table 4.6(b).

**Table 4.6 (a)**: Test scenarios for investigation of placing behavior

| Run no. | Type of Protection Element | Depth of flow (m) | Velocity (m/s) | Discharge ($m^3/h$) |
|---|---|---|---|---|
| 1-3 | CC block | 0.15 | 0.3 | 150 |
| 4-6 | CC block | 0.175 | 0.3 | 195 |
| 7-11 | Geobag | 0.15 | 0.3 | 150 |
| 12-15 | Geobag | 0.175 | 0.3 | 195 |

**Table 4.6 (b):** Test scenarios for investigation of incipient condition

| Run no. | Discharge range ($m^3/h$) | Water level range(m) | Type of Protection Element | Condition |
|---|---|---|---|---|
| 1 | 150 to 300 | 0.15 to 0.19 | Concrete block (C1) | Underwater construction |
| 2 | | | Concrete block (C2) | |
| 3 | | | Concrete block (C3) | |
| 4 | | | Concrete block (C4) | |
| 5 | 195 to 320 | 0.175 to 0.21 | Concrete block (C1) | Underwater construction |
| 6 | | | Concrete block (C2) | |
| 7 | | | Concrete block (C3) | |
| 8 | 130 to 270 | 0.15 to 0.22 | Geobag (G1) | Underwater construction |
| 9 | | | Geobag (G2) | |
| 10 | | | Geobag (G3) | |
| 11 | | | Geobag (G4) | |
| 12 | | | Geobag (G5) | |
| 13 | 165 to 295 | 0.175 to 0.24 | Geobag (G2) | Underwater construction |
| 14 | | | Geobag (G3) | |
| 15 | | | Geobag (G4) | |
| 16 | | | Geobag (G5) | |
| 17 | 100-320 | 0.10 to 0.25 | Concrete block (C2) | Dry bed condition |
| 18 | | | Geobag (G3) | |
| 19 | | | Geobag (G4) | |

## 4.6 Test procedure

The course of actions followed during all the experiments are stated below chronologically. Firstly, the placing behavior of protection element was investigated. Secondly, incipient condition for element in case of underwater construction was studied. Finally, incipient condition for element placed in a dry bed prior to flow of water was studied and compared with that of underwater construction. The shape of apron and number of element required per unit length was determined as mentioned previously. This amount was dumped during the run. Depth of flow was measured by point gauge. Point velocity data were collected by using ADV (Acoustic Doppler

Velocimeter) at apron and just upstream of the apron. At each cross section point velocity was collected at three vertical such as center of the right, middle and left segment of each section (Figure 4.18).

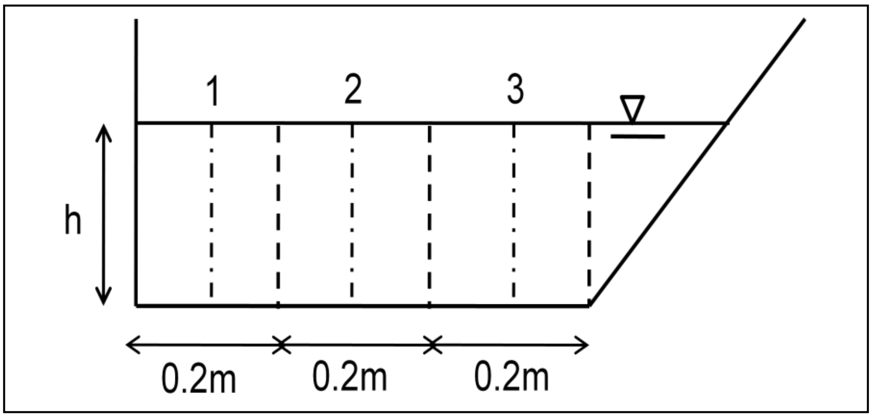


**Figure 4.18:** Cross section of the experimental reach

At each vertical point velocity data have been collected at three depths but near the bed, collected data showed very low correlation. So depth averaged velocity data have been used in analysis.

In order to observe the effect of proximity (Sides, at vertical 1 and vertical 3) velocity measurements close to the sides also measured in addition to the test vertical at the middle segment. Velocity distribution shows some proximity effect at sides compared to the middle section at vertical 2. Thus, velocity measurements at vertical 2 of middle segment have been used in analysis.

### 4.6.1 Procedure for placing behavior observation

Procedure for placing behavior observation in laboratory is given below:

i) Two different combinations of hydraulic parameters have been investigated. The elements have been dumped from 4 cm above the water surface in all tests run which is comparable with barge height.

ii) For a particular set up, the discharge has been controlled by the valve and the depth of flow has been fixed by adjusting the tail gate. Depth averaged flow velocity was measured using ADV.

iii) The duration of a run was determined by monitoring the movement of bags and blocks on the bed. As the movement was over, run continued for more ten minutes and the state of protection element was documented.

iv) The horizontal settling distance was measured from the initial dumping line to the center of each element.

### 4.6.2 Procedure for incipient condition experiment in case of underwater construction

i) Five types of bag and four types of block are used. Two different combinations of hydraulic parameters were investigated. The elements were dumped from 4 cm above the water surface in all run which is comparable with barge height.

ii) Blue, yellow and red colored blocks were used in first, second and third layers to observe their post dumping condition.

iii) For a particular set up, the initial discharge was set by the discharge controlling valve and the initial depth of flow was fixed by adjusting the tail gate. Depth averaged flow velocity at initial condition was measured using ADV.

iv) Then discharge was increased very slowly at a rate of $5m^3/h$ and observed for three to five minutes. After that if there was no movement in apron material flow was increased again. This process continued till the incipient condition occurred.

v) Incipient condition is considered as the displacement of an element from its initial position. When this condition was satisfied, the flow depth and velocity was measured at different section.

vi) The significant feature of the test is that elements were dumped in the flowing water rather placed in a dry bed prior to flow of water. This procedure depicts the real life practice.

### 4.6.3 Procedure for incipient condition experiment of protection elements on dry bed condition

i) Two types of bag and one type of block were used. One hydraulic condition was investigated for the purpose of comparison.

ii) Apron was constructed on dry bed prior to flow of water.

iii) Then pump was started to cause flow of water in the channel.

iv) When incipient condition was satisfied for apron constructed on dry bed, the flow depth and velocity was measured at different section.

## 4.7 Observations

During the experimentation, the following observations were made:

### 4.7.1 Observations on placing behavior of falling apron

i) Small cube shaped block spin while falling and rolled down 5 to 10 cm after touching the bed of the channel.

ii) Few blocks at the front side stopped the rolling of others coming behind them.

iii) Rectangular shaped bags traveled more distance than square shaped bags.

iv) The settling distance of geobags was relatively greater than that of CC blocks for similar condition.

v) The angle of settling distance with vertical was relatively greater for CC blocks than that of geobags.

vi) Geobag embedded with sand bed and among themselves relatively more compared to CC blocks.

Figure 4.19 is showing the placement of falling apron (CC blocks and Geobags).

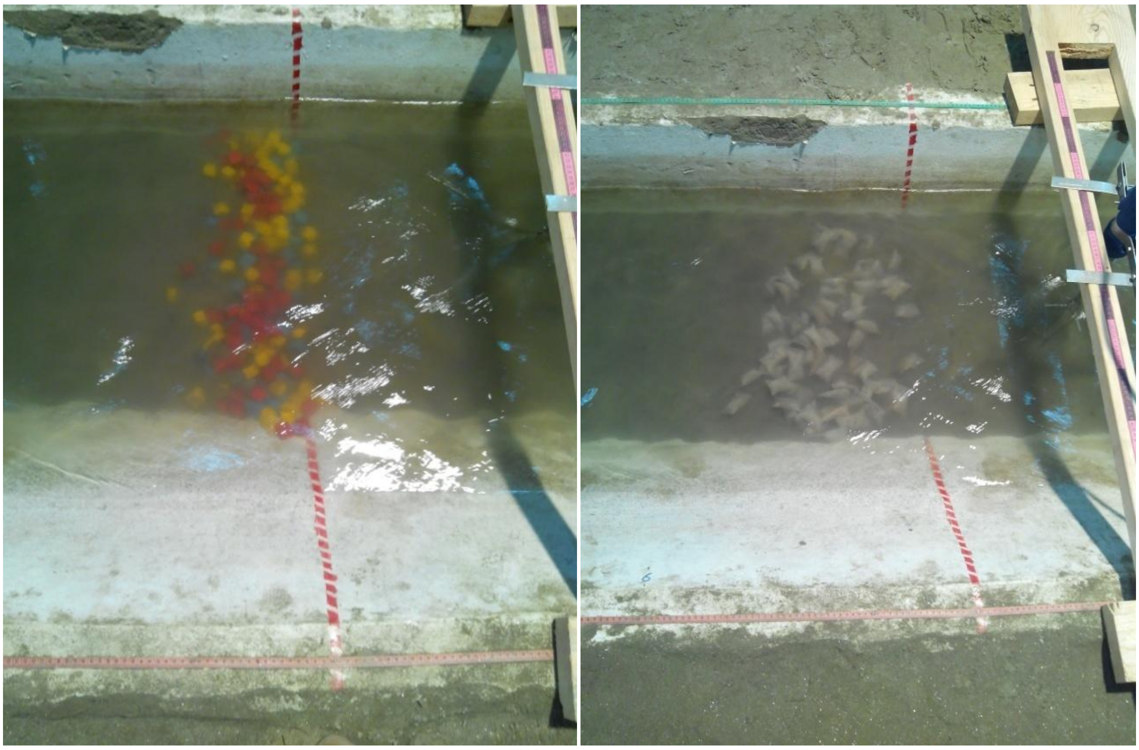

**Figure 4.19:** Investigation of placement of falling apron (CC blocks and Geobags)

### 4.7.2 Observations on incipient condition experiment in case of underwater construction

i) The water surface at the apron section was slightly lower than the upstream section.

ii) The velocity over the apron was higher than that of upstream and downstream.

iii) The larger the size of the protection element greater velocity required to cause incipient condition.

iv) The velocity at the centre was greater than that of both bank sides.

v) As the velocity was increased the protection elements started vibrating.

vi) For geobags, group movement or sliding was observed while blocks moved individually.

vii) Square shaped bags required higher velocity to reach incipient condition than that of rectangular bags.

The protection elements at incipient condition in case of underwater construction are shown in Figure 4.20 and Figure 4.21.

**Figure 4.20:** Displacement of CC blocks at incipient condition (Underwater construction)

**Figure 4.21:** Displacement of geobags at incipient condition (Underwater construction)

### 4.7.3 Observations on incipient condition experiment of protection elements in dry bed condition

i) As the flow starts the upper layers fell down immediately and the bottom layer started to settle down into the sand bed.

ii) After this immediate displacement the bed material made good packing prior to the water level reached the low water level. Due to this packing and interlocking protection elements attained incipient condition in higher velocity than that of underwater construction.

Figures 4.22 to 4.23 show the incipient condition experimentations in dry bed condition

**Figure 4.22:** Displacement of CC blocks at incipient condition (Dry bed Condition)

**Figure 4.23:** Displacement of geobags at incipient condition (Dry bed condition)

### 4.7.4 Bed form in the test run

i) Characteristics features of different bed forms can be recognized on the basis of bed material size and the relative velocity of stream or Froude Number. In present experimentation ripple has been observed with the fine bed material (generally with d< 0.5-0.7 mm).

ii) According to Simons and Richardson (1961), Athaullah (1968), Van Rijn's (1984) approach, ripple bed form has been observed

Figure 4.24 is showing the ripple bed form developed during all the experimentations.

**Figure 4.24:** Bed form during the experimentation

# CHAPTER FIVE

# RESULTS AND DISCUSSIONS

## 5.1 Introduction

Laboratory experiments have been conducted to investigate the placing behavior of toe protection elements (e.g. CC blocks and Geobags) of river bank protection works. First of all, the placement of different types of protection element was observed. Therefore, the investigations at incipient condition of CC blocks and geobags are described in this chapter. These results are utilized to analyze the relationship among dimensionless particle diameter, relative depth and dimensionless velocity. The depth factor and turbulent intensity of the CC blocks and geobags are analyzed here when they were dumped in the flowing water under live bed condition.

## 5.2 Results of the placing behavior of protection elements

Two set up were investigated for both block and geobag during the fifteen experimental run to observe the placement of different types of protection elements. These experimental observations have been presented in article 4.7 in Chapter 4. Fall velocities have been calculated by equations given by Raju and Matin (2013). For CC blocks and geobags, suggested equation based on earlier studies has been revised with the experimental data of present study.

### 5.2.1 Analysis of horizontal settling distance for CC block

The CC blocks followed the path of a projectile pattern during the course of its settling which created an angle of about $60^0$ with the vertical. Figure 5.1 represents a regression analysis of the experimental data with a coefficient of determination ($R^2$) of 0.86.

The final expression suggested in the present study is,

$$\frac{S}{h} = 1.46 \left(\frac{u}{w}\right)^{0.95} \tag{5.1}$$

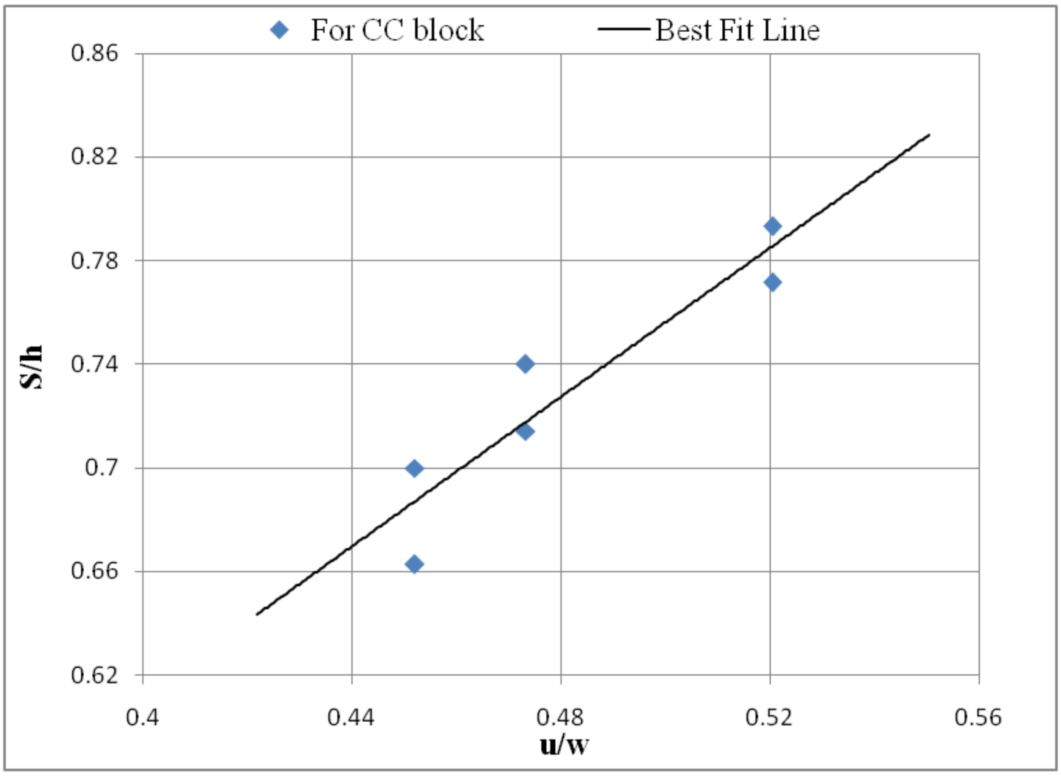


**Figure 5.1**: Plot of S/h against u/w for CC block

### 5.2.2 Comparison of proposed settling distance equation for CC block

For the determination of accuracy of a formula two different methods have been used in this study. Firstly, the average value of relative error where error is defined as

$$\text{Relative error} = \frac{|\text{Predicted}-\text{Observed}|}{\text{Observed}} \times 100$$

Secondly, discrepancy ratio which is referred as the ratio of predicted value to measured value.

$$\text{Discrepancy ratio} = \frac{\text{Predicted value}}{\text{Observed value}}$$

The function with the discrepancy ratio closest to 1.0 is considered as highest ranked (Thomas et. al. 2002).

In this present study comparison can be made by both methods to investigate the predictive performance of equation proposed in this study and also of different investigators.

Figure 5.2 represents the comparison of predicted settling distance by proposed empirical equation (equation 5.1) and Raju (2011) versus measured in this study. The average relative error for present study has been found 1.96%. According to earlier investigation all data lies below the line of perfect agreement i.e. earlier investigation predicted lower settling distance than that of measured in the present study for CC block.

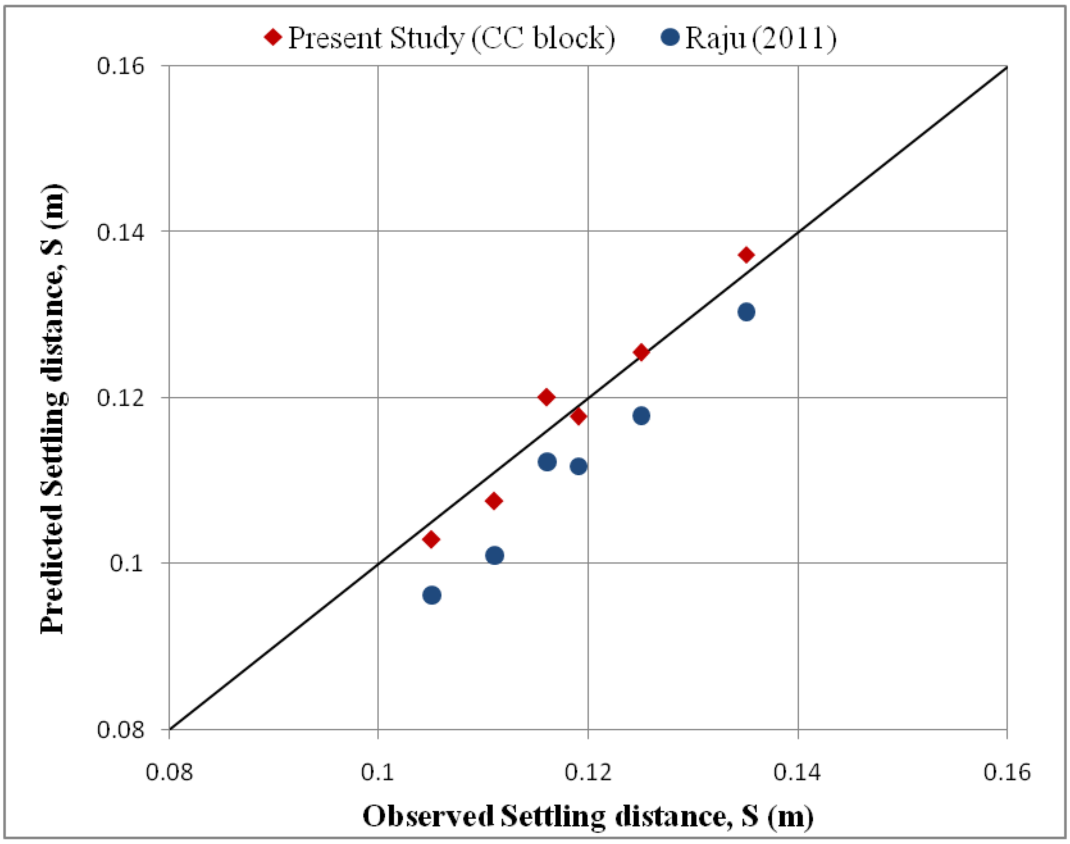


**Figure 5.2**: Comparison of observed and predicted horizontal settling distance using equation (5.1) and Raju (2011) for CC block

### 5.2.3 Analysis of horizontal settling distance for geobag

The geobags also followed the path of a projectile pattern during the course of its settling which created an angle of about $45^0$ with the vertical. Geobags traveled more distance during falling than that of CC blocks.

A regression analysis of the experimental data has been performed with a coefficient of determination ($R^2$) of 0.65 presented in Figure 5.3.

The final expression of horizontal settling distance becomes,

$$\frac{S}{h} = 1.534\left(\frac{u}{w}\right)^{1.16} \tag{5.2}$$

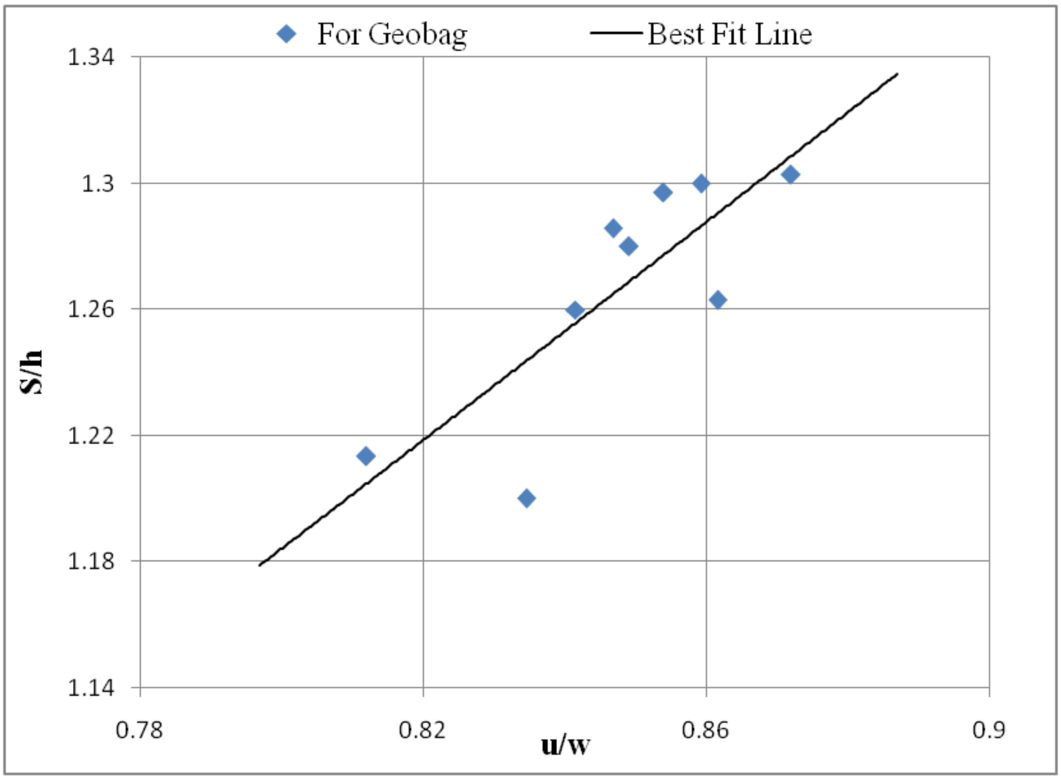


**Figure 5.3**: Plot of S/h against u/w for geobag

### 5.2.4 Comparison of proposed settling distance equation for geobag

The comparison of predicted settling distance by proposed empirical equation (equation 5.2) with earlier investigation (Raju, 2011) versus measured in this study for geobags is presented in Figure 5.4. The average relative error for present study has been found 1.38 %. Proposed equation by Raju (2011) shows satisfactory compliance with that of equation proposed in the present study for prediction of settling distance of geobags.

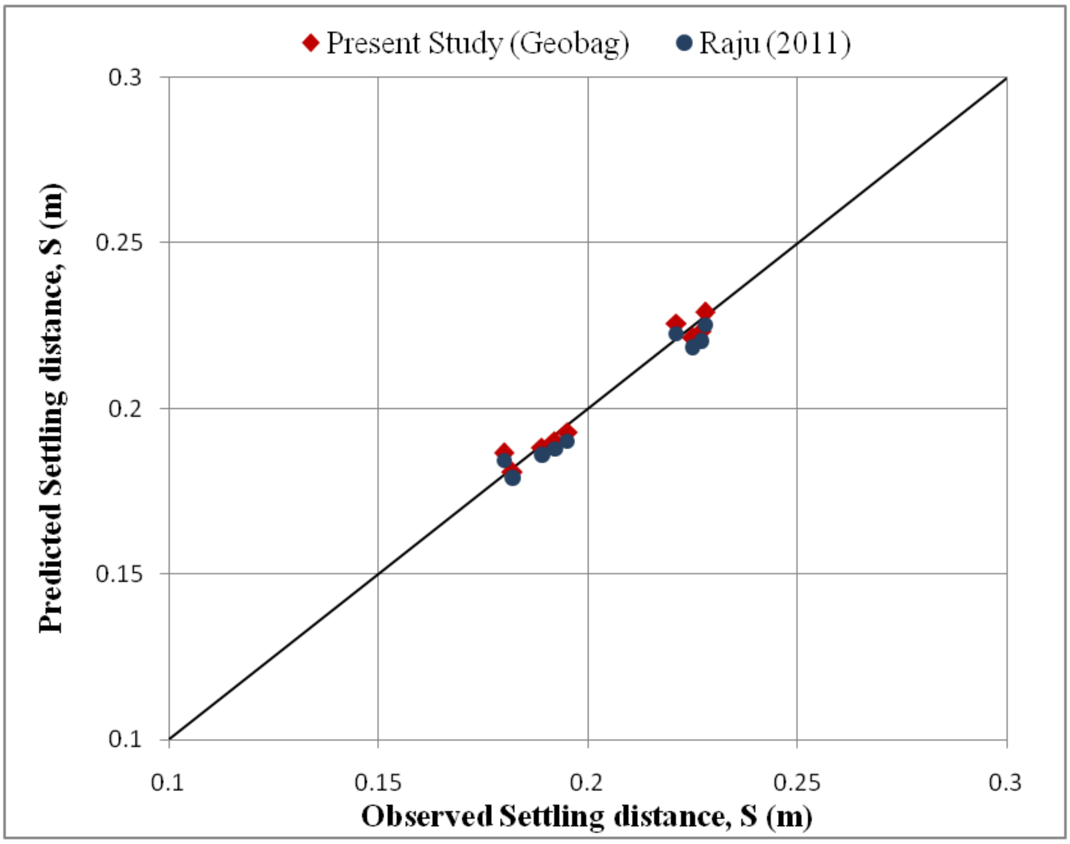


**Figure 5.4**: Comparison of observed and predicted horizontal settling distance using equation (5.2) and Raju (2011) for geobag

### 5.3 Results of incipient condition

The transition from the condition of 'no motion' to initial movement is defined as the critical or threshold condition or incipient condition (Paphitis, 2001). From a theoretical point of view, if the fluid forces are below that required for the motion of a particle, there will not be any movement. If they are greater than that required for motion, there will be movement. The boundary between the two may be described as 'incipient' condition i.e. the particle is about to move (Armitage and Rooseboom, 2010). The present study focuses on the incipient condition of toe protection elements (CC blocks and Geobags).

The value of different parameters at incipient condition in the experiment for CC block and geobags are summarized in Table 5.1 and Table 5.2 respectively. Parameters mentioned here are discussed during the literature review.

**Table 5.1:** Experimental results at incipient condition of CC block

| Setup | Location | CC Block Size, d (m) | Dimensionless Particle diameter, $d_*$ | Depth of flow, h (m) | Depth averaged Velocity, u (m/s) | Shear Velocity, $u_*$ (m/s) | Boundary Reynolds number, $R_*$ |
|---|---|---|---|---|---|---|---|
| 1 | Upstream of Apron | 0.01 | 247.23 | 0.1632 | 0.3688 | 0.0383 | 458.19 |
| | | 0.015 | 370.84 | 0.1648 | 0.3762 | 0.0384 | 689.72 |
| | | 0.02 | 494.46 | 0.1852 | 0.5061 | 0.0400 | 958.77 |
| | | 0.023 | 568.63 | 0.1872 | 0.5244 | 0.0402 | 1106.77 |
| | At Apron | 0.01 | 247.23 | 0.1630 | 0.4437 | 0.0382 | 457.99 |
| | | 0.015 | 370.84 | 0.1646 | 0.4589 | 0.0384 | 689.42 |
| | | 0.02 | 494.46 | 0.1850 | 0.5126 | 0.0400 | 958.40 |
| | | 0.023 | 568.63 | 0.1870 | 0.5677 | 0.0402 | 1106.35 |
| 2 | Upstream of Apron | 0.015 | 370.84 | 0.1887 | 0.5150 | 0.0403 | 723.84 |
| | | 0.02 | 494.46 | 0.1927 | 0.5230 | 0.0406 | 972.26 |
| | | 0.023 | 568.63 | 0.2021 | 0.6423 | 0.0413 | 1136.86 |
| | At Apron | 0.015 | 370.84 | 0.1885 | 0.5184 | 0.0403 | 723.57 |
| | | 0.02 | 494.46 | 0.1925 | 0.5234 | 0.0406 | 971.91 |
| | | 0.023 | 568.63 | 0.2019 | 0.6185 | 0.0413 | 1136.47 |

**Table 5.2:** Experimental results at incipient condition of geobag

| Setup | Location | Geobag Size, d (m) | Dimensionless Particle diameter, $d_*$ | Incipient Depth of flow, h (m) | Incipient Velocity, u (m/s) | Shear Velocity, $u_*$ (m/s) | Boundary Reynolds number, $R_*$ |
|---|---|---|---|---|---|---|---|
| 1 | Upstream of Apron | 0.0304 | 577.36 | 0.2052 | 0.5462 | 0.0415 | 1441.76 |
| | | 0.0232 | 440.86 | 0.1942 | 0.3991 | 0.0407 | 1079.96 |
| | | 0.0246 | 466.71 | 0.1992 | 0.4382 | 0.0411 | 1153.50 |
| | | 0.0256 | 486.87 | 0.2003 | 0.4247 | 0.0411 | 1205.62 |
| | | 0.0267 | 506.64 | 0.2162 | 0.4813 | 0.0422 | 1288.18 |
| | At Apron | 0.0304 | 577.36 | 0.205 | 0.5118 | 0.0415 | 1441.28 |
| | | 0.0232 | 440.86 | 0.194 | 0.4316 | 0.0407 | 1079.57 |
| | | 0.0246 | 466.71 | 0.199 | 0.4403 | 0.0411 | 1153.10 |
| | | 0.0256 | 486.87 | 0.2001 | 0.4429 | 0.0411 | 1205.20 |
| | | 0.0267 | 506.64 | 0.216 | 0.5077 | 0.0422 | 1287.77 |
| 2 | Upstream of Apron | 0.0232 | 435.56 | 0.2212 | 0.4643 | 0.0426 | 1129.76 |
| | | 0.0246 | 461.10 | 0.2287 | 0.5060 | 0.0431 | 1209.71 |
| | | 0.0256 | 481.01 | 0.2352 | 0.4664 | 0.0435 | 1274.01 |
| | | 0.0267 | 500.55 | 0.2372 | 0.4787 | 0.0436 | 1329.55 |
| | At Apron | 0.0232 | 435.56 | 0.221 | 0.4196 | 0.0426 | 1129.41 |
| | | 0.0246 | 461.10 | 0.2285 | 0.4997 | 0.0431 | 1209.35 |
| | | 0.0256 | 481.01 | 0.235 | 0.4596 | 0.0435 | 1273.64 |
| | | 0.0267 | 500.55 | 0.237 | 0.5401 | 0.0436 | 1329.18 |

### 5.3.1 Analysis of shear velocity for CC block

Two set up were investigated for both block and geobag during the sixteen experimental run (seven for block and nine for geobag) to obtain a correlation between dimensionless particle diameters with dimensionless flow parameter boundary Reynolds number. On the basis of expression shown in equation (3.11), a regression analysis of the experimental data has been performed with a coefficient of determination ($R^2$) of 0.997.

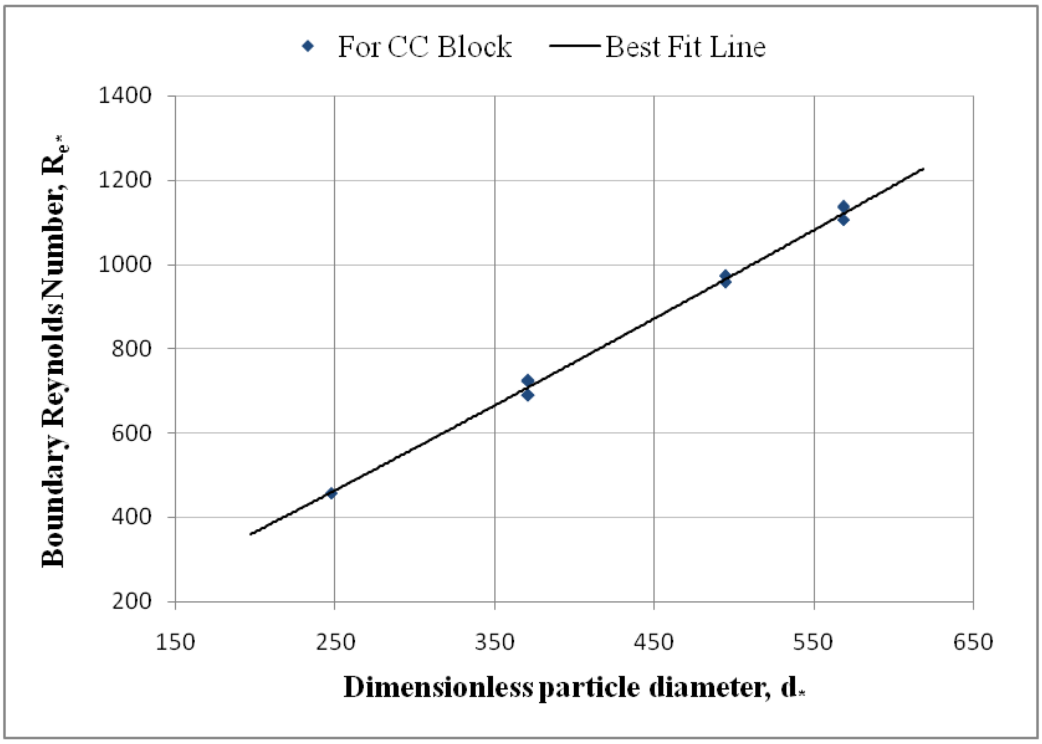


**Figure 5.5**: Boundary Reynolds number versus dimensionless particle diameter for CC Block

Finally equation (3.11) for CC blocks attains the form as:

$$R_{e*} = 1.212\, d_*^{\,1.076} \tag{5.3}$$

Where, $R_{e*} = \left(\frac{u_* d}{\nu}\right)$ and $d_* = d\left(\frac{\Delta g}{\nu^2}\right)^{1/3}$

It is seen that boundary Reynolds number increases as the dimensionless particle diameter increases.

Equation (5.3) is valid within the experimental ranges of 200<$R$*<1400 and 200<$d$*<600.

### 5.3.2 Comparison of proposed shear velocity equation for CC block

Figure 5.6 represents the values of discrepancy ratios of predicted shear velocity and observed shear velocity by proposed empirical equation (equation 5.3). Figure also shows the values of other researchers such as Keulegan (1938), Manning and Strickler equation and Melville (1988). Table 5.3 shows the percentage of discrepancy ratios within each discrepancy band.

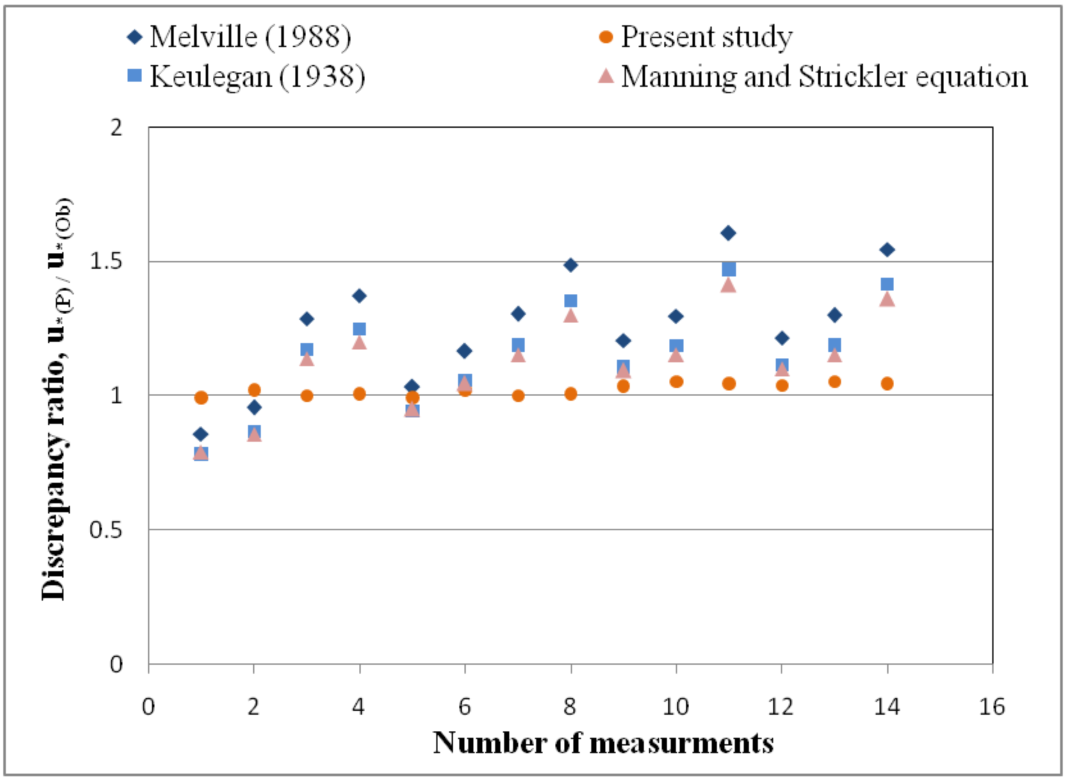


**Figure 5.6**: Values of discrepancy ratio of shear velocity for CC block

**Table 5.3:** Discrepancy band of shear velocity for CC block

| Discrepancy Band | Present Study (%) | Keulegan (1938) (%) | Manning & Strickler Eq. (%) | Melville (1988) (%) |
|---|---|---|---|---|
| 0.95 -1.05 | 100 | 0 | 15 | 15 |
| 0.85 -1.15 | - | 36 | 43 | 22 |
| 0.75 -1.25 | - | 79 | 79 | 43 |
| 0.65 -1.35 | - | 100 | 86 | 72 |

| Discrepancy Band | Present Study (%) | Keulegan (1938) (%) | Manning & Strickler Eq. (%) | Melville (1988) (%) |
|---|---|---|---|---|
| 0.5 -1.5 | - | - | 100 | 86 |
| 0.5 -2.0 | - | - | - | 100 |

The values of discrepancy ratio as shown in Figure 5.6 and Table 5.3 demonstrate that 100% of the present experimental data lies within the range of 0.95 to 1.05. The different percentage of discrepancy ratio of Keulegan (1938), Manning and Strickler equation and Melville (1988) equations are found within different bands. These analysis reveals that the present equation show comparatively better predictive performance of shear velocity than earlier investigations.

### 5.3.3 Analysis of shear velocity for geobag

On the basis of expression shown in equation (3.11), a regression analysis of the experimental data has been performed. The plot is shown in Figure 5.7.

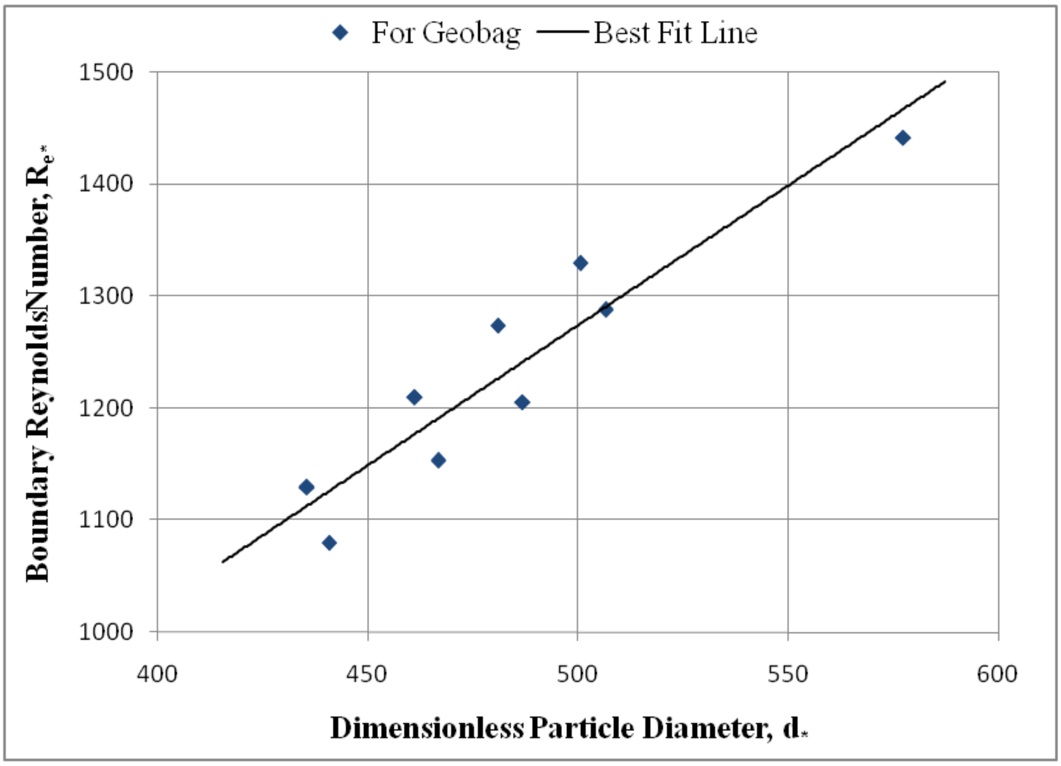


**Fgure 5.7**: Boundary Reynolds number versus Dimensionless particle diameter for geobag

The coefficient of determination ($R^2$) is found to be 0.87 indicating a good correlation. It is seen that as the dimensionless particle diameter increases the boundary Reynolds number also increases which is consistent with literature.

The final expression for shear velocity for geobag becomes:

$$R_{e*} = 2.883\ d_*^{\ 0.98} \tag{5.4}$$

It is seen that boundary Reynolds number increases as the dimensionless particle diameter increases.

Equation (5.4) is valid within the experimental ranges of $1x10^3<R*<1.5x10^3$ and $400<d*<600$.

### 5.3.4 Comparison of proposed shear velocity equation for geobag

Figure 5.8 represents the discrepancy ratio of predicted shear velocity and observed shear velocity by proposed empirical equation (equation 5.4) for geobag in this study. In this figure, the values of other researchers such as Keulegan (1938), Manning and Strickler equation and Melville (1988) also presented. According to present study all ratios are found to be very close to the perfect agreement line as shown in Figure 5.8. The discrepancy ratios of Keulegan (1938), Manning and Strickler equation and Melville (1988) equations lie between the bands 0.5 to 2.0. Table 5.4 represents the percentage of discrepancy ratios within each discrepancy band for geobags.

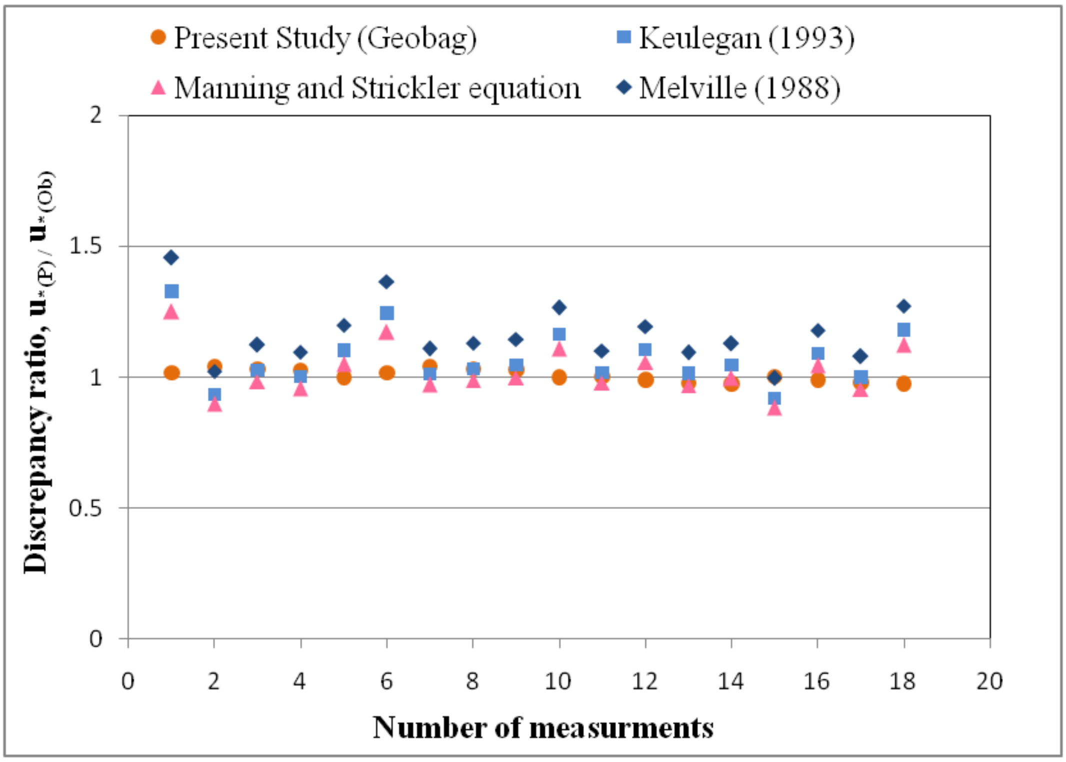


**Figure 5.8**: Values of discrepancy ratio of shear velocity for geobags

**Table 5.4:** Discrepancy band of shear velocity for geobag

| Discrepancy Band | Present Study (%) | Keulegan (1938) (%) | Manning & Strickler Eq. (%) | Melville (1988) (%) |
|---|---|---|---|---|
| 0.95 -1.05 | 100 | 50 | 62 | 12 |
| 0.85 -1.15 | - | 78 | 89 | 62 |
| 0.75 -1.25 | - | 95 | 100 | 78 |
| 0.65 -1.35 | - | 100 | - | 89 |
| 0.5 -1.5 | - | - | - | 100 |

From Table 5.4 it is found that 100% ratios within the range of 0.95 to 1.05. The different percentage of discrepancy ratio of Keulegan (1938), Manning and Strickler equation and Melville (1988) equations are found within different bands. These analysis reveals that the present equation show better predictive performance of shear velocity for geobags than earlier investigations.

### 5.3.5 Computation of relative error of shear velocity equations

Empirical equation 5.3 and equation 5.4 has been developed based on shear velocity by doing experimental investigations at incipient condition of nine different size protection elements for different set ups. Different formulas for shear velocity prediction along with proposed relationship have been compared with observed shear velocity in this study. The relative error of different formula and proposed equation is presented in Table 5.5.

**Table 5.5**: Performance of various shear velocity prediction formulas

| Shear Velocity Equation | Relative Error % | |
|---|---|---|
| | CC Block | Geobag |
| Present study | 2.50 | 1.97 |
| Keulegan (1938) | 20.84 | 8.69 |
| Manning and Strikler equation | 18.03 | 6.84 |
| Melville (1988) | 28.61 | 16.47 |

From the table 5.5, it is found that, the proposed empirical equations have the lowest average value of relative error for block and geobag. However, it is approved that equation (5.3) and (5.4) is always a better predictor for block and geobag, respectively, than that of earlier investigations.

The errors in predicting shear velocity by the previous investigations of similar condition are mainly due to the fact that the size of the elements used in this experiment is quite larger than those used in other studies.

### 5.3.6 Analysis of depth averaged velocity for CC block

Rubey (1948) found that the near bed velocity is, however, not very well defined and it is preferable to use the critical depth averaged velocity as the characteristic parameter. So in this present study depth averaged velocity for toe protection element at incipient condition has been analyzed also.

To analyze depth averaged velocity, relationship between dimensionless velocity ($u/u_*$) and relative depth (h/d) has been developed. The relative depth is the ratio of depth of flow and particle diameter. A regression analysis has been performed on the basis of expression shown in equation (3.13). Where, shear velocity, $u_*$ can be obtained by proposed equation 5.3.

The term relative depth is very important in bank protection design. So it is useful for the design. From Figure 5.9, it is seen that dimensionless velocity decreases as the relative depth increases.

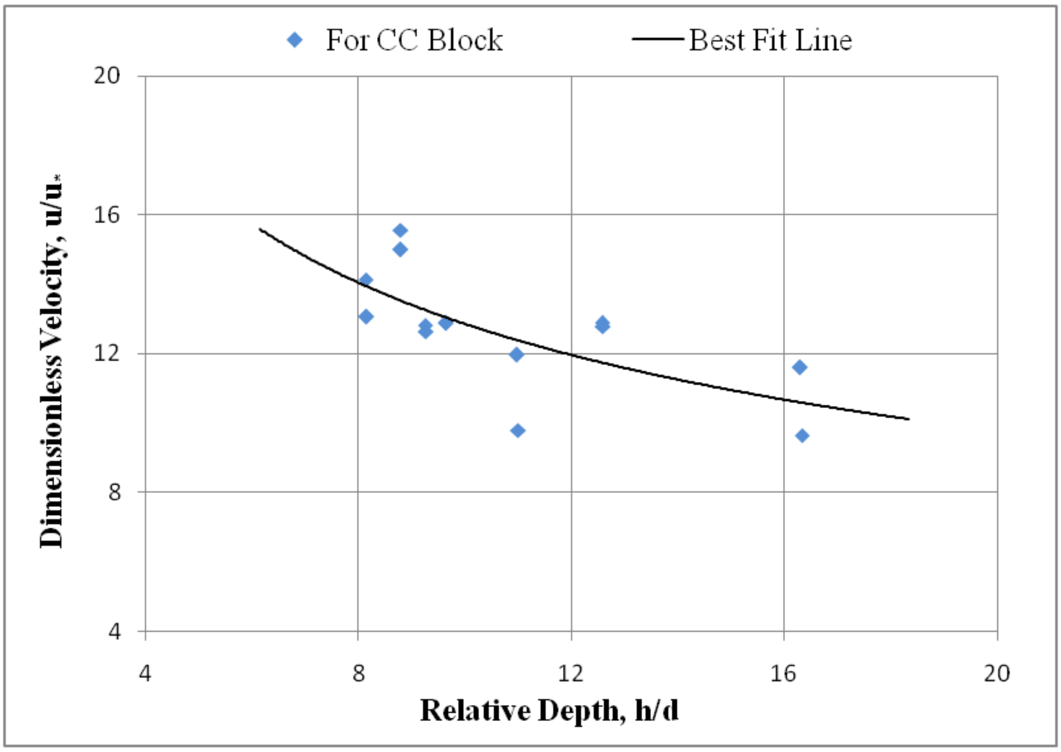


**Figure 5.9**: Dimensionless velocity versus relative depth for CC block

The final expression of the relationship for CC block becomes

$$\frac{u}{u*} = 31.85 \left(\frac{h}{d}\right)^{-0.39} \tag{5.5}$$

Equation (5.5) is valid within the range $7 < \frac{h}{d} < 17$ and $10 < \frac{u}{u*} < 15$.

### 5.3.7 Comparisons of proposed depth averaged velocity equation for CC block

Figure 5.10 represents the discrepancy ratio of predicted shear velocity and observed shear velocity by proposed empirical equation (equation 5.5) for CC block in this study. In this figure, the values of other researchers such as Isbash (1935), Inglis (1949), Niel (1967) and Maynord (1989) also presented. According to present study all ratios are found to be very close to the perfect agreement line as shown in Figure 5.10. The discrepancy ratios of Isbash (1935) depict better similarity with present study. Table 5.6 represents the percentage of discrepancy ratios within each discrepancy band for geobags.

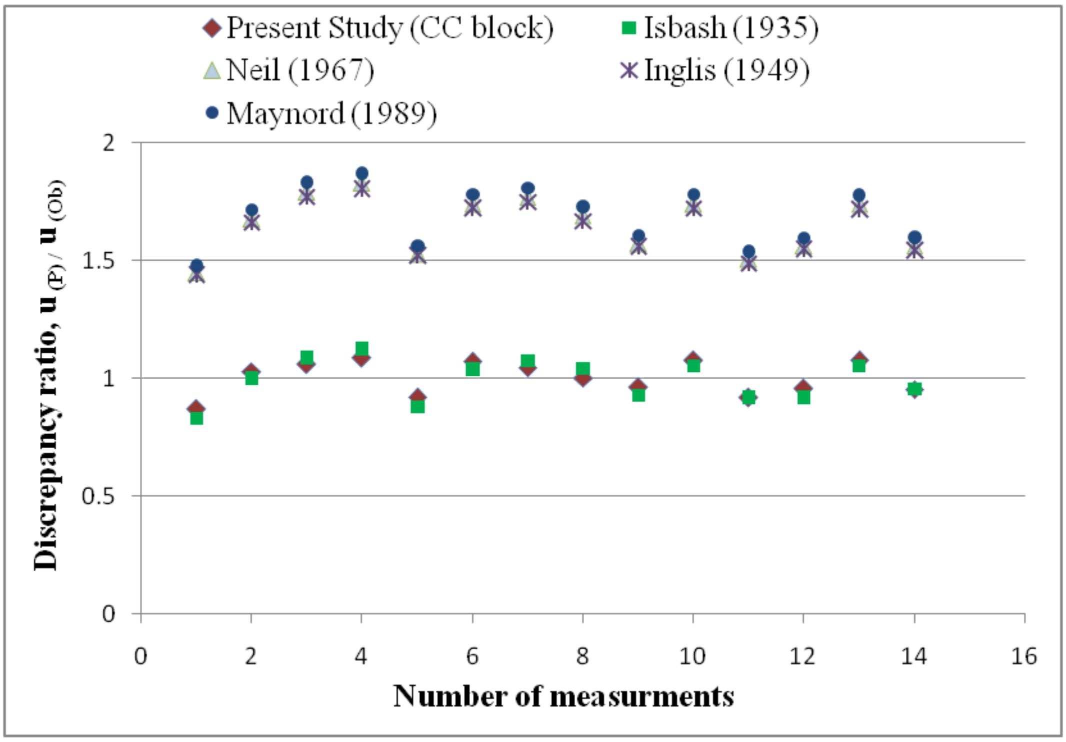


**Figure 5.10**: Values of discrepancy ratio of depth averaged velocity for CC block

**Table 5.6:** Discrepancy band of depth averaged velocity for CC block

| Discrepancy Band | Present Study (%) | Isbash (1935) (%) | Inglis (1949) (%) | Niel (1967) (%) | Maynord (1989) (%) |
|---|---|---|---|---|---|
| 0.95 -1.05 | 43 | 29 | 0 | 0 | 0 |
| 0.85 -1.15 | 100 | 93 | 0 | 0 | 0 |
| 0.75 -1.25 | - | 100 | 0 | 0 | 0 |
| 0.65 -1.35 | - | - | 0 | 0 | 0 |
| 0.5 -1.5 | - | - | 15 | 8 | 8 |
| 0.5 -2.0 | - | - | 100 | 100 | 100 |

Results in Table 5.6 shows that, 43% discrepancy ratios are found within the range 0.95 to 1.05 and 100% discrepancy ratios lie within the discrepancy band 0.85 to 1.15.

Earlier investigations show differences with present study because the condition of their analyses differs from present study.

### 5.3.8 Analysis of depth averaged velocity for geobag

To develop relationship between dimensionless velocity ($u/u_*$) and relative depth (h/d) for geobag, a regression analysis of experimental data has been performed, where $u_*$ is obtained from equation 5.4.

From Figure 5.11 it is seen that dimensionless velocity decreases as the relative depth increases.

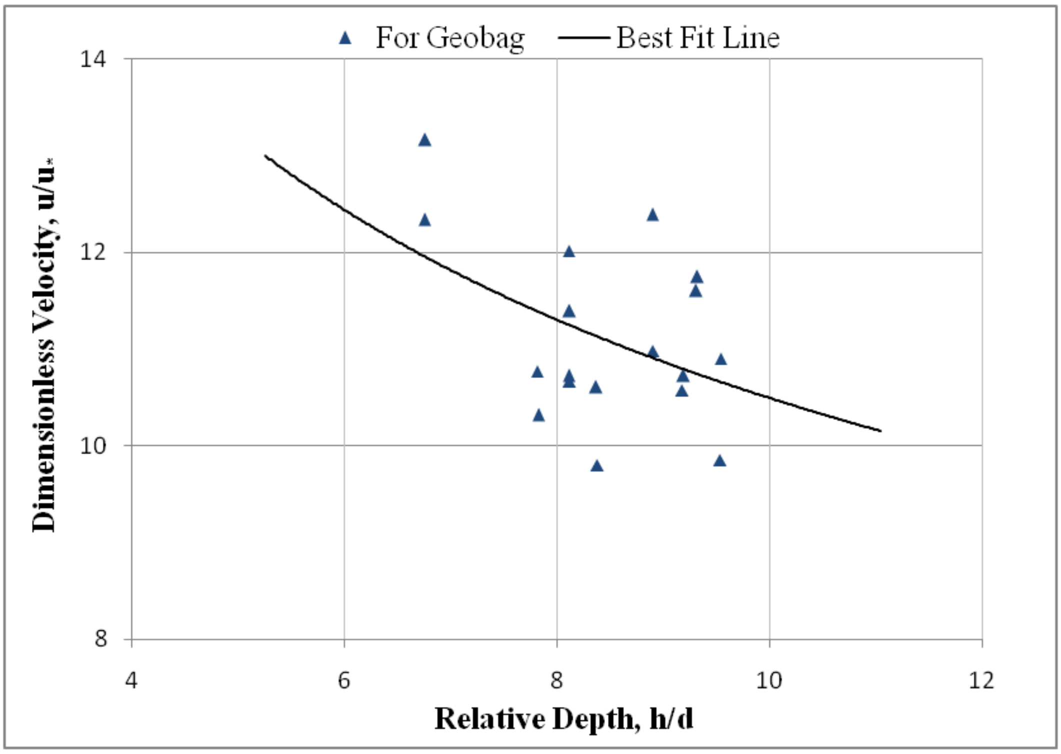


**Figure 5.11**: Plot of dimensionless velocity versus relative depth for geobag

The final expression of the relationship becomes

$$\frac{u}{u_*} = 22.58 \left(\frac{h}{d}\right)^{-0.33} \tag{5.6}$$

Equation (5.6) is valid within the range $5 < \frac{h}{d} < 11$ and $10 < \frac{u}{u_*} < 14$.

### 5.3.9 Comparisons of Proposed depth averaged velocity equation for geobag

Figure 5.12 represents the values of discrepancy ratios of predicted shear velocity and observed shear velocity by proposed empirical equation (equation 5.6) for geobag. Figure 5.12 also shows the values of other researchers such as Isbash (1935), Inglis (1949), Niel (1967) and Maynord (1989). According to present study all ratios are found to be very close to the perfect agreement line as shown in Figure 5.12. These analysis reveals that the present equation show satisfactory compliance with the Isbash (1935) investigation. Table 5.7 represents the percentage of discrepancy ratios within each discrepancy band for geobags.

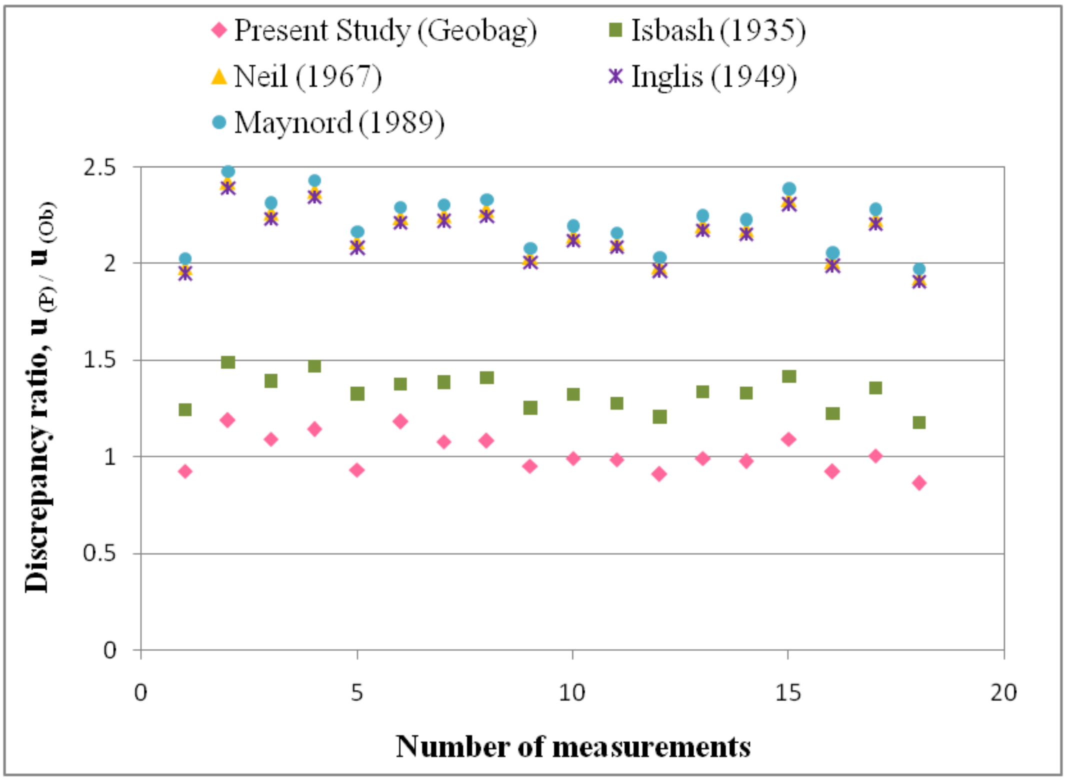


**Figure 5.12**: Values of discrepancy ratio of depth averaged velocity for geobag

**Table 5.7:** Discrepancy band of depth averaged velocity for geobag

| Discrepancy Band | Present Study (%) | Isbash (1935) (%) | Inglis (1949) (%) | Niel (1967)(%) | Maynord (1989) (%) |
|---|---|---|---|---|---|
| 0.95 -1.05 | 34 | 0 | 0 | 0 | 0 |
| 0.85 -1.15 | 89 | 0 | 0 | 0 | 0 |
| 0.75 -1.25 | 100 | 23 | 0 | 0 | 0 |

| Discrepancy Band | Present Study (%) | Isbash (1935) (%) | Inglis (1949) (%) | Niel (1967)(%) | Maynord (1989) (%) |
|---|---|---|---|---|---|
| 0.65 -1.35 | - | 56 | 0 | 0 | 0 |
| 0.5 -1.5 | - | 100 | 0 | 0 | 0 |
| 0.5 -2.0 | - | - | 23 | 17 | 6 |

From Table 5.7, 34% discrepancy ratios are found within the range 0.95 to 1.05 and 100% discrepancy ratios are within the discrepancy band 0.75 to 1.25 for geobag. Earlier investigations show differences with present study because the condition of their analyses may not be similar with the present study.

### 5.3.10 Computation of relative error of depth averaged velocity equations

Empirical equations (Eq. 5.5 and Eq.5.6) of incipient condition based on depth averaged velocity have been developed by doing experimental investigations on incipient behavior of nine different size protection elements. Different incipient velocity formulas along with proposed relationship have been compared with predicted depth averaged velocity equation. The relative error of different formula and proposed relationship is presented in Table 5.8.

**Table 5.8**: Performance of depth averaged velocity prediction formulas

| Shear Velocity Equation | Relative error % | |
|---|---|---|
| | CC Block | Geobag |
| Present study | 8.64 | 7.8 |
| Isbash (1935) | 9.4 | 34.56 |
| Inglis (1949) | 69.95 | 114.56 |
| Niel (1967) | 73.94 | 118.42 |
| Maynord (1989) | 75.48 | 122.28 |

From the Table 5.8 it is seen that the proposed empirical equations have the lowest average value of relative error for block and geobag. Equation (5.5) has the lowest average value of relative error 8.64% and equation (5.6) has also lowest average value of relative error 7.78 % where Isbash (1935) equation performs better than the rest with 9.4% and 34.56% for CC blocks and geobags respectively. However, it is needless to mention that equations proposed in present study comparatively better predictor for both CC block and geobag.

Inglis (1949) has large value of relative errors in predicting incipient velocity because he reported some experimental results with isolated and close-packed blocks, but apparently not arranged in a random fashion as riprap. The reason behind the large relative error obtained by Neil (1967) is, Neil (1967) proposed a relationship on the basis of experiments with natural gravels, glass spheres and low-density spheres, to just maintain stability of stones on a flat bed. Maynord (1989) has the largest value of relative error because Maynord (1989) presented a relationship for incipient movement of riprap on a flat bed considering 30% passing size of stone.

All these formula considered stones/blocks on flat bed. But present study investigated incipient condition of protection element dumped in flowing water on a live bed to better understand the real life phenomena and all the proposed equations have lowest value of relative error comparing with the previously established formula.

### 5.3.11 Analysis of shear stress for CC Block

According to theoretical analysis of the experiment, relationship between Shield's number and dimensionless particle diameter for CC block has been developed. The plot is shown in Figure 5.13.

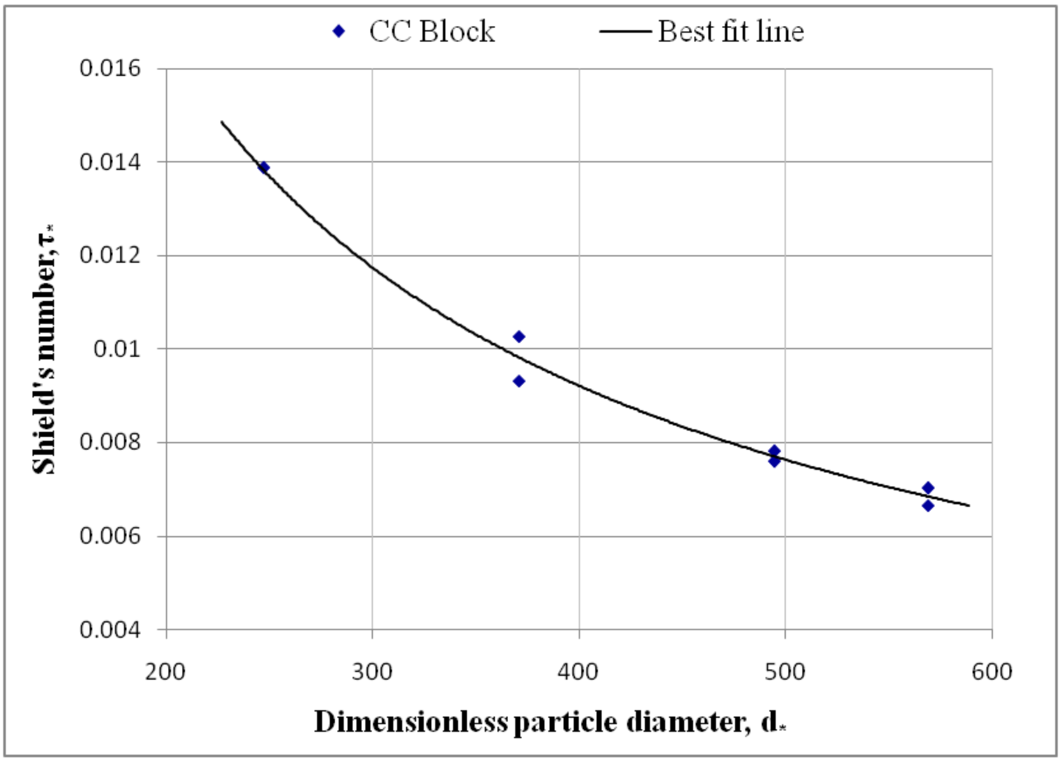


**Figure 5.13**: Shield's number versus dimensionless particle diameter for CC block

The coefficient of determination ($R^2$) is found to be 0.98 indicating a good correlation. It is seen that as the dimensionless particle diameter increases Shield's number decreases.

The final expression of shear stress for block becomes

$$\tau_* = 1.471\, d_*^{-0.84} \tag{5.7}$$

Equation (5.7) is valid within the experimental ranges of $0.006 < \tau_* < 0.015$ for Shield's number and $200 < d_* < 600$ for dimensionless particle diameter.

### 5.3.12 Comparison of proposed relationship for CC block with others

Figure 5.14 shows the comparison of various equations for predicting Shield's number against dimensionless particle diameter with present study for CC block. From this figure, it is clear that Brownile (1981) and Cao et al. (2006) predicts greater value than equation proposed in present study and Dey and Raju(2002) ) predicts smaller value than equation proposed in present study. However, for higher dimensionless particle diameter the value of Shield's number quite similar as predicted by Dey and Raju (2002).

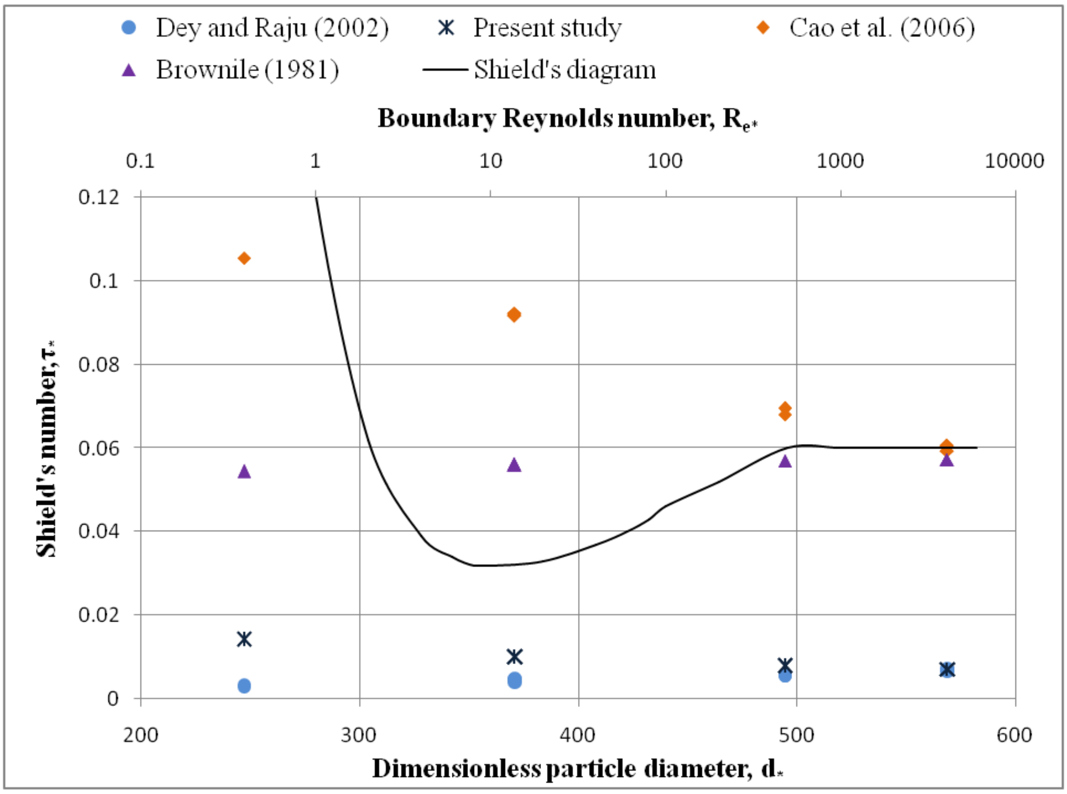


**Figure 5.14**: Comparison of Shield's number for CC block with others

From Figure 5.14 it is also clear that according to present study Shield's number slightly decreases with increasing dimensionless particle diameter which is consistent with Cao et.al. (2006). On the other hand, Shield's number increases with increasing dimensionless particle diameter according to Brownile (1981) and Dey and Raju (2002).

Shield's diagram established to calculate the incipient condition of bed material. Figure 5.14 also demonstrates the difference between incipient condition of bed material and protection elements.

### 5.3.13 Analysis of shear stress for geobag

Figure 5.15 depicts the relationship between Shield's number and dimensionless particle diameter for geobag.

The coefficient of determination ($R^2$) is found to be 0.76 indicating a good correlation. It is seen that as the dimensionless particle diameter increases Shield's number decreases.

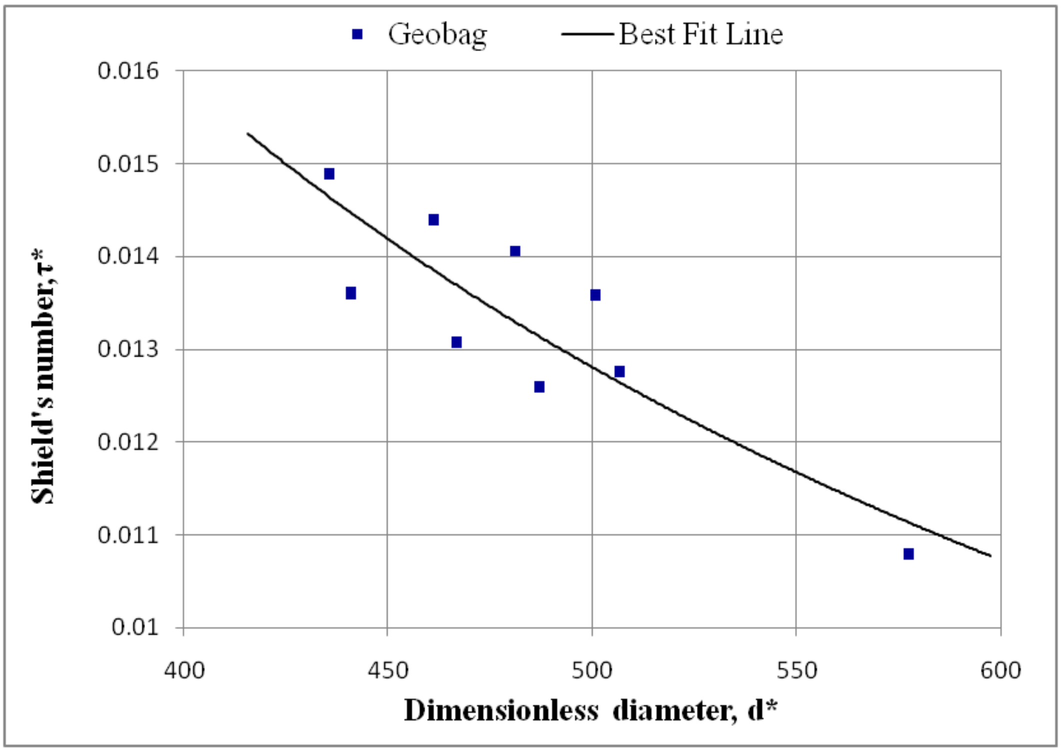


**Figure 5.15**: Shield's number versus dimensionless particle diameter for geobag

The final expression of shear stress for block becomes

$$\tau_* = 5.259\, d_*^{\,-0.96} \tag{5.8}$$

Equation (5.8) is valid within the experimental ranges of $0.01 < \tau_* < 0.016$ for Shield's number and $400 < d_* < 600$ for dimensionless particle diameter.

### 5.3.14 Comparison of proposed relationship for geobag with others

The comparison of various equations for predicting Shield's number against dimensionless particle diameter with present study for Geobag is presented in Figure 5.16. From the figure it can be mentioned that Brownile (1981) and Cao et al. (2006) predicts greater value than equation proposed in present study and Dey and Raju(2002) predicts smaller value than equation proposed in present study.

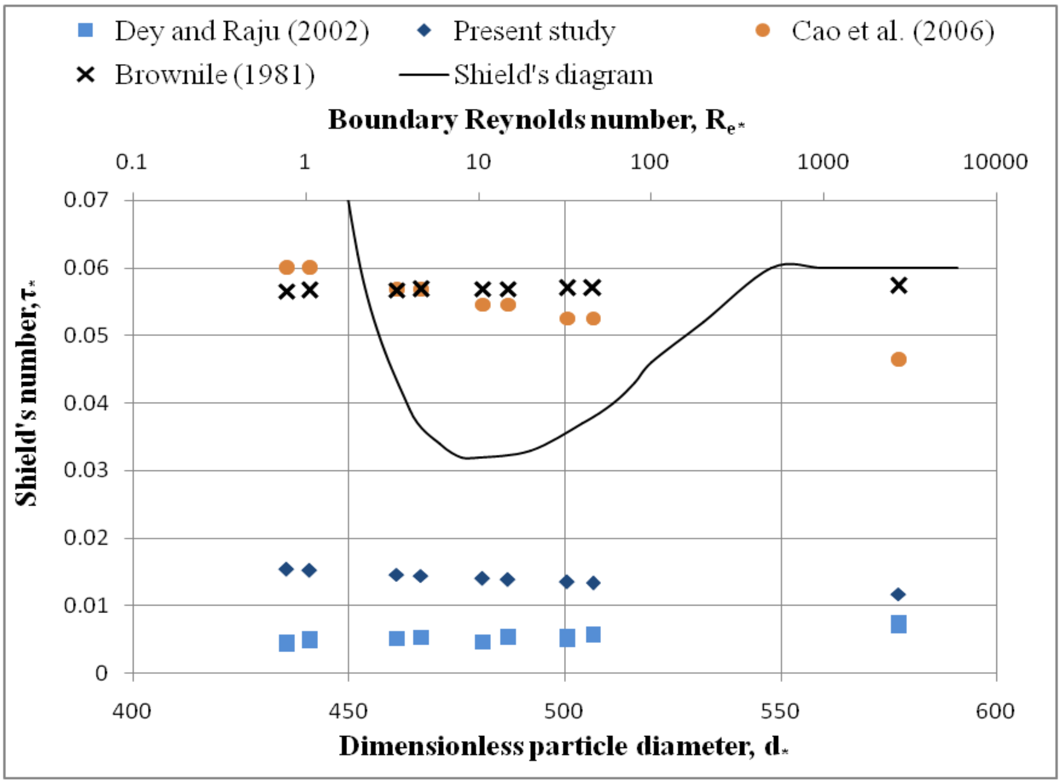


**Figure 5.16**: Comparison of Shield's number for geobag with others

From Figure 5.16 it is evident that according to present study Shield's number slightly decreases with increasing dimensionless particle diameter which is consistent with Cao et.al. (2006). On the other hand, Shield's number increases with increasing dimensionless particle diameter according to Brownile (1981) and Dey and Raju (2002).

From Shield's diagram established incipient condition of bed material can be evaluated which is different for the large sized protection element. Figure 5.16 demonstrates the difference between incipient condition of bed material and protection element.

### 5.3.15 Analysis of turbulence intensity for CC blocks

Protection element is most likely to be entrained when turbulent fluctuations act to increase the local velocity around the elements above the average velocity. These downstream directed turbulent fluctuations, therefore, are included in the present study. The turbulence intensity (root mean square of fluctuating velocity, m/s) r.m.s. (u′) should be considered in determining mobility of protection elements.

A regression analysis of the experimental data has been performed. Figure 5.17 presents the relationship between non-dimensional turbulence intensity with relative depth for CC blocks with a coefficient of determination ($R^2$) of 0.67.

The final empirical relationship of the equation (3.18) becomes

$$\frac{\mathrm{r.m.s}(u')}{u_*} = 0.251\left(\frac{h}{d}\right)^{0.647} \tag{5.9}$$

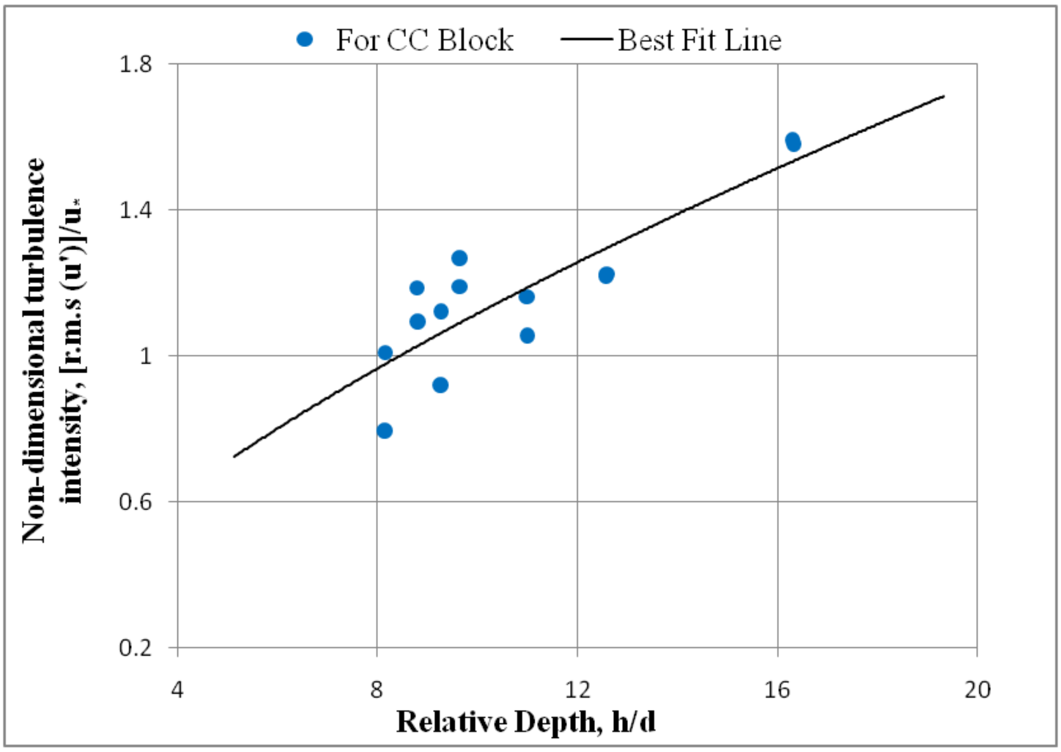


**Figure 5.17**: Relationship between non-dimensional turbulence intensity with relative depth for CC blocks

Equation 5.9 is valid within the experimental range $0.65 < \frac{\mathrm{r.m.s}\,(u')}{u_*} < 1.75$ and $4.5 < \frac{h}{d} < 19$.

From Figure 5.17 it is evident that non-dimensional turbulence intensity increases with increasing relative depth for CC blocks.

### 5.3.16 Analysis of turbulence intensity for geobags

A regression analysis of the experimental data has been performed. Figure 5.18 presents the relationship between non-dimensional turbulence intensity with relative depth for geobag with a coefficient of determination ($R^2$) is 0.52.

The final empirical relationship of the equation (3.18) becomes

$$\frac{\mathrm{r.m.s}(u')}{u_*} = 0.14 \left(\frac{h}{d}\right)^{0.923} \tag{5.10}$$

Equation 5.10 is valid within the experimental range $0.6 < \frac{\mathrm{r.m.s}\,(u')}{u_*} < 1.4$ and $5 < \frac{h}{d} < 12$.

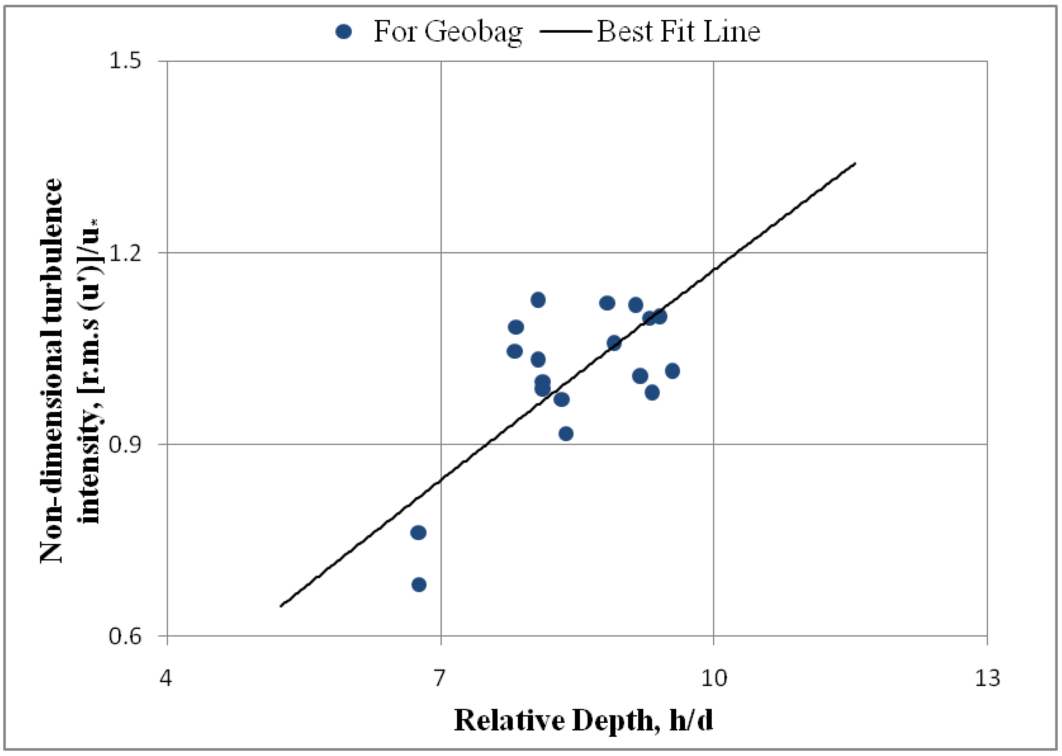


**Figure 5.18**: Relationship between non-dimensional turbulence intensity with relative depth for Geobag

Figure 5.18 shows that non-dimensional turbulence intensity increases with increasing relative depth for geobag.

### 5.3.17 Performance of proposed turbulence intensity relationship

A unified model for the turbulence intensity as a function of relative depth has yet to be proposed. In the literature dealing with turbulence intensity, only one empirical equation by Lamb et al. (2008) is found so far and the equations of the present study (Eq. 5.9 and Eq. 5.10) are compared with it by the computation of relative error. The relative error of Lamb et al. (2008) formula and proposed relationship is presented in Table 5.9.

**Table 5.9**： Performance of turbulent intensity prediction formulas with observed values

| **Relative error %** | **CC block** | **Geobag** |
|---|---|---|
| Present Study | 8.71 | 7.26 |
| Lamb et al. (2008) | 66 | 63 |

### 5.3.18 Effect of relative roughness on turbulent intensity

Figure 5.19 depicts the relationship between non-dimensional turbulence intensity and relative roughness for CC block. The relationship shows good agreement with the reduction in turbulence intensity with increasing relative roughness is due to reduced macro-scale turbulent motions as earlier study by Lamb et al. (2008).

Figure 5.20 depicts the relationship between non-dimensional turbulence intensity and relative roughness for geobag. The relationship also compliance with earlier investigation by Lamb et al. (2008), as turbulence intensity is inversely proportional with relative roughness.

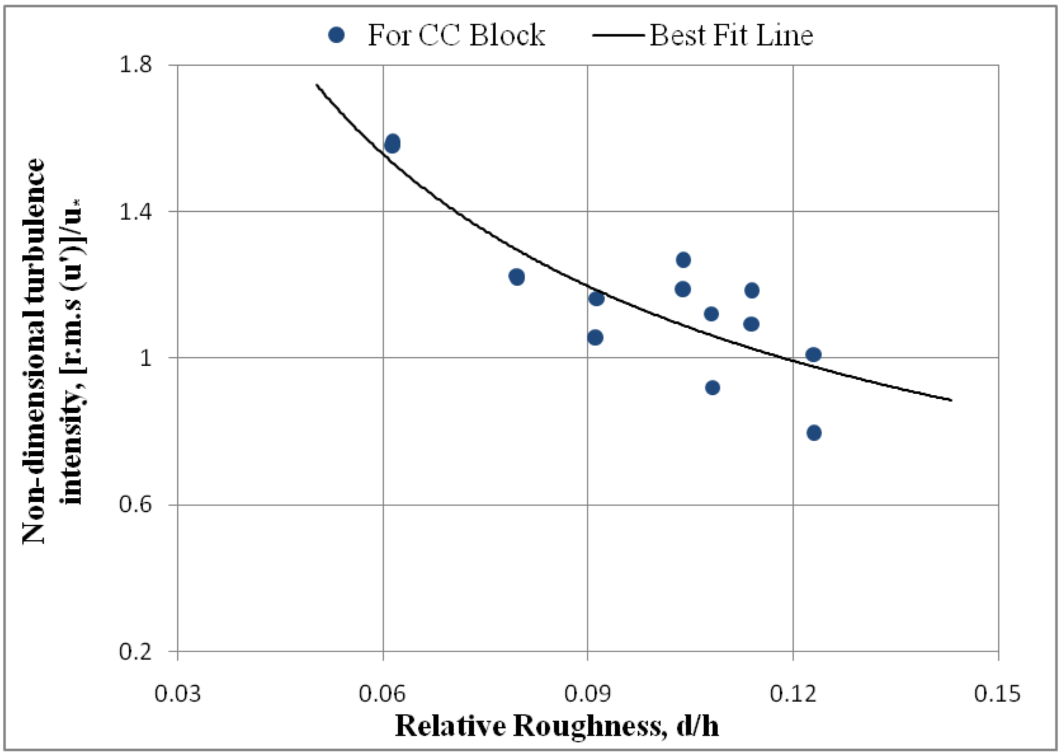


**Figure 5.19**: Relationship between non-dimensional turbulence intensity with relative roughness for CC block

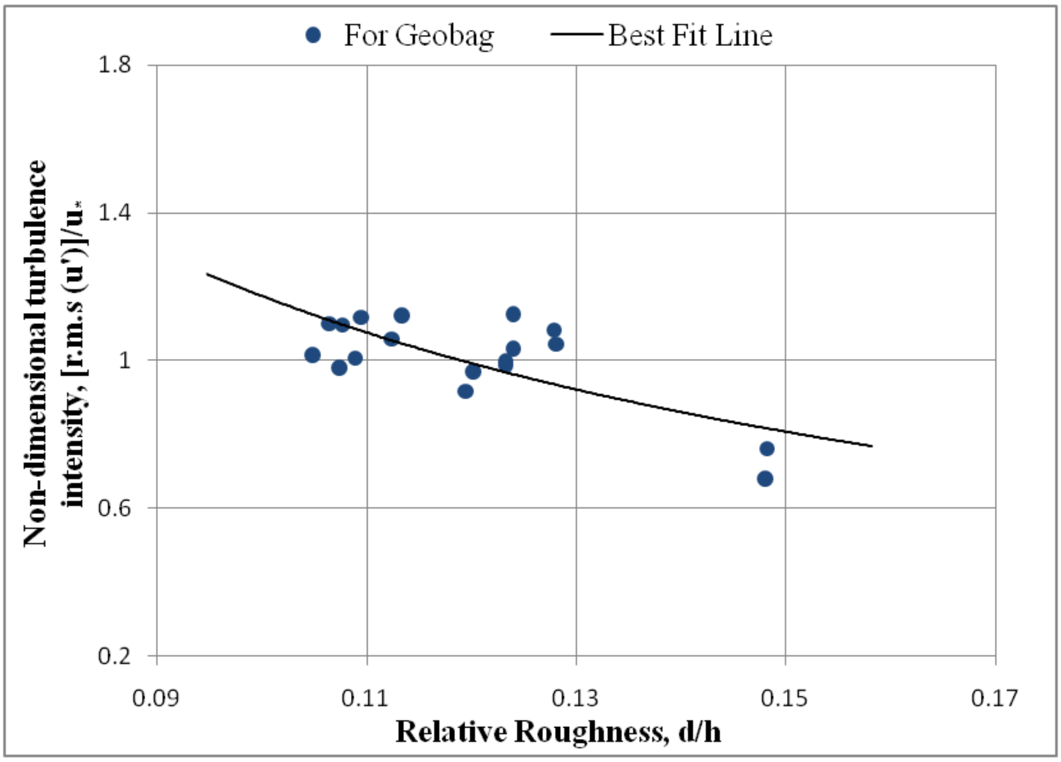


**Figure 5.20:** Relationship between non-dimensional turbulence intensity with relative roughness for Geobag

### 5.4 Analysis of depth factor

Depth factor is very important for the bank protection design. To analyze depth factor sixteen experimental runs have been conducted.

#### 5.4.1 Depth factor for the design of CC block

With the flow velocity well known Pilarczyk's relation (1990) is applicable. Depth factor ($k_h$) was calculated by using Pilarczyk's (1990) relation for both CC block and Geobag of different sizes. A regression analysis of the experimental data has been performed with a coefficient of determination ($R^2$) of 0.83.

Figure 5.21 represents the relationship between depth factor ($k_h$) and relative depth (h/d) for CC block.

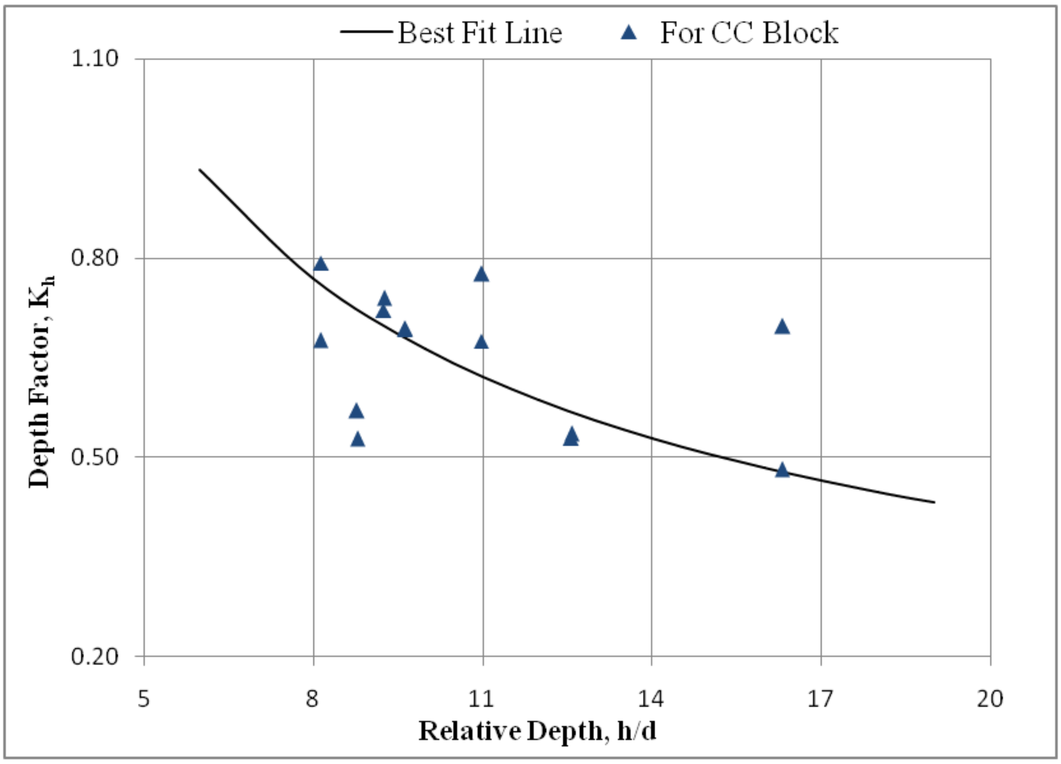


**Figure 5.21**: Depth factor versus relative depth for CC block

The Figure 5.21 depicts that as the relative depth increases the depth factor decreases.

The final expression of depth factor equation (3.15) for CC blocks becomes

$$K_h = 3.102 \left(\frac{h}{d}\right)^{-0.67} \tag{5.11}$$

Equation (5.11) is valid within the experimental ranges of $5 < h/d < 20$ for relative depth and $0.5 < k_h < 0.8$ for depth factor.

### 5.4.2 Depth factor for the design of geobag

Pilarczyk's relation (1990) is applicable for the computation of depth factor ($k_h$) if the flow velocity is well known. Depth factor ($k_h$) was calculated by using Pilarczyk's (1990) relation for Geobag of different sizes. A regression analysis of the experimental data has been performed with a coefficient of determination ($R^2$) of 0.40.

The final expression of depth factor for Geobag becomes,

$$k_h = 5.218\left(\frac{h}{d}\right)^{-0.72} \qquad (5.12)$$

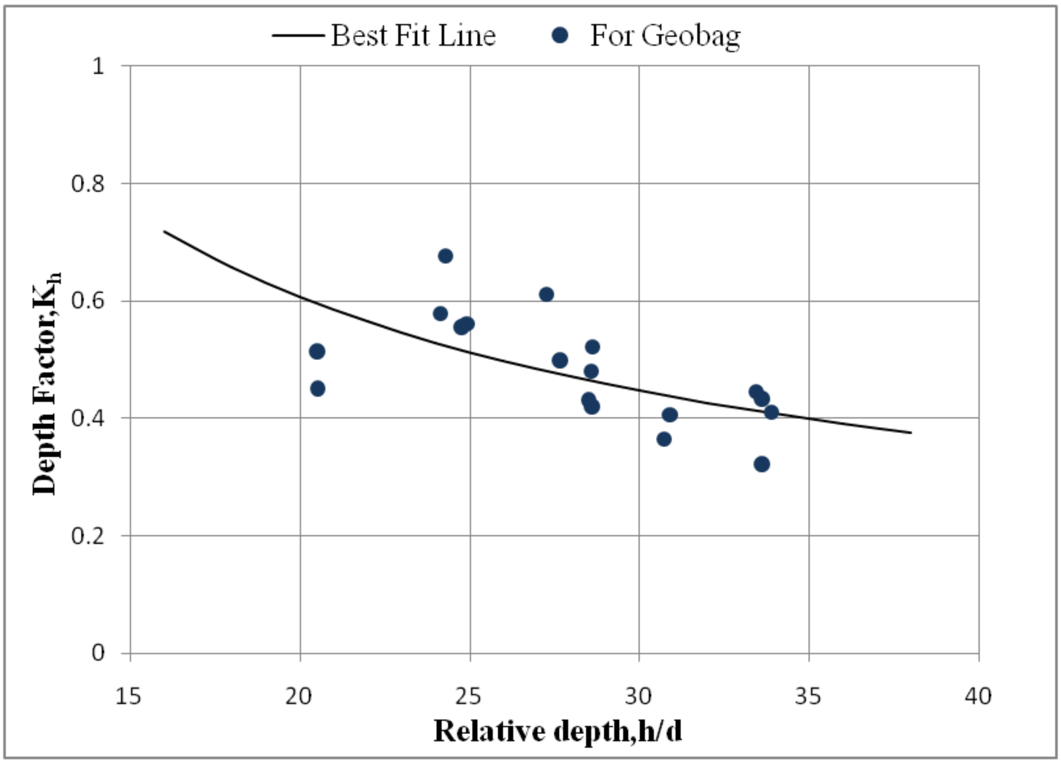


**Figure 5.22**: Depth factor versus relative depth for geobag

Figure 5.22 represents the relationship between depth factor ($k_h$) and relative depth (h/d) for Geobag. It is proved that depth factor is inversely proportional with relative depth.

Equation (5.12) is valid within the experimental ranges of 16 < h/d < 38 for relative depth and 0.35 < $k_h$ < 0.7 for depth factor.

### 5.4.3 Comparison of proposed depth factor relationship

From reviewing different literature it has been found that only Pilarczyk gave the relation between relative depth and depth factor. So in present study equation (Eq. 5.11 and Eq.5.12) has been compared with Pilarczyk (2008). The relative error of Pilarczyk (2008) formula and proposed relationship is presented in Table 5.10.

**Table 5.10**: Performance of depth factor prediction formulas

| **Relative error %** | **CC block** | **Geobag** |
|---|---|---|
| Present Study | 11.87 | 12.24 |
| Pilarczyk (2008)_ non developed velocity profile | 13.87 | 16.17 |
| Pilarczyk (2008)_ fully developed velocity profile | 28.95 | 33 |

These analysis reveals that the present equation show good compliance with the Pilarczyk (2008) investigations.

## 5.5 Analysis of the effect of live bed at incipient condition

The well-known Shields curve is essentially an empirical result where a line of best fit has been applied to the scattered experimental data. In this experiment dimensionless critical shear stress ($\tau_{*c}$) and the particle shear Reynolds number ($R_{e*}$) values have been calculated from experimental data to predict its behavior. Experiments have shown that dimensionless critical shear stress, or Shields parameter is independent of the Boundary Reynolds number, or particle Reynolds number greater than 200, which is consistent with literature. Dimensionless shear stress, $\tau_{*c}$ obtained from the experiments for CC block ranges from 0.0067 and 0.0139. For geobag dimensionless shear stress, $\tau_{*c}$ are found to be in the range between 0.011 and 0.015. The results demonstrate that the protection elements studied are in ‘no motion’ condition according to Shield’s diagram. For underlying sand bed material (size 0.23 mm) $\tau_{*c}$ are found 0.04 which is in ‘motion’ condition according to Shield’s diagram. Under the live bed condition, the material on the bed has an additional impact on the incipient condition of the protection elements.

Table 5.11 is showing the comparisons of shear velocity and shear stress on fixed bed with live bed for both type of protection elements (CC block and geobag).

**Table 5.11:** Comparisons of shear velocity and shear stress on fixed bed and live bed

| **Type of protection elements** | **Size (m)** | **Set up** | **Shear velocity (m/s)** | | | **Shear Stress ($N/m^2$)** | | |
|---|---|---|---|---|---|---|---|---|
| | | | **Fixed bed (Raju, 2011)** | **Live bed (Present Study)** | **Range of % error** | **Fixed bed (Raju, 2011)** | **Live bed (Present Study)** | **Range of % error** |
| **CC block** | 0.015 | 1 | 0.03724 | 0.03791 | 0.14-5.45 | 1.387 | 1.437 | 0.28-6.62 |
| | 0.02 | | 0.03737 | 0.03952 | | 1.397 | 1.562 | |
| | 0.023 | | 0.03834 | 0.03968 | | 1.470 | 1.574 | |
| | 0.015 | 2 | 0.03986 | 0.03979 | | 1.589 | 1.583 | |
| | 0.02 | | 0.04036 | 0.04008 | | 1.629 | 1.607 | |
| | 0.023 | | 0.04070 | 0.04075 | | 1.656 | 1.661 | |
| **Geobag** | 0.0316 | 1 | 0.00373 | 0.04097 | 6.02-10.87 | 1.387 | 1.679 | 11.69-20.56 |
| | 0.0236 | | 0.00327 | 0.04019 | | 1.363 | 1.615 | |
| | 0.0245 | | 0.00409 | 0.04055 | | 1.329 | 1.644 | |
| | 0.0253 | | 0.00364 | 0.04063 | | 1.368 | 1.651 | |
| | 0.0259 | | 0.00454 | 0.04172 | | 1.382 | 1.740 | |
| | 0.0236 | 2 | 0.00257 | 0.04258 | | 1.601 | 1.813 | |
| | 0.0245 | | 0.00290 | 0.04307 | | 1.613 | 1.855 | |
| | 0.0253 | | 0.00332 | 0.04348 | | 1.613 | 1.890 | |
| | 0.0259 | | 0.00339 | 0.04360 | | 1.617 | 1.901 | |

From Table 5.11, it is evident that shear velocity on a live bed is about 2% greater than that of fixed bed for CC Block. For geobag shear velocity is about 8% greater on a live bed than that of fixed bed. Both CC block and geobag shows greater shear stress in case of live bed than fixed bed. The shear stress on live bed for CC block and geobag is about 4% and 16% greater than fixed bed respectively. This investigation shows consistency with earlier investigations done by Novaka and Nalluria (1984).

Most of the available literatures dealing with incipient motion, the bed was considered fixed. The fixed bed condition was used to improve underwater visibility of the placing and dumping of the protection elements. However, in Bangladesh, river bed is composed of alluvial material and toe protection is constructed in underwater condition. It is apprehended, there is an underlying effect of alluvial bed on the incipient condition of protection elements. This study is therefore can be an attempt to an investigation of a situation of underwater protective works prevailing in practice.

### 5.6 Comparison of incipient condition with dry bed condition

For designing of bank protection works in perennial rivers the construction works have always been a challenge and not considered in design. It is suggested that the designer should consider the hydraulic parameters which should be commensurate with underwater constructional aspects. Therefore a comparison has been made between underwater and dry bed toe protection to observe the incipient parameters.

Results of the shear velocity and incipient velocity for both underwater and dry bed condition are shown in Table 5.12.

**Table 5.12:** Results of underwater and dry bed condition at incipient condition

| **Type of Protection element** | **Dry bed condition** | | | **Underwater construction** | | |
|---|---|---|---|---|---|---|
| | **Depth, h (m)** | **Velocity, u (m/s)** | **Shear velocity, $u_*$ (m/s)** | **Depth, h (m)** | **Velocity, u (m/s)** | **Shear velocity, $u_*$ (m/s)** |
| CC Block | 0.2012 | 0.55 | 0.0412 | 0.1927 | 0.52 | 0.0406 |
| Geobag | 0.2072 | 0.57 | 0.0416 | 0.1992 | 0.44 | 0.0411 |

It is seen from the results that, flow depth, velocity and shear velocity are greater at dry bed condition for both CC block and geobag.

# CHAPTER SIX
# CONCLUSIONS AND RECOMMENDATIONS

## 6.1 Introduction

The experimental study of the placement of toe protection elements and incipient condition of toe protection elements under live bed condition has been conducted. Relationships for governing parameters of the incipient velocity, shear velocity, shear stress, turbulence intensity and depth factor of toe protection elements have been theoretically analyzed. These relationships then verified using laboratory data. A total of two types of elements (CC block and geobag) consisting of four sizes CC blocks and five different sizes of geobags have been used to conduct experiments. In this chapter, the conclusions and recommendations are made.

## 6.2 Conclusions

From this study the following conclusions can be made:

i) Placing behavior of protection elements has been observed. The CC blocks and geobags followed the path of a projectile pattern during falling which has created an angle of about $60^0$ and $45^0$ with the vertical respectively. The geobag traveled relatively more distance than CC block during the course of its settling.

ii) The settling distance relationship proposed in this study was found to be satisfactory i.e. for horizontal settling distance prediction equation; the error was 1.96% for CC block and 1.38% for geobags.

iii) Proposed relationships for shear velocity have been compared with other available equations. It was found that the predictive capacity of proposed relationships (Eq. 5.3 and Eq. 5.4) showed satisfactory performance (discrepancy ratios were between 0.5 to 2.0 and the error is 2.5% for CC block and 1.97% for geobags).

iv) Predictive performances of the proposed relationships for depth-averaged velocity, shear stress and turbulence intensity at incipient condition have been compared with other available equations. It was found that the predictive capacity of proposed relationships show satisfactory compliance with earlier investigations.

v) At incipient condition geobags showed comparatively higher shear velocity and shear stress than that of CC blocks. These higher values were due to the embedded effect of geobag with sand bed compared to that of CC blocks.

vi) As such, from the present experiment it has been found that, the incipient velocity of geobag was much higher than that of CC block.

vii) The proposed equations for the estimation of depth factor (Eq. 5.11 and Eq. 5.12) were found to be complying satisfactorily with the equation developed by Pilarczyk (2008).

viii) It has been observed that the shear velocity and shear stress for protection elements dumped in flowing water on live bed condition higher (2% for CC block and 8 % for geobag) than that of fixed bed condition.

ix) Relationship between non-dimensional turbulence intensity and relative roughness has been developed. The Figures (Fig. 5.19 and Fig. 5.20) demonstrated that, turbulence intensity is inversely proportional with relative roughness.

x) Finally, it is anticipated that the findings summarized above have applications in design and construction of river bank protection works.

## 6.3 Recommendations

Following recommendations can be suggested for further study, these are as follows:

i) The proposed equation to determine shear velocity, depth averaged velocity, turbulence intensity and depth factor of protective element has been verified based on laboratory data and in future it may be verified in field condition.

ii) The results of the present study can be assessed further with experimental works of large capacity physical model facilities.

iii) Similar study can be done with the equipment which can measure accurately near bed flow situations under live bed conditions.

iv) A prototype example can be verified with experimental channel of similar nature using mathematical model.

## REFERENCES


1. Ashiq, M and Doering, J.C. (2006). “How incipient motion determination judgment affects different parameters in sediment transport investigation”. Proceedings of 8th FISC, 264-271.

2. Armitage, N., & Rooseboom, A. (2010). “The link between Movability Number and Incipient Motion in river sediments”. Water SA, 36(1), 89-96.

3. Bathurst, J. C. (1985). “Flow resistance estimation in mountain rivers”. Journal of Hydraulic Engineering, 111(4), 625-643

4. Beheshti, A. A., and Ashtiani, B. A. (2008). “Analysis of threshold and incipient conditions for sediment movement”. J. Coastal Eng., Elsevier, 55 (2008), 423-430.

5. Brahms, A. (1753). Anfangsgründe der deich-und. Wasserbaukunst, Aurich (Source: Raju, K.M.A.H., 2011).

6. Brownlie, W. R. (1981). “Compilation of Alluvial Channel Data”. Technical Report KH-R-43B. Pasadena, California, USA: California Institute of Technology. (Source:Miedema, S. A., 2010)

7. Breusers, H. N. C, Nicollet, G., and Shen, H. W. (1977). "Local scour around cylindrical piers." J. Hydr. Res., 15(3), 211-252. (Source: Chiew, 1992).

8. Bridge scour manual, (2013). State of Queensland (Department of Transport and Main Roads) 2013.

9. BWDB, (2010). “Guidelines for river bank protection”, prepared for Bangladesh Water Development Board under Jamuna-Meghna River Erosion Mitigation Project, Government of the People’s Republic of Bangladesh.

10. Cao, Z., Pender, G., & Meng, J. (2006). “Explicit formulation of the Shields diagram for incipient motion of sediment”. Journal of Hydraulic Engineering, 132(10), 1097-1099.

11. Celik, A. O. (2011). “Experimental investigation of the role of turbulence fluctuations on incipient motion of sediment”. Doctoral dissertation, Virginia Polytechnic Institute and State University.

12. Chang, H. H. (1988). “Fluvial Processes in River Engineering”. John Willey& Sons, Inc. USA, 1988.

13. Cheng, N. S. (2006). “Influence of shear stress fluctuation on bed particle mobility”. Physics of Fluids (1994-present), 18(9), 096602.

14. Chiew, Y. M. (1992). “Scour protection at bridge piers”. Journal of Hydraulic Engineering, 118(9), 1260-1269.

15. Dey S and Raju U (2002). “Incipient motion of gravel and coal beds”. Sādhan ā, 27 (5), 559–568.

16. Dey, S., (2003). “Threshold of sediment motion on combined transverse and longitudinal sloping beds”. Journal of Hydraulic Research, Vol. 41, No. 4, p. 405-415.

17. Dey, S., & Sarkar, A. (2006). “Scour downstream of an apron due to submerged horizontal jets”. Journal of hydraulic engineering, 132(3), 246-257.

18. Desonneville, B., Vanvelzen, G., Verheij, H., & Dorst, K. (2012). “Falling aprons at circular piers under currents”. ICSE6 Paris - August 27-31, 2012.

19. Elkholy, M., & Chaudhry, M. H. (2012). “Investigations on the Trajectory of Large Sandbags in Open Channel Flow”. Journal of Hydraulic Engineering, 138(12), 1060-1068.

20. FAP 21 (2001). “Guidelines and design manual for standardized bank protection structures”, Flood Action Plan, Bank Protection Pilot Project, prepared for Water Resources Planning Organization.

21. Gales, R. (1938). “The principles of river training for railway bridges and their application to the case of the Hardinge Bridge over the lower Ganges of Sara”. Journal of the Institution of Civil Engineers, December 1938. Paper No, 5167, India.

22. García, C. M., Cantero, M. I., Niño, Y., & García, M. H. (2005). “Turbulence measurements with acoustic Doppler velocimeters”. Journal of Hydraulic Engineering, 131(12), 1062-1073.

23. Göğüş, M., and Defne, Z. (2005). “Effect of shape on incipient motion of large solitary particles”. J. Hydraul. Eng. Div, ASCE, 131 (1), 38-45.

24. Grass, A. J. (1971). “Structural features of turbulent flow over smooth and rough boundaries”. Journal of Fluid Mechanics, 50(02), 233-255.

25. Halcrow and Associates, (2002). “Feasibility Study - Final Report”, Jamuna-Meghna River Erosion Mitigation Project, Volume 1 (Phase II), main report prepared for Bangladesh Water Development Board, Government of the People’s Republic of Bangladesh, and Asian Development Bank.

26. Hasan, M. R. (2003). “Experimental study of local scour at the toe of protected embankment”. M. Engg. Thesis, Department of Water Resources Engineering, BUET, Dhaka.

27. Haque, M. E. (2010). “An experimental study on flow behavior around launching apron”. M.Sc. Thesis, Department of Water Resources Engineering, BUET, Dhaka.

28. Hickin, E. J. (2004), "River Hydraulics and Channel Form". Chapter 5.

29. Hoeven, M. A. V. (2002). “Behaviour of a falling apron”. M.Sc. Thesis, Hydraulic and Geotechnical Engineering Department, Delft University of Technology.

30. Hofland, B., Battjes, J. A., & Booij, R. (2005). “Measurement of fluctuating pressures on coarse bed material”. Journal of Hydraulic Engineering, 131(9), 770-781.

31. Inglis, C. C. (1949). “The behavior and control of rivers and canals (with the aid of models)”, Part II. Central Waterpower Irrigation and Navigation Research Station, Poona, India.

32. Keulegan, G. H. (1938). “Laws of turbulent flow in open channels”. (Vol. 21, pp. 707-741). US: National Bureau of Standards.

33. Lamb, M. P., W. E. Dietrich, and J. G. Venditti (2008). "Is the critical Shields stress for incipient sediment motion dependent on channel-bed slope?" J. Geophys. Res., 113, F02008, doi: 10. 1029/2007JF000831.

34. Marsh, N. A., Western, A. W., & Grayson, R. B. (2004). "Comparison of methods for predicting incipient motion for sand beds". Journal of Hydraulic Engineering, 130(7), 616-621.

35. Maynord, S. T., Ruff, J. F. and Abt, S. R. (1989). "Riprap Design". J. Hydraul. Eng., ASCE, 115 (7), 937-949.

36. Miedema, S.A. (2010). "Constructing the Shields curve, a new theoretical approach and its applications". WODCON XIX, Beijing China.

37. Melville, B. W., & Sutherland, A. J. (1988). "Design method for local scour at bridge piers. Journal of Hydraulic Engineering". 114(10), 1210-1226.

38. Neill, C. R. (1967). "Mean velocity criterion for scour of coarse uniform bed material". Proceedings 12$^{th}$ Congress, International Association for Hydraulic Research, Vol. 3. (Source: NHC,2006).

39. NHC, (2006). Northwest Hydraulic Consultants: Physical Model Study (Vancouver Canada), Final Report. Prepared for Jamuna-Meghna River Erosion Mitigation Project. Bangladesh Water Development Board.

40. Nikora, V.I., Goring, D.G. (2000). Flow turbulence over fixed and weakly mobile gravel beds. J. Hydraul. Eng., ASCE 126(9), 679-690.

41. Novak, P. and Nalluri, C.(1984). "Incipient motion of sediment particles over fixed beds". Journal of Hydraulic Research, 22: 3, 181 — 197

42. Oberhagemann, K., & Hossain, M. M. (2011). Geotextile bag revetments for large rivers in Bangladesh. J. Geotextiles and Geomembranes, Elsevier, 29(4), 402-414.

43. Paphitis, D. (2001). "Sediment movement under unidirectional flows: an assessment of empirical threshold curves". Coastal Engineering, 43(3-4), 227-245.

44. Peirson, W. L., Figlus, J., Pells, S. E., & Cox, R. J. (2008). “Placed rock as protection against erosion by flow down steep slopes”. Journal of Hydraulic Engineering, 134(9), 1370-1375.

45. Pechlivanidis, G. I., Keramaris, E., Pechlivanidis, I. G., & Samaras, G. A. (2012). “Measuring the Turbulent Characteristics in an Open Channel Using the PIV Method”. Global Nest Journal, 14(3), 378-385.

46. Perng, A.T.H. and H. Capart (2008). “Underwater sand bed erosion and internal jump formation by travelling plane jets”. Journal of Fluid Mechanics 595, 1-43.

47. Pilarczyk, K. W. (1990). Coastal Protection, a. A. Balkema (Publisher), Rotterdam. (Source: BWDB, 2010).

48. Pilarczyk, K. W. (2008).”Design of alternative revetments”. Handbook of coastal and ocean engineering, edited by Kim Young, World Scientific publishers.

49. Raju, K.M.A.H. (2011). “An experimental study on settling behavior of toe protection elements of river bank protection works”. M.Sc. Thesis, Department of Water Resources Engineering, BUET, Dhaka.

50. Raju, K.M.A.H. and Matin M. A. (2013). “An experimental study on settling velocity of regular shaped elements for underwater erosion protection.” Journal of Civil Engineering, IEB, 41(1) (2013), 41-58.

51. Rao, T. S. N. (1946). “History of the Hardinge Bridge upto 1941,” Railway Board, Government of India, New Deldi, Technical paper no. 318.

52. Recking, A., & Pitlick, J. (2012). “Shields versus Isbash”. Journal of Hydraulic Engineering, 139(1), 51-54.

53. Reico, J., and Oumeraci, H. (2009). “Process based stability formulae for coastal structures made of geotextile sand containers” J. Coastal Eng., Elsevier, 56 (2009), 632-658.

54. Restall, S. J., Jackson, L. A., Heerten, G., and Hornsey, W. P. (2002). “Case studies showing the growth and development of geotextile sand containers: an

Australian perspective". J. Geotextiles and Geomembranes, Elsevier, 20 (2002), 321-342.

55. RRI (2010). River Research Institute. "Additional test to carryout investigation regarding performance of falling apron, drop test for dumping of geobag and outflanking problem by physical model to address bank erosion of Bangladesh". Prepared for Bangladesh Water Development Board.

56. Saathoff, F., Oumeraci, H., and Restall, S. (2007). "Australian and German experiences on the use of geotextile containers". J. Geotextiles and Geomembranes, Elsevier, 25 (2007) 251–263.

57. Sadat-Helbar, S. M., & Farhoudi, J. (2008). "Shear velocity method to riprap sizing at downstream of stilling basins". World Applied Sciences Journal, 4(1), 116-123.

58. Smith, D.A., Cheung, K.F., 2004. "Initiation of motion of calcareous sand". J. Hydraul. Eng. ASCE, 130 (5), 467–472.

59. Spring, F. J. (1903). "River training and control on the guide bank system", Railway Board Technical Paper No. 153, New Delhi.

60. Sternberg, H. (1875). "Untersuchungen über das Längen und querprofil geschiebeführender". Flüse Zeitschrift Bauwesen, vol. 25. (Source: Raju, K.M.A.H., 2011).

61. Stevens, M. A., and Oberhagemann, K. (2006). SpecialReport 17: Geobag Revetments. Prepared for Jamuna-Meghna River Erosion Mitigation Project. Bangladesh Water Development Board.

62. Thomas, W. A., Copeland, R. R., & McComas, D. N. (2002). "SAM hydraulic design package for channels". US Army Corps of Engineers Engineer Research and Development Center, Coastal and Hydraulics Laboratory. Final report September.

63. USACE, (1994). "Hydraulic design of flood control channels". U. S. Army Corps of Engineers, Manual EM 1110-2-1601.

64. Vollmer, S., and M. G. Kleinhans (2007). “Predicting incipient motion, including the effect of turbulent pressure fluctuations in the bed”. Water Resour. Res., 43, W05410, doi: 10.1029/2006WR004919.

65. Wu, F. C., and Yang, K. H. (2004). “Entrainment probabilities of mixed-size sediment incorporating near-bed coherent flow structures”. Journal of Hydraulic Engineering, 130(12), 1187-1197.

66. Zaman, M. U., and Oberhagemann, K. (2006). SpecialReport 23: “Design brief for river bank protection implemented under JMREMP.” Prepared for Jamuna-Meghna River Erosion Mitigation Project. Bangladesh Water Development Board.

67. Zhu, L., Wang, J., Cheng, N. S., Ying, Q., and Zhang, D. (2004). “Settling distance and incipient motion of sandbags in open channel flows”. Journal of waterway, port, coastal, and ocean engineering, 130(2), 98-103.